METAL-ORGANIC MONOLAYERS AS SUBSTRATES FOR BIOMOLECULE MICROARRAYS

By

SARAH MARIE LANE

A DISSERTATION PRESENTED TO THE GRADUATE SCHOOL
OF THE UNIVERSITY OF FLORIDA IN PARTIAL FULFILLMENT
OF THE REQUIREMENTS FOR THE DEGREE OF
DOCTOR OF PHILOSOPHY

UNIVERSITY OF FLORIDA

2007

To my family
(Papa, Mom, Margaret, Zac, Mellita, Peter and, of course, Jorge and Victoria)

ACKNOWLEDGMENTS

I would like to thank my advisor, for mental and moral support; the University of Florida Chemistry Department for providing me with an outstanding education; Marcela Morado for her hard work on the lanthanide self-assembled monolayer project; and Eric Lambers and the members of MAIC for allowing me unbridled access to the XPS instrument. Finally, I would like to thank the National Science Foundation for funding.

TABLE OF CONTENTS

LIST OF TABLES

LIST OF FIGURES

LIST OF ABBREVIATIONS

AFM:	Atomic Force Microscopy
APTES:	3-Aminopropyltriethoxysilane
DNA	Deoxyribonucleic acid
dsDNA:	Double-stranded deoxyribonucleic acid
EAL	Effective Attenuation Length
LB	Langmuir-Blodgett
NIST	National Institute of Standards and Technology
ODPA	Octadecylphosphonic acid
OTS	Octadecyltrichlorosilane
QCM	Quartz crystal microbalance
RNA	Ribonucleic acid
SAM	Self-assembled monolayer
SDS	Sodium dodecylsulfate
SPR	Surface plasmon resonance
SSC	Saline sodium citrate buffer
XPS	X-ray photoelectron spectroscopy

Abstract of Dissertation Presented to the Graduate School
of the University of Florida in Partial Fulfillment of the
Requirements for the Degree of Doctor of Philosophy

METAL-ORGANIC MONOLAYERS AS SUBSTRATES FOR BIOMOLECULE MICROARRAYS

By

Sarah Marie Lane

August 2007

Chair: Daniel R. Talham
Major: Chemistry

It has previously been shown that a zirconium-phosphonate surface can immobilize 5'-phosphorylated ssDNA and that this system can be used for DNA microarrays. These DNA microarrays had been studied with fluorescence imaging, but the probe surface density and hybridization efficiency was unknown. X-ray photoelectron spectroscopy was used to study the surface density of DNA and dsDNA on a zirconium-phosphonate substrate. A model was developed for the quantitative calculation of DNA surface density for the N 1s and Zr 3d peak intensities. It was found that a ssDNA probe with a poly-dG spacer gave a surface density of 2.8 $\times 10^{11}$ ssDNA molecules/cm^2. While the same ssDNA probe with a poly-dA spacer gave a surface density of 1.4 $\times 10^{11}$ ssDNA molecules/cm^2. It was also found that the surface density of the probe with the poly-dA spacer, unlike the probe with the poly-dG spacer, was highly dependent on the rinsing conditions. This indicated that the poly-dA spacer caused higher non-specific adsorption. In addition to the ssDNA studies, the use of the zirconium-phosphonate monolayer as a substrate for dsDNA microarrays was investigated, where the dsDNA would act as a probe for proteins. To supplement this research, the surface coverage of dsDNA with phosphate linkers and poly-dG spacers on the 5' and 5'ends; 3' and 3'ends; and 3' and 5'ends was calculated using the XPS data for the N 1s peak and Zr 3d peak. The surface coverage

results followed the same trend seen with fluorescence imaging of protein binding studies, where phosphate linkers on opposite ends of the dsDNA gave the highest surface coverages. A dsDNA sample with a random oligonucleotide spacer and phosphate linkers on the 5' and 5' ends showed a lower surface density than the dsDNA with phosphate linkers and poly-dG spacers on the 5' and 5' ends, which also followed the trend seen in the fluorescence studies of the protein binding.

Finally, this dissertation addresses research aimed at making lanthanide monolayers, which could act as supports for protein microarrays. Monolayers of lanthanide phosphonates were prepared using the Langmuir-Blodgett method, but it was found that these films were not stable in water. Using self-assembly of a siloxane modified ethylenediamine triacetic acid/lanthanide complex a more robust monolayer was formed, which was stable in water. Protein binding studies have not yet been performed on these more robust surfaces. Also, research was performed towards synthesizing a ligand which would sensitize the luminescence and immobilize lanthanides on a surface by means of a chelidamic acid ligand containing an amine. This molecule was made, but the purification and use of this molecule was hindered by its poor solubility.

CHAPTER 1
INTRODUCTION: XPS ANALYSIS OF DNA

Introduction

As technology and science advance, researchers have found many valuable reasons for immobilizing DNA on surfaces.[1-5] One reason is to study and analyze DNA itself. For example, to code a genome, microarrays of DNA can be used.[3] The general design of a DNA microarray is a surface covered with an array of many different spots of known ssDNA sequences called the probe, which should be well attached to the surface. The surface is then exposed to a solution of unknown ssDNA sequences called the target, which are often fluorescently labeled. The target ssDNA binds the probes of complementary sequence, allowing the target sequences to be determined by following the probe-target interaction with an analytical technique such as fluorescence imaging. One of the first examples of a DNA array used to study ssDNA interactions was given by Rease *et al.* This array was synthesized directly on a surface using photolithographic techniques and phosphoramidite activated deoxynucleosides (protected at the 5'-hydroxyl with a photolabile group).[3] The oligonucleotides were coupled together where the surface was exposed to light. Then selective photodeprotection and coupling cycles were repeated until the desired sequences were obtained. Using this method they made a 1.28 x 1.28 cm array containing 256 spots. The spots were tested for hybridization specificity with target molecules. After this example of in situ prepared oligonucleotides, many other different methods for preparing ssDNA microarrays have been reported.

Another use of immobilized DNA is for directed assembly. One of the first reports of using DNA for directed assembly came from Alivisatos *et al.*, where they had derivatized 1.4 nm gold particles with a single DNA strand.[1] Then using the specific interactions of complementary DNA strands they created dimers and trimers of the gold particles which had very specific inter-

particle distances based on the length of the DNA sequence. Similarly, Mucic *et al.*, using complementary interactions between ssDNA on 31 nm Au nanoparticles and 8 nm Au particles, created a network of the larger particles surrounded by the smaller particles.[6] Another example of DNA directed assembly is seen in a paper by Becker *et al.*, where ssDNA was spotted onto a substrate and then exposed to a solution of the complementary strand modified with a protein.[7] This second DNA strand bound to the complement creating a protein microarray which could then be used to probe protein-protein interactions with mass spectrometry.

These examples are just a drop in the bucket of the many uses scientists have found for surface immobilized DNA. With these many different uses for immobilized DNA, the chemistry of the DNA on the great variety of surfaces plays an important role. For instance, the surface density has been seen to affect hybridization efficiency[8] and it has been observed that the different bases of DNA result in different non-specific binding.[9] A number of methods have become more common for the quantitative surface analysis of DNA. These methods include surface plasmon resonance,[8] radiometric quantification using ^{32}P,[10] quartz crystal microbalance[11] and x-ray photoelectron spectroscopy (XPS)[12]. Surface plasmon resonance requires the DNA to be immobilized on either a gold or silver planar surface. Radiometric quantification requires that the DNA be modified with a radioactive isotope. Quartz crystal microbalance again requires the DNA to be immobilized on a specific metal surface like gold. Unlike the other methods, with XPS, unmodified DNA on almost any surface can be analyzed. In addition, XPS can give both qualitative information about the chemical environment of the different surface components through the shifts in the photoelectron binding energies and also quantitative information by looking at the peak areas of the photoelectrons.

The concept of XPS is fairly simple. A sample under ultra-high vacuum is bombarded with X-rays, usually from an aluminum or magnesium source, kicking out photoelectrons from the different energy levels of the atoms. The photoelectrons are ejected in all directions, with some traveling towards the analyzer. They then pass through the analyzer which is adjusted to allow only photoelectrons with a specific kinetic energy to reach the detector. Thus the kinetic energies of the photoelectrons are known and with the known energy of the X-rays the initial binding energy of the electron can be calculated.

As the electrons travel towards the analyzer, they pass through the rest of the sample. As they travel through the solid, there is a certain probability they will collide with another atom, resulting in an elastic collision, where their trajectory is changed, or an inelastic collision, where they lose kinetic energy. The further the electron must travel through the sample to reach the analyzer the higher the probability it will undergo a collision. Thus the photoelectrons originating from deep within the sample are more likely to arrive at the analyzer with a kinetic energy less than its original kinetic energy. The photoelectrons that have lost kinetic energy do not contribute to their respective peak, but to the background. Elastic collisions increase the path length the photoelectron must travel to get to the analyzer, increasing the probability they will undergo a collision.

Each electronic energy level of each element has an inherent efficiency with which it interacts with the X-rays called the photoelectric cross-section; this also affects the peak intensity. The peak intensity is also dependent on the concentration of the material in the sample, which allows quantitative or semi-quantitative information to be obtained from XPS. In addition to quantitative data, information about the chemical environment of the element can be drawn from slight shifts in the binding energy. This is because the electron binding energy

depends on the energy level, which can be affected by its chemical environment. For example, a photoelectron leaving an Fe^{3+} atom will have a higher binding energy than one leaving an Fe^{2+}.

As mentioned before, XPS is an analytical method that can be used on most solid surfaces. In 2004, our group published a paper showing that a zirconium-phosphonate surface can selectively immobilize 5'-phosphorylated ssDNA over nonphosphorylated ssDNA and that this system can be used for DNA microarrays. Little was known about the nature of the DNA on the surface, such as the probe surface density or the hybridization efficiency. With the help of XPS analysis, we attempted to answer some of these questions. This PhD dissertation discusses these XPS studies. This chapter introduces the topic of using XPS and outlines what other scientists have done in the way of studying DNA with XPS.

In addition to studying DNA on a zirconium-phosphonate surface, research was performed in order to make lanthanide monolayers, which would act as substrates for protein microarrays and also which would provide a system to study the luminescence of lanthanides in monolayers. More background information for these projects can be found in their respective chapters.

Qualitative and Semiquantitative XPS

XPS has been used a number of different ways to analyze DNA on a surface. One of the common uses is to simply look at a binding energy spectrum for the one of the elemental components of DNA, such as phosphorus or nitrogen, to confirm that the DNA is present on the surface being studied.[13-16] The binding energy of the N 1s photoelectron is around 400 eV while the P 2p peak has a binding energy around 133 eV. With a sufficient presence of DNA, both the N 1s and P 2p peak can be observed; however nitrogen is slightly more sensitive than phosphorus. Carbon and oxygen are not often used as an unconditional indicator for the presence of DNA due to the fact that they are often present on the surface either as contamination or a modification. This qualitative study often involves minimal analysis of the

peak shape or exact binding energy. For example, Wang *et al.* looked at the desorption of thiolated DNA on gold after applying a potential across the metal surface.[15] They observed a loss of the N 1s peak and an increase in the Au 4f peak. The increase in the Au 4f peak means that there is less attenuation of this peak by the DNA overlayer. Another interesting example, involving the use of dsDNA to self assemble lysine-capped gold colloidal nanoparticles, comes from Kumar *et al*. They used the P 2p peak as a positive indicator for the presence of DNA. According to the exact binding energy of the P 2p peak, they claimed no degradation of the DNA.[14]

XPS also easily offers semiquantitative results in the form of atomic percentages. The atomic percentages are calculated from either the peak intensity or peak area using a sensitivity factor for each energy level of each element. However, care needs to be taken when looking at the atomic percentages calculated this way because attenuation of the peaks by elastic and inelastic collisions has not been taken into account. There are quite a few examples of scientists using semiquantitative XPS to study DNA. This is often combined with other studies such as an examination of the binding energies measured with high resolution.[17-23] Frequently, when chemical information needs to be obtained from XPS by studying the binding energies, the element under analysis is present in more then one chemical environment. The multiple species give rise to more than one peak in XPS, which may be resolvable, but more often overlap. When the peaks overlap, peak fitting is often used to deconvolute the different species in the peak. An early example looked at the binding energy shifts studied the interaction of DNA with cis-dichlorodiamine platinum(II).[23] In this case, the DNA was not actually on a surface. One of the earliest examples of using semiquantitative XPS to study DNA on a surface was given by Herne *et al.*, who looked at thiolated and non-thiolated DNA self-assembling on gold.[17] They observed

that post-spotting treatment with mercaptohexanol dramatically decreased the non-thiolated DNA N 1s peak, but only slightly decreased the thiolated DNA N 1s peak. They also explored different potassium phosphate buffer concentrations. They saw, by following the N 1s normalized peak intensity, that increasing buffer concentrations up to 1 M increased the DNA immobilization. Very recently, Lee *et al.* also looked at posttreatment with a mercapto-alcohol, mercaptoundecanol, on thiolated DNA adsorbed onto gold.[19] They studied both elemental percentages and binding energies. They observed that posttreatment resulted in, not surprisingly, an increase in the elements associated with mercaptoundecanol, such as carbon and sulfur. More interestingly, after treatment with the mercaptoundecanol, the binding energies of most of the elements associated with the DNA shifted to lower binding energies especially the N 1s peak, which they thought indicated the DNA was standing upright and no longer interacting with the gold surface. Mohaddes *et al*. saw similar behavior in their work. They reported shifts to lower binding energies while studying the influence of mercaptohexanol on thiol-modified DNA immobilized onto GaAs.[21] On the other hand, Sastry *et al.* focused solely on studying the binding energies while looking at DNA immobilized in thermally evaporated films of octadecylamine (ODA).[22] The DNA was incorporated into the ODA by simply dipping the film into a DNA solution. The DNA was held in the film by the often-used electrostatic interactions between the positively charged protonated amine and negatively charged backbone of the DNA. They looked at the C 1s, P 2p, and N 1s peaks with XPS. With peak fitting of the C 1s peak they found two components: one at 285.5 eV and another at 287.5 eV. They attributed the low binding energy component to the hydrocarbon peak of ODA and the DNA sugars and bases. The higher binding energy component was attributed to carbons coordinated to the oxygen in the backbone. They also looked at the P 2p peak which arises from the phosphate backbone. Its

binding energy at 132.8 eV, they report, is similar to others of immobilized DNA, which they say indicates there is no degradation of the DNA.

An interesting study performed by Lee *et al.*, which also used semiquantitative XPS and binding energies, in addition to time-of-flight secondary-ion mass spectrometry (TOF-SIMS), studied the variation in the purity of thiolated ssDNA from three different vendors: Alpha, TriLink, and Synthegen.[18] They looked at the atomic percentage of phosphorus, carbon, nitrogen, oxygen, sulfur, and gold in the immobilized DNA. In the films from Alpha and Synthegen, they obtained less intense P 2p and N 1s peaks and more intense Au 4f peaks, which indicated that the DNA from those two vendors self assembled with a lower density. In addition, the films made from the DNA from Synthegen and Alpha contained excess sulfur. The C 1s percentages were the same for the films from all three vendors. However, upon studying the C 1s peak of the Synthegen and Alpha films with high resolution XPS, they saw a larger portion of the peaks with a lower binding energy. The lower binding energy portion indicated an excess amount of C-C and C-H species. They proposed that excess C-C and C-H plus the excess sulfur mentioned before was due to contamination with dithiothreitol, a reductant used to cleave disulfide precursors. With the help of TOF-SIMS, they were able to confirm the contamination with dithiothreitol. They also looked at the atomic percentages while varying the adsorption time and studied high resolution XPS scans of the sulfur region while varying the adsorption time to gain insight into how the contamination affected the kinetics of immobilization.

Quantitative

The semiquantitative results offered by XPS are useful, but valuable more quantitative information can also be obtained with XPS. One important piece of information that can be calculated from XPS data is the thickness of an overlayer on a substrate. This is based on the

simple equation which relates the intensity I_0 of a peak from an element in the bare substrate to the intensity I of the peak after it has been attenuated by an overlayer:

$$I = I_0 \exp(-d/\lambda \sin\theta) \qquad (1\text{-}1)$$

Here λ is the photoelectron mean free path, d is the thickness of the overlayer, and θ is the photoelectron take-off angle with respect to the surface. The photoelectron mean free path is the average distance a photoelectron will travel before it undergoes an inelastic collision. The mean free path depends on the kinetic energy of the photoelectron and on the material it is traveling through. Instead of the mean free path, an effective attenuation length can be used which takes into account elastic collisions as well. Equation 1-1 has been used in several instances to calculate the thickness of a DNA overlayer on a substrate.[12, 24-26] Higashi immobilized dsDNA on a gold surface, which had been modified with a binary SAM with one of the compounds containing an acridine group (Figure 1-1).[24] The acridine group can intercalate into the dsDNA leading to the dsDNA adsorption. Using Equation 1-1 and the Au 4f peak, they were able to calculate the thickness of the binary SAM (1.9 nm), and then the binary SAM plus the dsDNA layer (4.7 nm). From these thicknesses they estimated the dsDNA film thickness at 2.8 nm, which they say indicates that the dsDNA can be no more than a bilayer structure since the thickness of a dsDNA helix is 2 nm.

Another way to take advantage of the relationship in Equation 1-1 is to analyze the sample at multiple photoelectron take off angles. Leavitt *et al.* performed a similar study of ssDNA, which contained a sulfur atom replacing one of the oxygens in the phosphate backbone (Figure 1-2).[27] However, they sought a depth profile of the atomic percentages which requires the following equation which relates the intensity I_i of a specific element i with the different parameters of XPS:

$$I_i \propto F_i \sigma_i \int_0^\infty c_i(z) \exp(-z/\lambda_i \sin\theta) \mathrm{d}z \qquad (1\text{-}2)$$

In Equation 1-2, F_i is the spectrometer transmission function, σ_i the photoionization cross section, and $c_i(z)$ the concentration at depth z from the sample surface. The other variables have the same significance as in Equation 1-1. The exponential portion of the equation takes into account the attenuation of photoelectrons due to inelastic collisions. As is customary, Leavitt *et al.* used Equation 1-2 as a ratio of two elemental peaks. However, when using angle dependent data, Equation 1-2 cannot be solved directly. To get around this problem, Leavitt *et al.* treated the DNA layer as a series of flat homogeneous parallel layers and used an iterative method to find the atomic percentages of nitrogen, oxygen, phosphorus, carbon, sulfur and gold at different depths. In their depth profile, they saw that in the top 5 Å carbon, nitrogen, and oxygen reached their maximum atomic percentages. Then at a depth between 2.5 to 10 Å sulfur and phosphorus reached their maximum atomic percentages, while Au increased steadily in this region. This depth profile indicates that the sulfur and phosphorus are oriented towards the gold as would be expected if the sulfur is bound to the gold.

One of the most important works in quantitative XPS of DNA on gold was published by Petrovykh *et al*.[12, 26] They looked at a thiolated 25-mer of thymine binding to gold. They first used Equation 1-1 to get the thickness of the film. Then, as mentioned before, Equation 1-2 can be used to describe the ratio of concentration of gold to an element in the DNA, nitrogen or phosphorus:

$$\frac{c_i}{c_{Au}} = \frac{I_i}{I_{Au}} \frac{F_{Au}\sigma_{Au}L_{Au}^Q}{F_i\sigma_i L_i^Q} \frac{\exp[-z/L_{Au}]}{1-\exp[-z/L_i]} \qquad (1\text{-}3)$$

In this case, they used either quantitative effective attenuation lengths L_i^Q or average effective attenuations lengths L_{Au} instead of photoelectron mean free paths. To calculate the

effective attenuation lengths, they used a program called Electron Effective-Attenuation-Lengths Database Version 1.0 written by Powell and Jablonski at NIST.[28] In Equation 1-3, the $1-\exp[-z/L_i]$ portion of the equation accounts for the attenuation of the DNA film by itself. They could then use the density of gold to calculate the density of nitrogen and finally the surface coverage of the DNA, which they found to be 3.7×10^{13} DNA molecules per cm^2 for a DNA immobilization time of 20 hours.

Since Petrovykh's publication of this method for calculating the surface coverage of DNA other reports have emerged with similar calculations. Saprigin *et al.* immobilized ssDNA homo 20-mers through a covalent linkage on amine-coated oxidized aluminum.[25] To attach the DNA to the surface, they reacted phosphorylated DNA with carbodiimide to form a phosphoramidate linkage on the amine surface. They used the ratio of the Al 2p peak to P 2p peak and then the density of the aluminum to find the surface coverage of the DNA. Their calculation, similar to Equation 1-3, must also take into account the attenuation of the Al 2p peak by the aluminum oxide layer, the amine modification as well as the DNA layer. The surface density they found for a guanine oligomer is 2.8×10^{13} DNA molecules per cm^2. In addition to Saprigin's paper, Shen *et al.* also used a similar method to quantify thiolated DNA immobilized on maleimide-modified fused silica. One difference in their method is that they sputter the DNA and maleimide modification off the silica support *in situ* to get a reading of the bare silica surface. They use the ratio of P 2p to Si 2p and Si 2s to perform the surface coverage calculation, but in their equation they use the intensity of the bare silica support negating the need to correct for the attenuation of Si signal by the DNA layer. The surface density they find under the optimum conditions is 9.2×10^{12} DNA molecules per cm^2.

A final example involves the calculation of DNA surface coverage on silica nanoparticles.[29] The nanoparticles were first coated with an amine and then with 6-hexanedioic acid to create a carboxylic acid terminated surface which could then bind an amine modified oligonucleotide. They followed each step of the silica nanoparticle modification and DNA immobilization using XPS. To determine the DNA surface coverage, first the surface coverage of amine on the nanoparticles was determined using a ninhydrin fluorescence test. Then when the DNA was bound, they assumed that any increase in the N 1s signal was from the DNA and they could calculate the surface coverage of the DNA as 4.7×10^7 DNA molecules per bead.

Conclusion

This chapter offers an overview of the possibilities for using XPS to investigate DNA. However, XPS has its limitations and the data shown in most papers is often supported by other independent analytical techniques. Furthermore, some authors reporting quantitative results caution the readers that the data should be taken to be only semiquantitative because of the assumptions that must be made when performing the calculations for overlayer thickness and surface coverage.[27]

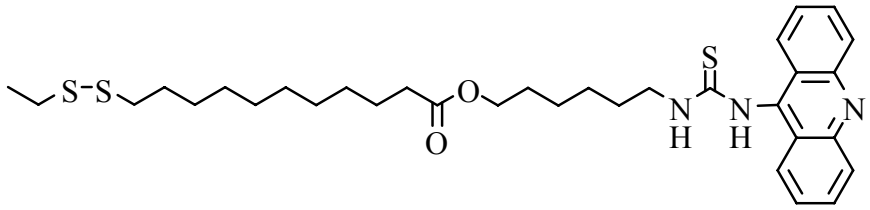

Figure 1-1. Compounds used by Higashi *et al.* in their in binary SAM to immobilize DNA.

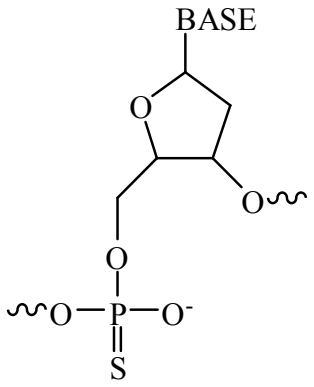

Figure 1-2. DNA with sulfur modified phosphate backbone used by Leavitt *et al.*

CHAPTER 2
USE OF XPS TO STUDY OLIGONUCLEOTIDES AT A ZIRCONIUM-PHOSPHONATE SURFACE

Introduction

Oligonucleotide microarrays, which allow high throughput, highly parallel investigation, have been used to probe a number of different biological phenomena including the analysis of gene expression.[30] There are many platforms on the market which are used for DNA and RNA microarrays and with each new platform there are often different protocols. The oligonucleotide probes can be prepared either *in situ*, for which the DNA or RNA sequences are synthesized directly on the surface,[31] or *ex situ*, where complete sequences are spotted on the surface.[30]

Our group recently reported that glass slides modified with a zirconium-phosphonate surface layer are effective substrates for covalently immobilizing oligonucleotides for array applications.[32] This concept, illustrated in Figure 1, uses specific metal/ligand interactions to covalently attach the oligonucleotide to the surface. Zirconium-phosphonate surfaces are known to strongly immobilize phosphate and phosphonate functionalized molecules.[33, 34] For example, these surfaces can be used to prepare self-assembled monolayers of densely-packed alkylphosphonates and other functional organophosphonates.[35] In a related fashion, phosphate terminated oligonucleotides can be immobilized and we demonstrated the zirconium-phosphonate surface selectively binds phosphorylated oligonucleotides over nonphosphorylated oligonucleotides.

Some of the surface chemistry parameters affecting the performance of oligonucleotide arrays include the density of the probe, the non-specific adsorption of DNA or RNA to the surface, and the distance of the probe from the surface. For example, it is now well documented that a high probe surface density can lead to low hybridization efficiencies and slow hybridization kinetics.[8, 36] Also the use of a spacer between the linker and the probe, which is

surmised to lift the DNA off the surface and prevent steric hindrance caused by the surface, can increase hybridization efficiencies.[37] To study the surface chemistry of immobilized probes several different quantitative techniques have been used including surface plasmon resonance (SPR), quartz crystal microbalance(QCM) and X-ray photoelectron spectroscopy (XPS).[26]

XPS, traditionally a materials science analytical technique, has been shown to be an efficient, label-free method for studying DNA on a surface. Leavitt *et al.* used angle-resolved XPS to study DNA with a thiol-modified backbone and determine its orientation on the surface of gold.[27] More recently, Petrovykh *et al.* used single-angle XPS with a substrate-overlayer model to determine the density of thiol-modified DNA on gold.[12] It has also been demonstrated that XPS can be used to distinguish between the different DNA and RNA bases.[25]

In this thesis, we report our initial results quantifying DNA attached to a zirconium-phosphonate support using XPS. Using the probe spotting conditions optimized for microarray applications we immobilized phosphorylated ssDNA on the surface and quantified the surface density using XPS and a modified substrate-overlayer method.

Experimental

Materials

Glass substrates were purchased from Gold Seal Products. Oligonucleotides were ordered lyophilized with HPLC purity from Invitrogen (Carlsbad, California). The ssDNA sequence used, which includes a spacer consisting of nine guanines, was 5'-H_2O_3PO-$(G)_9$-CCGCCGGTAACCGGAGGTTAAGATCGAGATCCA (**$PO_4G_9O_{33}$**). Reagents were of analytical grade and used as received from commercial sources, unless indicated otherwise.

Zirconium-Phosphonate Substrates

Hydrophobic glass slides were made using octadecyltrichlorosilane (OTS) following a method by Sagiv.[38] The glass slides were cleaned with piranha etch (3:1 H_2O_2:H_2SO_4, boiling 20

minutes) and followed by the RCA method (4:1:1 H_2O_2:NH_4OH:H_2O, boiling 20 minutes and then 5:1:1 H_2O_2:HCl:H_2O, boiling 20 minutes). Then they were made hydrophobic by treating with a 5mM solution of octadecyltrichlorosilane (OTS) in bicyclohexyl for 2 minutes, rinsing with toluene for 30 seconds, and then drying with N_2. The slides were treated again with the OTS, rinsed with toluene, and finally dried with N_2.[22]

A KSV 2000 LB double-barrier Teflon trough, supplied through KSV Instruments (Stratford, CT), was used to form the ODPA monolayers at the air-water interface. A filter-paper Wilhelmy balance attached to a KSV microbalance was used to measure surface pressure.

The zirconium-phosphonate films were made by first spreading a 0.3mg/mL solution of ODPA in chloroform on a 2.6 mM aqueous $CaCl_2$ subphase, which had a pH adjusted to 7.8 using a KOH solution. The ODPA was compressed at the rate of 10 mm/min to a pressure of 20 mN/mm. Once the target pressure was reached, a hydrophobic glass slide was dipped 50mm into the subphase at a rate of 8 mm/min. The slide was then lowered into a glass vial in the trough. The vial with the slide was removed from the trough and an amount of a zirconyl chloride ($ZrOCl_2$) solution was added to reach a concentration of 3 mM of Zr^{4+} in the vial with the slide. The slides sat for 7 days in the Zr^{4+} solution. If the slides were not used right away, they were stored in water until later use.

DNA Immobilization

To immobilize the oligonucleotides to the zirconium-phosphonate surface, first the appropriate amount of water was added to make a 100 μM solution and then the oligonucleotides were aliquoted into smaller one-time-use volumes. The aliquoted oligonucleotides were stored in a freezer at -20°C. The ssDNA were prepared in a 1 x SSC (saline sodium citrate) buffer, pH 6 at a concentration of 40 μM. The saline sodium citrate buffer solutions are prepared from a

stock solution of 20 x SSC, which corresponds to a 3.0 M NaCl and 0.30 M sodium citrate solution. Thus for a 1 x SSC solution, the concentrations are 0.15 M NaCl and 0.015 M sodium citrate, creating a solution which has an ionic strength of 0.225 M. To create a spot large enough for XPS analysis, 30 μL of the DNA was pipetted onto the rinsed and dried zirconium-phosphonate surface. Once the DNA had been spotted, the slides were incubated overnight in Petri dishes at room temperature. Then the slides were submerged for 1 hour in 3.5 x SSC, 0.3% SDS at 42°C, followed by rinsing 5 times with nanopure water and spin drying. The slides then underwent a mock hybridization, which should give the true probe concentration if they were to undergo hybridization, by treatment with 25μL per spot of 3 x SSC, 0.1% SDS overnight at 42°C. Finally, the slides were rinsed in 2 x SSC, 0.1% (2 min), 1 x SSC (2 min), and 0.2 x SSC (2 times, 2 min), followed by rinsing in water 5 times.

XPS was performed using a UHV XPS/ESCA PHI 5100 system. Survey scans and multiplex scans (Zr 3d, P 2p, and N 1s) were taken with a Mg Kα X-ray source using a power setting of 300 W and a take off angle of 45° with respect to the surface. Survey scans were taken for all samples with a pass energy of 89.4 eV and multiplex scans were taken with a pass energy of 22.36 eV. Using commercial XPS analysis software and Shirley background subtraction, the peak areas were determined. Four different spots were analyzed to determine the scatter of the data. The analyzer transmission function, which is necessary for the surface coverage calculations, was determined using a method by Weng.[39] To find the analyzer transmission function with this method, the XPS intensities of the C 1s, O 1s, Zr 3d, and Zr 3p3 peaks of a zirconium-phosphonate substrate were analyzed at nine different pass energies: 179.0, 143.0, 89.5, 71.5, 44.7, 35.7, 22.4, 18.0 and 11.2 eV.

Results and Discussion

The Zirconium-Phosphonate Surfaces

Zirconium-phosphonate surfaces can be made a number of ways, including adsorption of Zr^{4+} onto phosphorylated groups covalently attached to silica or gold, or also by adsorption of Zr^{4+} onto organicphosphonic acid monolayers prepared by Langmuir-Blodgett (LB) deposition.[40-43] We have found that zirconium monolayers made using the LB technique provide a reproducible, highly-active surface for the binding of phosphate and phosphonate containing molecules.[43] As shown in Figure 2-2, to prepare the zirconium-phosphonate monolayers using the LB technique, octadecylphosphonic acid (ODPA) is spread at the air-water interface, is compressed into a monolayer, and then transferred onto a hydrophobic substrate. The ODPA-coated substrate is then exposed to a solution of $ZrOCl_2$. The Zr^{4+} binds strongly to more than one phosphonate group creating a robust surface that is stable in water for months.

X-ray Photoelectron Spectroscopy

In a typical instrument setup for XPS, X-rays impinge a sample causing photoelectrons to be released from the core orbitals. The photoelectrons are then retarded to a certain kinetic energy called the pass energy and then they enter the analyzer and finally the detector. Retarding the electrons does not change the absolute energy spread, but does increase resolution. Differences in the pass energy and also the photoelectron kinetic energies can causes variations in the analyzer and detector efficiencies. An analyzer transmission function, T, can be used to correct these variations. In a paper by Weng et. al., several methods were laid out for determining the analyzer transmission function.[39] The most suitable method for our instrument was chosen. This involved using XPS peaks at different kinetic energies (E_k) taken with different pass energies. For this the C 1s, O 1s, Zr 3d, and Zr 3p3 peak intensities for a zirconium-phosphonate slide were obtained at nine different pass energies (E_a): 179.0, 143.0,

89.5, 71.5, 44.7, 35.7, 22.4, 18.0 and 11.2 eV. The intensity data, *I*, for a given kinetic energy was scaled with a multiplicative factor to take into account the different inherent sensitivities for the different photoelectrons of the elements. The data was then used to make a $\log(I/E_a)$ vs $\log(E_a/E_k)$ plot, shown in Figure 2-3. The following third order polynomial equation was used to describe the trend of the data:

$$\log(I/E_a) = 0.0222\log(E_a/E_k)^3 - 0.4708\log(E_a/E_k)^2 - 0.9387\log(E_a/E_k) + C \quad (2\text{-}1)$$

When Equation 2-1 is solved for the intensity, the analyzer transmission function is obtained:

$$T \propto (E_a)(E_a/E_k)^n \quad (2\text{-}2)$$

where

$$n = \left(-0.987 - 0.4708\log(E_a/E_k) + 0.0222\log(E_a/E_k)^2\right) \quad (2\text{-}3)$$

Using Equations 2-2 and 2-3; the kinetic energy of the Zr 3d photoelectron, 1067 eV; and the pass energy of 22.36 eV, the analyzer transmission function for Zr was found to be 31.2 eV. Similarly with the kinetic energy of the N1s photoelectron, 851.6 eV, and again an analyzer energy of 22.36 eV, the analyzer transmission function for the N 1s photoelectron was found to be 37.1 eV. The analyzer transmission function for Zr and N are used in the calculations for the surface density of the DNA, as shown later.

Substrate-Overlayer Model

XPS is often used to determine the thickness and surface coverage of thin films by quantifying the attenuation of the substrate photoelectrons as they pass through the thin film on their way to the analyzer. This technique, called the substrate-overlayer model (shown in Figure 2-4 A), has been used several times to quantify the surface coverage of DNA on a substrate.[25, 26] The calculation generally uses the intensity of an infinitely thick substrate and a finitely thick overlayer. The intensity of an elemental peak coming from the substrate, I_s, can be written as

$$I_S = FN_S\sigma_S T_S L_S \sin\theta \exp\left(-t/\left(L_S^{eff}\sin\theta\right)\right) \qquad (2\text{-}4)$$

or

$$I_S = I_S^{\infty} \exp\left(-t/\left(L_S^{eff}\sin\theta\right)\right) \qquad (2\text{-}5)$$

where F is the X-ray photon flux; N_S is the atomic density of the element; σ_S is the effective cross section of the photoelectron for the specific energy level of the element; T_S is the analyzer transmission function of the spectrometer for the given kinetic energy; L_S is the effective attenuation length (EAL) of the substrate photoelectron as it travels through the substrate; t is the overlayer film thickness; L_s^{eff} is the EAL of the substrate photoelectron as it travels through the overlayer; θ is the angle of the photoelectron detection with respect to the sample surface; and I_S^{∞} is the intensity of the bare substrate. Scofield coefficients are usually used for the cross section of the photoelectron.[44] Equation 2-4 can be simplified to Equation 2-5, and if the intensity of the bare substrate, I_S^{∞}, is known or measured, the thickness of the overlayer can be determined.

Similarly, the intensity of a peak coming from an element in the overlayer, I_X, can be written as

$$I_X = FN_X\sigma_X T_X L_X \sin\theta\left(1-\exp\left(-t/\left(L_X^{eff}\sin\theta\right)\right)\right) \qquad (2\text{-}6)$$

where, N_X, σ_X, T_X, L_X, and L_X^{eff} signify the same parameters as in Equation 2-4 except with respect to an element from the overlayer. Equations 2-4 and 2-5 can be combined, cancelling some of the instrumental parameters, to give the atomic density ratios of an element from the substrate and from the overlayer:

$$\frac{N_X}{N_S} = \frac{I_X\sigma_S T_S L_S \exp\left(-t/\left(L_S^{eff}\sin\theta\right)\right)}{I_S\sigma_X T_X L_X\left(1-\exp\left(-t/\left(L_X^{eff}\sin\theta\right)\right)\right)}. \qquad (2\text{-}7)$$

As shown by Petrovykh *et al.*,[12] Equation 2-7 can be modified using the relationship of the atomic density, N_X, to the atomic surface coverage, n_X, and the overlayer thickness:

$$N_X = n_X t \,. \qquad (2\text{-}8)$$

When this is combined with Equation 2-7, the ratio of overlayer surface coverage to substrate density is obtained:

$$\frac{n_X}{N_S} = \frac{I_X \sigma_S T_S L_S t \exp\left(-t/\left(L_S^{eff} \sin\theta\right)\right)}{I_S \sigma_X T_X L_X \left(1-\exp\left(-t/\left(L_X^{eff} \sin\theta\right)\right)\right)}. \qquad (2\text{-}9)$$

In the quantitative determination of DNA on a substrate such as gold, *X* could be the N 1s peak, or P 2p, but probably not C 1s or O 1s due to possible contaminants on the surface also containing these elements. While *S* can be any element from the substrate, it is best to use a peak specific to the substrate. Using the known atomic density of the chosen substrate element and the number of nitrogens in the DNA strand, the surface coverage of the DNA can be calculated.

Model for the Zirconium-Phosphonate Surface

Our system, as shown in Figure 2-4B, requires a slightly different approach due to the fact that we use the zirconium-phosphonate layer as our modifying substrate. We choose to use the Zr 3d peak as the substrate signal instead of the silicon XPS peaks, because these are strongly attenuated by the zirconium-phosphonate modifying layer. The zirconium coverage corresponds to a monolayer and is therefore assumed not to attenuate itself.[43] Thus the intensity of the Zr 3d peak attenuated by the DNA overlayer can be written as

$$I_{Zr} = F n_{Zr} \sigma_{Zr} T_{Zr} \sin\theta \exp\left(-t/\left(L_{Zr}^{eff} \sin\theta\right)\right) \qquad (2\text{-}10)$$

Equation 2-10 can then be used with Equations 2-7 and 2-8 to give

$$\frac{n_N}{n_{Zr}} = \frac{I_N \sigma_{Zr} T_{Zr} t \exp\left(-t/\left(L_{Zr}^{eff} \sin\theta\right)\right)}{I_{Zr} \sigma_N T_N L_N \left(1-\exp\left(-t/\left(L_N^{eff} \sin\theta\right)\right)\right)} \qquad (2\text{-}11)$$

Using the number of nitrogens in the DNA sequence and the known surface coverage of zirconium, the DNA coverage can be calculated. The surface coverage of zirconium, 4.2×10^{14} atoms/cm^2, was previously determined from the 24 Å^2 cross sectional area of the zirconium-phosphonate sites in the LB monolayer.[43]

To calculate the EALs needed for Equation 2-11, the NIST SRD-82 software was used.[28] This program requires the input of several parameters including the kinetic energy of the photoelectrons, the stoichiometry of the DNA, the band-gap energy of the DNA,[45] the film density of DNA,[46] and the instrumental geometry. The software[28] "average practical EAL" output number was used for L_N^{eff} and L_{Zr}^{eff} and the output number of the "EAL for quantitative analysis" was used for L_N. The EAL values were calculated as 25.5, 31, and 27 Å, for L_N^{eff}, L_{Zr}^{eff}, and L_N, respectively.

After spotting the probe on the zirconium-phosphonate modified slides and performing the washing procedures, survey scans and multiplex scans of the Zr 3d binding energy (BE) peak region (194 – 180 eV), P 2p3 peak region (143 – 131 eV) and N 1s (143 – 131 eV) were obtained on the DNA spot areas. The average peak areas after Shirley baseline subtraction are shown in Table 1. Nitrogen, which is more sensitive in XPS analysis than phosphorus and also more abundant in DNA than phosphorus, is a good choice as the element from the DNA overlayer. Furthermore, phosphorus is present in the zirconium-phosphonate films and would complicate the calculations if it were used. For these reasons, the N 1s and Zr 3d peak areas were used in Equation 2-11 to calculate the nitrogen to zirconium surface coverage ratio. This ratio was then used with the number of nitrogens per DNA strand and the known surface coverage of zirconium to calculate the surface coverage of the probe.

The average of the measured peak intensities are given in Table 1. With these intensities and Equation 2-11, the probe surface density can be calculated. In Equation 2-11, the Scofield coefficients for N 1s, σ_N, is 1.77 and for Zr 3d, σ_Z, is 7.3. As explained previously, Equation 2-5 can be used to calculate the thickness. To perform this calculation, the intensity of the Zr 3d peak from a bare zirconium-phosphonate substrate is needed, which was found to be 11800. Finally, using the average N 1s peak intensity of 691 and Zr 3d peak intensity, 11618, coming from the substrate with DNA, the following calculation can be performed:

$$\frac{n_N}{n_{Zr}} = \frac{691 \times 7.3 \times 31.2\,\text{eV} \times 0.25\text{Å} \times \exp\left(-0.25\text{Å}/\left(31.1\text{Å} \times \sin 45\right)\right)}{11618 \times 1.77 \times 37.1\,\text{eV} \times 27\text{Å}\left(1 - \exp\left(-0.25\text{Å}/\left(25.5\text{Å}\sin 45\right)\right)\right)}$$

$$\frac{n_N}{n_{Zr}} = 0.0875$$

$$\text{DNA surface coverage} = 0.0875 \times \frac{4.2 \times 10^{14}\,\text{Zr atoms cm}^{-1}}{177\ \text{N atoms per DNA molecule}}$$

$$\text{DNA surface coverage} = 2.4 \times 10^{11}$$

The measured peak intensities and corresponding surface coverage are given in Table 1. The calculated coverage from these measurements of ssDNA on the surface is 2.8×10^{11} DNA molecules/cm^2. This surface coverage is lower than what other researchers have measured for DNA immobilized on gold. For example, the average maximum ssDNA coverage found by Georgiadis *et al.* on gold was 12×10^{12} molecules/cm^2 and Petrovykh *et al.* found a maximum coverage on gold using XPS as 37×10^{12} molecules/cm^2.[8, 12] Despite some differences in immobilization procedures, such as the salt concentration in the probe buffer solution,[47] there seem to be other factors, inherent to the zirconium-phosphonate surface, affecting the probe surface coverage. On the other hand, others have reported similar coverages. Zammatteo *et al.* studied the immobilization of DNA through a number of covalent coupling reactings including

the immobilization of amine-modified DNA on an aldehyde surface.[48] They used scintillation counting of ^{32}P-labeled ssDNA strands and found a maximum surface coverage of 3.6×10^{11} DNA molecules/cm^2. They were, however, using much longer strands, 250 bp, compared to our 42 bp, which might cause them to have lower surface coverages.

From fluorescence microarray studies comparing hybridization using nonphosphorylated and phosphorylated probes, it is seen that the phosphodiester backbone of the oligonucleotides does not covalently bind to the zirconium surface for permanent immobilization.[32] Nevertheless, once the oligonucleotides are covalently bound through the 5' phosphate, the phosphodiester backbone can physisorb to the surface causing the oligonucleotide to lie down on the surface, kinetically hindering further attachment of oligonucleotides. This observation is consistent with film thickness measurements that show far less then complete monolayer coverage. Therefore, although other molecular systems such as alkylphosphonate molecules self-assemble into close-packed monolayers on the zirconium-phosphonate surface, the phosphorylated DNA does not.

Although the measured DNA coverage appears low, these conditions have been shown to be useful for array applications. The XPS quantification of the DNA surface coverage gives a reasonable answer. There are, however, several possible sources of random and systematic error in these experiments. The sources of random error include slight differences in the preparation of the sample and also error coming from the instrument, such as changes in the X-ray flux and slight differences in the placement of the sample in the XPS chamber. The random error can be seen in the standard deviation of the surface coverage, which is around 20%. This error can perhaps be improved by improving the consistency of the rinsing steps.

The systematic error can come from a number of factors, including the surface coverage of zirconium ions and the choice of EALs. The intensity of the bare zirconium peak is taken from

an XPS of a rinsed unmodified zirconium-phosphonate surface. The zirconium-modified surface most likely has a monolayer of oxides and hydroxides on the surface, which would be displaced by the DNA. The oxides and hydroxides could attenuate the zirconium peak, thus the measured peak area of the Zr 3d peak would be systematically lower than the true value of the bare substrate. If this were true, it would give rise to a systematically lower DNA film thickness than the true value. Because in Equation 2-11, the EALs and overlayer thickness are always taken as a ratio to each other, the equation is not very sensitive to the value of the film thickness or EALs, and would only affect the surface coverage slightly.

Conclusions

The surface coverage of ssDNA on a zirconium phosphonate monolayer was calculated from XPS N 1s and Zr 3d peak intensities. The surface coverage of ssDNA is lower than reported values for thiol-modified DNA on gold. The DNA immobilization conditions were those optimized using fluorescence imaging and that indicated maximum DNA adsorption. Based on these findings, it indicates that, although the phosphodiester backbone cannot hold the DNA on the zirconium throughout the rinsings, an interaction between the zirconium surface and the backbone may cause the DNA to lay down on the surface, thus limiting the covalent binding of more DNA during spotting.

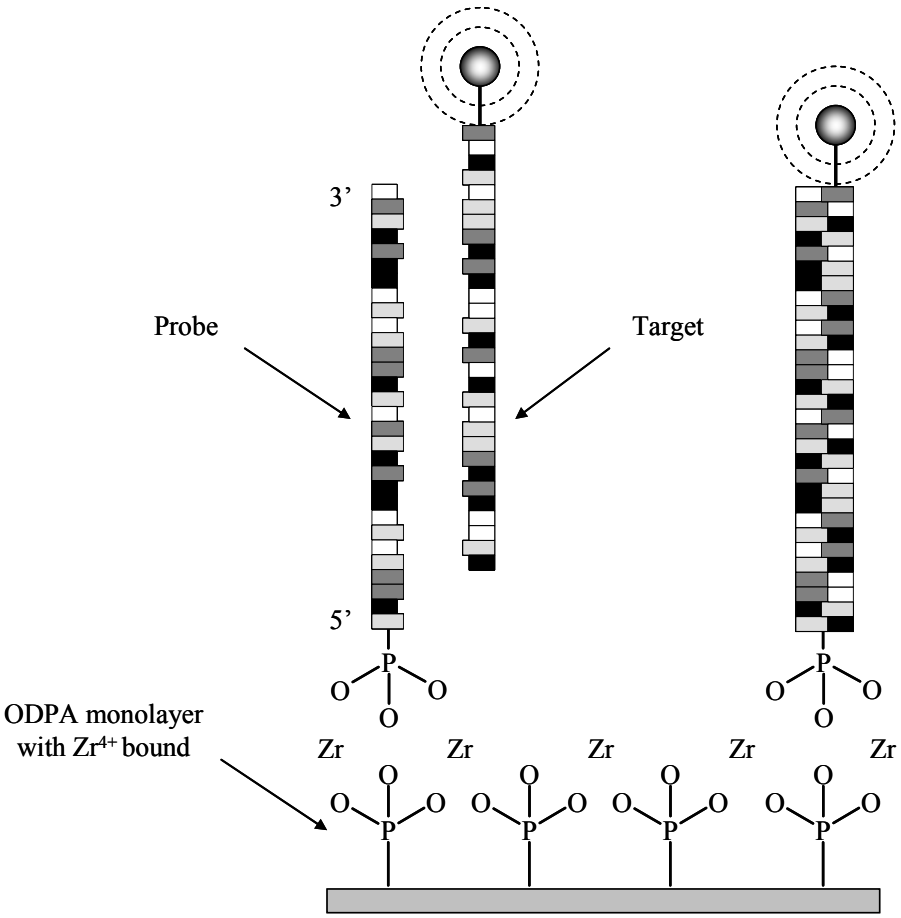

Figure 2-1. Illustration of the immobilization of the phosphorylated ssDNA and subsequent hybridization.

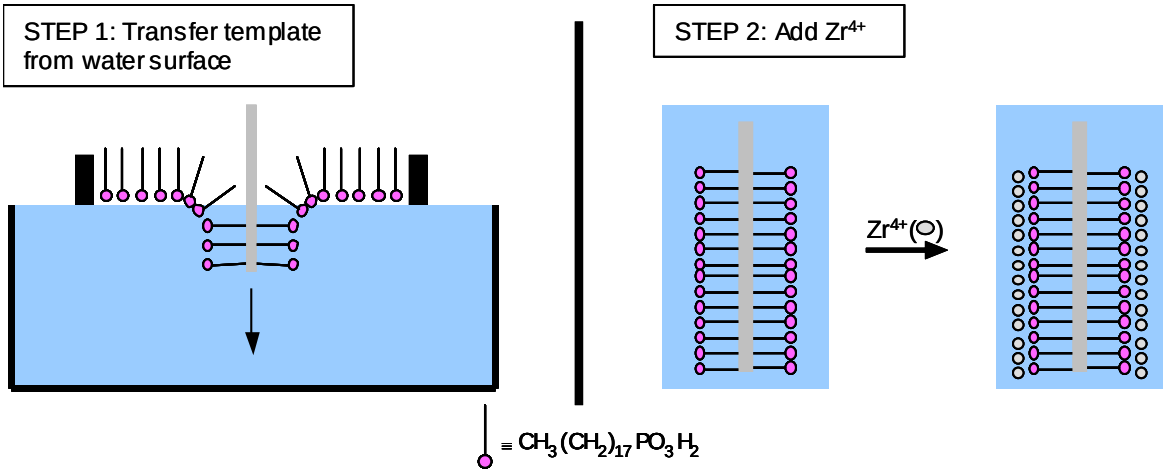

Figure 2-2. Procedure for making the zirconium-phosphonate monolayers. First the ODPA is spread at the air-water interface and then transferred onto a hydrophobic support. This followed by the addition of zirconyl chloride which forms a network with the phosphonate headgroups.

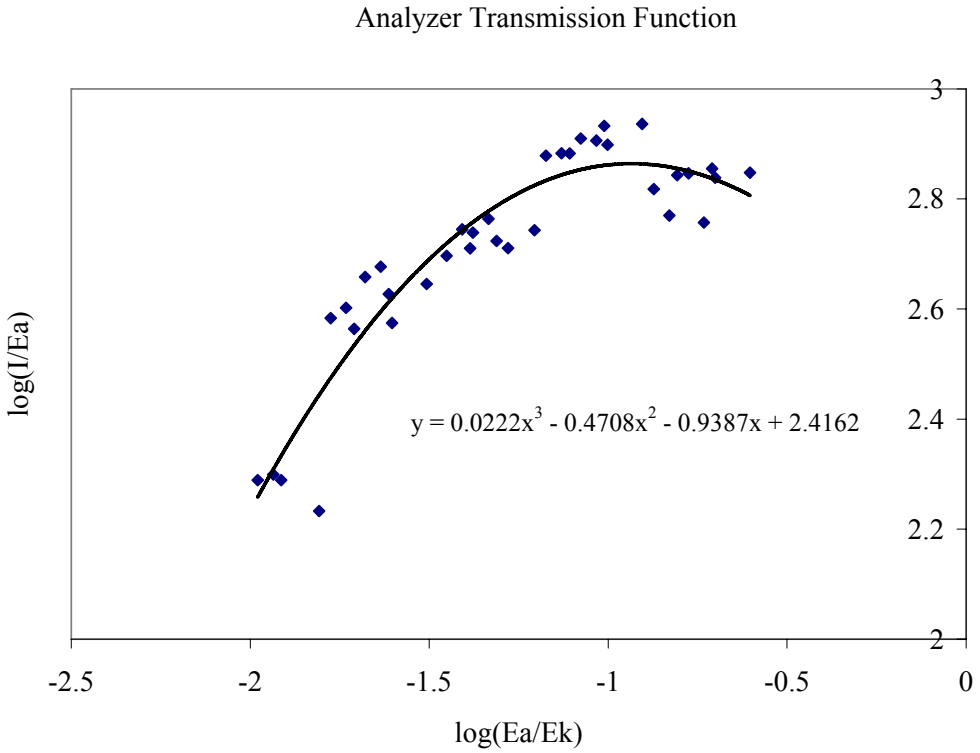

Figure 2-3. Graph of the analyzer transmission function. E_a is the analyzer energy (pass energy) and E_k is the kinetic energy of the photoelectron. The diamonds are the scaled data points.

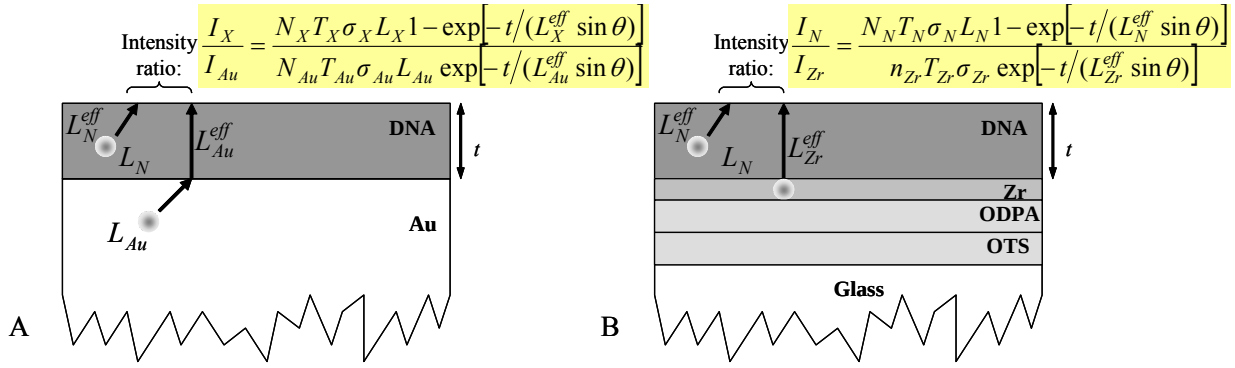

Figure 2-4. Parameters that are used to calculate the DNA surface coverage. A) The parameters for the gold-DNA system. B) The parameters for the zirconium-phosphonate-DNA system.

Table 2-1. Intensities of the N 1s and Zr 3d peaks for a zirconium surface with and without DNA. The table also includes the surface coverage of DNA that was calculated with the peak intensities.

	N 1s Area	Zr 3d Area	DNA Surface Coverage (ssDNA/cm^2)
With ssDNA	691	11618	$2.8 \times 10^{11} \pm 0.5 \times 10^{11}$
Without ssDNA	-	11800	-

CHAPTER 3
SPACER AND RINSING EFFECTS ON SSDNA SURFACE COVERAGE

Introduction

One of the many parameters changed to improve the performance of DNA microarrays is the use of a spacer between the probe sequence and the surface-linking group.[32, 37, 49, 50] The spacer, which creates distance between the linking group and the probe sequence, is used with many different DNA microarray platforms. It is thought to lift the probe off the surface to bring it more in contact with the solution phase. With our zirconium-phosphonate surface, we have shown that when a stretch of at least 5 guanines are used as the spacer, compared to the other nucleotides, increased hybridization is seen.[32] Beyond 7 guanines there is no further increase in hybridization. We call this increase in hybridization when using the poly-guanine spacer the "poly-dG effect."

This chapter discusses the surface coverage measurements made with XPS of a probe sequence with either a poly-guanine or poly-adenine spacer. This data allows us to determine if the poly-dG effect is due to a difference in the surface coverage or an increase in hybridization efficiency. Also in this chapter are details on rinsing experiments which give insight into non-specific binding of these two sequences.

Experimental

Zirconium-phosphonate substrates were prepared as stated in the experimental section of Chapter 1 of this dissertation. The general ssDNA sequence used was 5'-H_2O_3PO-$(X)_{9,12}$-CCGCCGGTAACCGGAGGTTAAGATCGAGATCCA. In the sequence, X represents either guanine or adenine, which was either 11 or 9 nucleotides long. The ssDNA were prepared in a 1 x SSC (saline sodium citrate) buffer, pH 6 at a concentration of 40 μM. To create a spot large enough for XPS analysis, 30 μL of the DNA was pipetted onto the rinsed and dried zirconium-

phosphonate surface. Once the DNA had been spotted, the slides were incubated overnight in Petri dishes at room temperature. Several different rinsing conditions were explored before XPS was taken. In one set, which we are calling Rinsing 1, the slide was submerged successively in 2 x SSC, 0.1% SDS (sodium dodecylsulfate) (2 min), 1 x SSC (2 min), and 0.2 x SSC (2 times, 2 min), followed by dipping twice in water. Rinsing 1 experiments were done with a spacer 11 nucleotides long. Another set of rinsing conditions, Rinsing 2, began with the spotted slide being immersed for 1 hour in 3.5 x SSC, 0.3% SDS at 42°C, followed by rinsing 5 times with nanopure water and spin drying. A final set of rinsing conditions was explored, Rinsing 3, which used the 1 hour submersion in 3.5 x SSC, 0.3% SDS at 42°C, followed by rinsing 5 times with nanopure water and spin drying. These slides then underwent a mock hybridization, which should give the true probe concentration if they were to undergo hybridization, by treatment with 25μL per spot of 3 x SSC, 0.1% SDS overnight at 42°C. Finally, the slides were rinsed in 2 x SSC, 0.1% (2 min), 1 x SSC (2 min), and 0.2 x SSC (2 times, 2 min), followed by rinsing in water 5 times. At least four spots were examined at each different rinsing condition.

Streaming surface potential measurements were performed using an asymmetric clamping cell on a Paar Physica Kinetic Analyzer. An excellent description of this system is given by Walker *et al*.[51] A 1 mM KCl solution with a pH of 6 was used as the electrolyte solution. A zirconium phosphonate slide was carefully clamped (the film can be easily disturbed during this process) onto the cell and 16 measurements were performed per slide.

Results and Discussion

There are a several different types of surfaces employed for DNA microarrays that use ex-situ prepared DNA. These surfaces can use the non-specific interactions between the DNA and the surface, such as in the case of the negatively-charged DNA phosphodiester backbone binding

to the positively charged amine-coated surface.[30] On the other hand, the surface can use a specific interaction between a linker on the DNA and the surface; for example, a thiol-modified DNA molecule binding to a gold surface.[17] With each different surface, there are different protocols for immobilization, rinsing, and hybridization, the conditions of which are usually suggested by the manufacturer. The different surfaces using specific interactions require different linkers. We use a zirconium-phosphonate surface, which uses a coordinate covalent bond between a 5'-phosphorylated DNA and the zirconium-phosphonate surface to immobilize the DNA. The two parameters explored here, the spacer identity and the rinsing conditions, both make a considerable difference in the amount of DNA on the surface. The two seemingly discrete parameters are discussed together in the same chapter because one affects the other.

The use of a spacer on the probe DNA began around the same time as the advent of the DNA microarray.[52] The spacer is a moiety added between the linker and probe sequence, which is found to give increased hybridization. It is believed that the spacer lifts the probe sequence off the surface so that it has more contact with the solution phase. There are a number of different spacers used depending on the type of surface. For DNA microarrays on gold, a simple alkyl chain, often 6-carbons long, is frequently used.[8] On the other hand, a stretch of different nucleotides can also be used. Guo *et al*. studied the immobilization and hybridization of 5'-amine-functionalized probes on an isocyanate-functionalized surface.[52] They used poly-dT spacers of 0, 3, 6, 9, 12, or 15 nucleotides long. When no spacer was used, they observed no hybridization, but starting with 9 nucleotides an increase in hybridization was seen, which continued up to 15 nucleotides. However, they did not study spacers longer than 15 nucleotides. On the other hand, Shchepinov *et al.* built spacers from a number of different monomers using phosphoramidite chemistry, by condensation onto an amine-functionalized polypropylene

support.[37] They found that using a spacer of about 40 atoms gave a 150-fold increase in the hybridization.

For our surface, fluorescence imaging was used to study hybridization when a stretch of adenine, guanine, thymine, or cytosine was added as spacers between the 5' phosphate linker and the probe sequence.[32] It was observed that the use of a poly-dG spacer over any other nucleotide or no spacer gave increased hybridization, as shown in Figure 3-1. This demonstrated the ability of a poly-dG spacer to give increased hybridization. The length of the spacer was also investigated, and it was found that beyond 7 guanines, no further significant increase in hybridization was seen. It remained unknown whether the poly-dG spacer caused an increase of probe on the surface or an increase in hybridization efficiency. However, it was suspected that this was related to the ability of oligomers of guanines to form quadruplex structures as shown in Figure 3-2, which is seen in the DNA of telomeres.[53, 54] In this structure, which is seen in the DNA of telomeres, the guanine bases form a hydrogen bonding scheme, as seen in Figure 3-3, where N(1) and N(2) act as hydrogen donors to O(6) and N(7). To determine if the poly-dG effect was caused by an increase in probe density, probes with either a poly-dG or poly-dA were studied with XPS.

The other parameter investigated here, rinsing, is a critical step in the DNA microarray process. After the DNA is spotted onto a surface, the surface is generally rinsed before hybridization. The rinsing solutions often contain a buffer, such as SSC, and a detergent such as SDS. A rinsing solution that contains less salt and more surfactant is considered more stringent. The slide may be heated or not during the rinsing process. There are only a few papers that investigate the importance of rinsing.[55, 56] One paper demonstrated that automated rinsing compared to manual decreases variability across microarray slides.[55] Another study showed that

more stringent washing conditions improved signal to background ratios; however they concluded that the hybridization step played a greater role in improving signal to background ratios.[56] A passivation step can also be used in between the rinsing and hybridization. This employs a molecule, such as bovine serum albumin (BSA), which binds to the surface where there is no probe. The BSA prevents the target molecule from physisorbing to the surface, ultimately improving the signal to noise. After a rinsing step, the passivation step and the hybridization can rinse off more probe. The experiments discussed in this chapter attempt to take into account the rinsing from passivation and hybridization.

Three different rinsings were investigated in this study. Rinsing 1, involves successively dipping the slide in 2 x SSC, 0.1% SDS (2 min), 1 x SSC (2 min), and 0.2 x SSC (2 times, 2 min), successively, followed by dipping twice in water. In Rinsing 2, which is actually a modified passivation step, the slide is submerged in a 3.5 x SSC, 0.3 % SDS solution at 42°C for 1 hour. Normally, this solution would contain BSA, but it was found that the BSA physisorbed onto the surface, causing nitrogen contamination. This contamination would hinder efforts to determine the DNA coverage based on the nitrogen signal in XPS. Rinsing 2 is more stringent than Rinsing 1 because of the increased surfactant concentration, the heating and the increased time the slide stays in the solution. Also the increased number of water rinsings at the end of Rinsing 2 raises the stringency. In Rinsing 3, again the slide is submerged in a 3.5 x SSC, 0.3% SDS 42°C for 1 hour, then the spot area is subjected to a step which is supposed to mimic a hybridization step. In this blank hybridization step, the spot area is treated with 25μL of 3 x SSC, 0.1% SDS overnight at 42°C. Often the hybridization solution contains formamide and other additives which are supposed to reduce non-specific interactions, but these molecules contain nitrogen and again it was found that they physisorbed onto the surface contributing to

nitrogen contamination. Due to the increased length of the rinsings and heating, Rinsing 3 should be more stringent than Rinsing 1 and 2.

To investigate how these two different parameters, rinsing and spacer identity, affected the surface coverage, XPS was taken after each of the different rinsing conditions while using a 5'-phosphorylated probe molecule containing a poly-dA spacer and one containing a poly-dG spacer. To improve the statistics of the data, at least 4 different spots were analyzed for each different condition. The N 1s and Zr 3d peaks were used to calculate the surface coverage using the model shown in Chapter 2.

A comparison of the average surface coverages of the poly-dA containing probe and poly-dG containing probe is shown in Figure 3-4. As the graph demonstrates, while the surface coverage of the poly-dG containing probe stayed relatively constant with the different rinsing procedures, the surface coverage of the probe containing the poly-dA spacer decreased with increasing rinsing stringency. With the less stringent SSC rinsing conditions (Rinsing 1) the calculated surface coverage of the poly-dA, $6.5 \times 10^{11} \pm 6.2 \times 10^{10}$ ssDNA molecules/cm^2, is twice that of the poly-dG containing probe, $3.2 \times 10^{11} \pm 3.5 \times 10^{10}$ ssDNA molecules/cm^2. After Rinsing 2, the surface coverages are almost equal, with the surface coverage of the poly-dA containing probe at $2.6 \times 10^{11} \pm 4.8 \times 10^{10}$ ssDNA molecules/cm^2 and that of the poly-dG containing probe at $2.6 \times 10^{11} \pm 5.9 \times 10^{10}$ ssDNA molecules/cm^2. Finally after rinsing with Rinsing 3, the surface of coverage of the poly-dG containing probe, $2.8 \times 10^{11} \pm 5.1 \times 10^{10}$ ssDNA molecules/cm^2, is twice that of the surface coverage of the poly-dA containing probe, $1.4 \times 10^{11} \pm 3.4 \times 10^{10}$ ssDNA molecules/cm^2. The error shown with the surface coverages is the standard deviation of the mean.

The final probe coverage after Rinsing 3, shows that the poly-dG containing probe has a higher surface coverage than the poly-dA containing probe after the mock hybridization. From this we can conclude that the reason an increase in hybridization is seen when a poly-dG spacer is used is due to a higher probe surface density. Although this is the first report of a poly-dG spacer giving increased probe surface density, Saprigin did an XPS study of 3'-phosphorylated homo-oligonucleotides which were reacted to a carbodiimide to form an *O*-phosphoryl isourea intermediate that reacts with surface-bound amine to produce a phosphoramidate linkage.[25] They found that homopolymers of guanines gave a higher surface coverage than the other oligonucleotides. They surmised that this behavior was due to the formation of non-Watson Crick base-pairing. How these quadruplexes of DNA might increase the probe surface density is not yet known. The poly-dG quadruplex most likely forms in solution, before the probes are spotted onto the surface. This more rigid structure likely takes up less space on the surface. The quadruplex may require the poly-dG quadruplex to stand erect on the surface, preventing some non-specific binding of the ssDNA. Another possibility is that the quadraplex requires the DNA to be more closely packed. A third possibility is that the quadraplex, with its four phosphate groups fairly close to each other, may have increased avidity towards the zirconium surface.

The fact that the poly-dA sequence starts at a higher surface coverage after Rinsing 1, but rinses off the surface with more stringent rinsing conditions, while the poly-dG sequence remains fairly constant, indicates that the sequence with the poly-dA exhibits stronger non-specific binding onto the surface than the sequence containing the poly-dG. It is assumed that the bond between the 5'-phosphate on the DNA and the zirconium surface is stable under the rinsing conditions. The conclusion that poly-dA exhibits stronger non-specific binding is supported by studies that looked at the specific and non-specific binding of homo-oligomers of

oligonucleotides. One study done by Wolf *et al.* compared the binding of thiolated and non-thiolated 25-mers of homo-oligomers on gold.[57] They did not look at poly-dG because they said the non-Watson Crick base-pairing makes synthesis of long homo-oligomers of guanines inefficient. They found that on gold there was considerable non-specific binding, which was sequence dependent. They found that non-thiolated poly-dA exhibited more non-specific binding than non-thiolated poly-dC and poly-dT. When they studied the binding of thiolated poly-dA,-dT, and -dC, they found that the strands with the most non-specific binding (poly-dA) bound at a slower rate. The non-specific binding slowed down the binding kinetics of the thiolated poly-dA and that during rinsing, more of the poly-dA rinsed off. These studies help support the belief that the poly-dA exhibits higher non-specific binding, limiting the specific binding and thus perhaps limiting the final surface coverage after all the rinsing steps.

Wolf *et al.* did not attempt to explain why the different bases had different non-specific binding. Why the poly-dA would give rise to more non-specific than poly-dG binding is not apparent in the structure of the base (Figure 3-5). It was thought that the charge of the zirconium-phosphonate surface may help to explain this behavior. Streaming surface potential – also known as zeta (ζ) potential – measurements were performed on the zirconium-phosphonate surface. The surface potential is the charge that develops at the interface between a solid surface and liquid medium. Two zirconium-phosphonate films were analyzed giving an average surface potential of +19.22 mV. Apparently, the oxides and hydroxides, which are assumed to cap the zirconium surface, do not completely mask the positive charge of the zirconium. What this could mean is that some of the non-specific binding is coming from the negatively charged phosphodiester backbone sticking to the somewhat positively charged surface. On the other hand, at pH 6 gold is reported to have a negative surface potential of approximately -20 mV.[58]

This indicates the reason that poly-dA appears to physisorb strongly both on gold and zirconium-phosphonate is not due to similar surface potentials. The final reason for the apparent physisorption of poly-dA is unclear.

This data indicates that there may be two different reasons why the poly-dG probe after sufficient rinsings has a higher surface density. One, is likely the formation of non-Watson Crick base pairs in solution, resulting in the quadruplex structure. The other is increased non-specific binding of poly-dA's increased non-specific binding which can limit the specific binding. While this non-specific binding is not capable of holding the oligonucleotide on the surface during the rinsings it is most likely interfering with the specific binding of the phosphate linker with the surface.

Conclusion

From the XPS quantitation, it is seen that after rinsings, the surface coverage of the probe with the poly-dA spacer decreases with each rinsing step, while that of poly-dG remains constant. The final surface coverage of the probe with the poly-dG spacer after a mock hybridization is about twice that of the probe with the poly-dA spacer. From this data it is concluded there could be two factors contributing to the higher surface coverage for the poly-dG containing probe. The first one is the formation of a quadruplex between the guanine bases. However, it is not completely clear how this structure leads to higher surface coverage. The second is non-specific binding of the poly-dA sequence with the surface limiting the specific binding. Finally, these results show that the poly-dG spacer leads to a higher probe surface coverage which is most likely the cause of the increased hybridization.

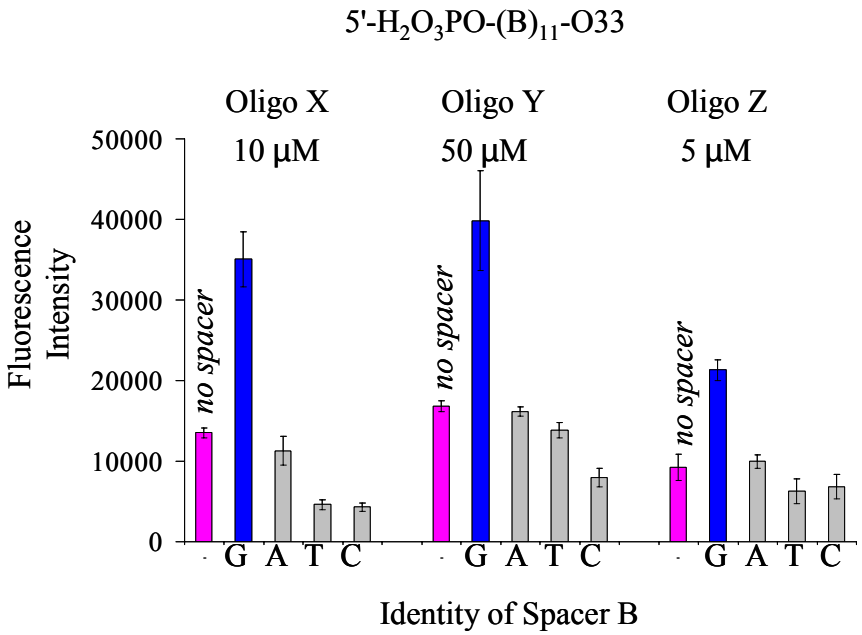

Figure 3-1. Fluorescence intensity after hybridization comparing the four different spacers on three different probe sequences.

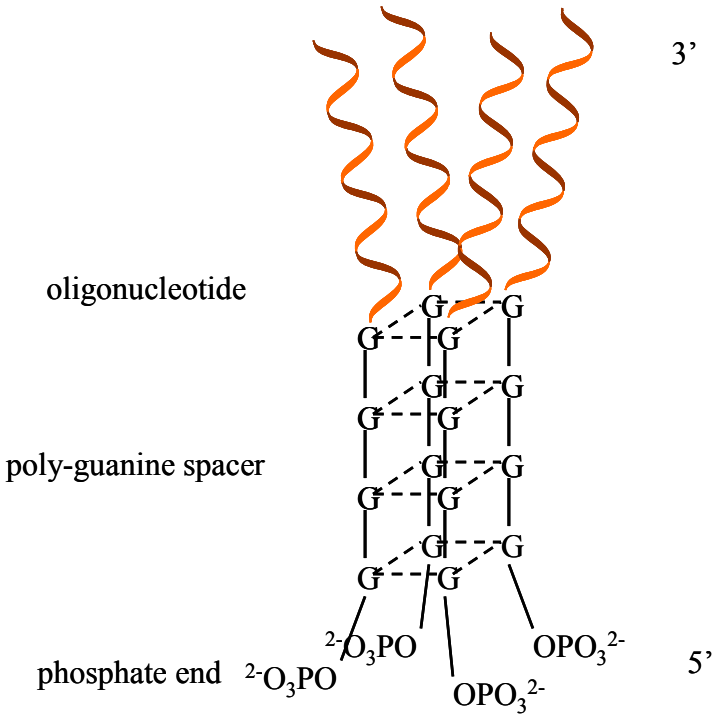

Figure 3-2. Illustration of how the poly-dG quadruplex might hold together the probe DNA.

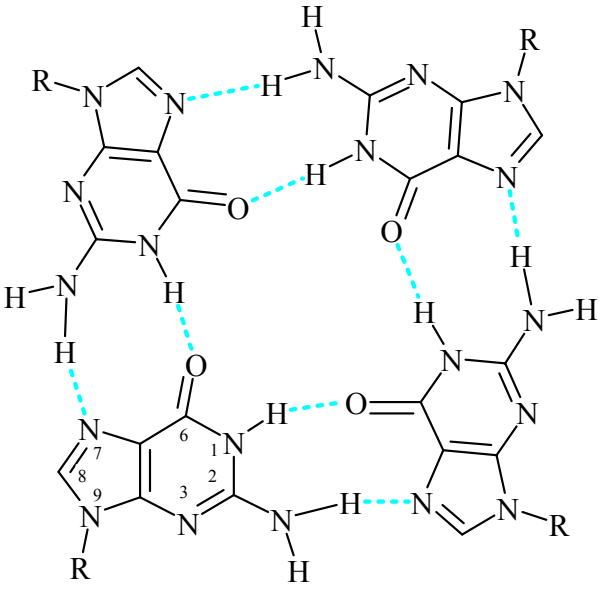

Figure 3-3. Poly-dG quadruplex. Illustrates the hydrogen bonding between the bases of guanosine.

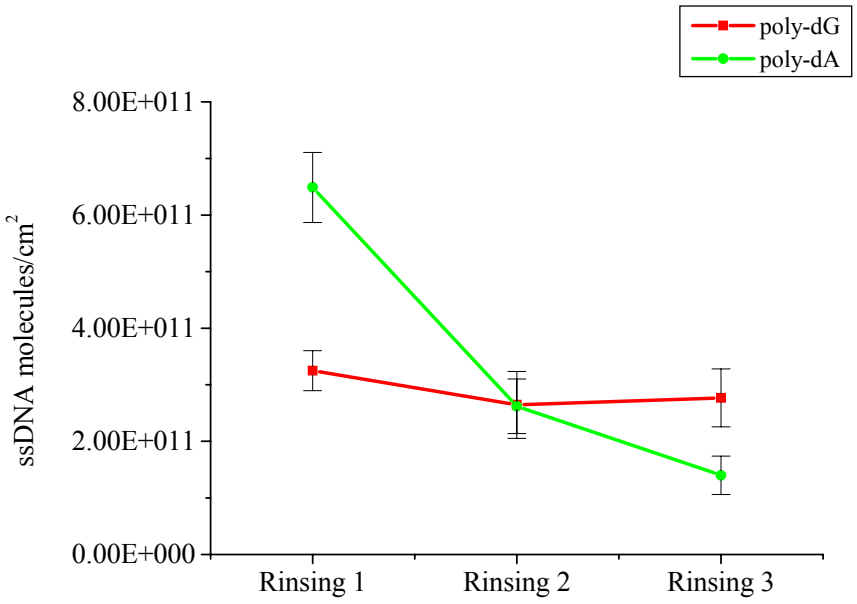

Figure 3-4. Surface coverage of probe after each different rinsing condition.

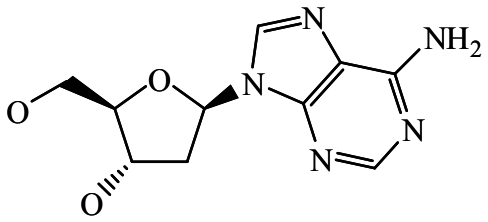

Deoxyadenosine

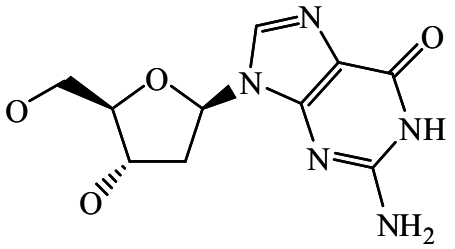

Deoxyguanosine

Figure 3-5. The bases and sugar deoxyadenosine and deoxyguanosine. From these structures, it is not apparent why a poly-dA strand would physisorb more strongly to the zirconium-phosphonate surface.

CHAPTER 4
EFFECT OF PHOSPHATE LINKER PLACEMENT ON THE BINDING OF DOUBLE-STRANDED DNA TO ZIRCONIUM-PHOSPHONATE SURFACES

Introduction

Soon after the advent of the ssDNA microarray, came the dsDNA array.[59-66] The main use of the dsDNA microarray is to follow the interactions of DNA and proteins, like transcription factors.[63] Transcription factor proteins, like the name suggests, regulate transcription by regulating the binding of RNA polymerase. They are generally modular proteins that bind to dsDNA at a specific region called the promoter sequence, or they can also bind to other transcription factor proteins. By doing this, they can initiate or inhibit transcription. Their influential role in the translation of the genetic code makes them an important area of research. The more commonly used methods of studying transcription factors and determining the promoter sequence includes gel shift analysis,[67] DNA footprinting,[68] and fluorescence polarization.[69] While these methods are reliable, they are not convenient for multiplexed studies of DNA-protein interactions, which is why dsDNA microarrays are becoming a valuable analytical technique.

Just as for ssDNA arrays, there are a number of different proposed methods for making dsDNA arrays. The dsDNA array was first reported by Bulyk *et al.*, who used primer extension of an ssDNA array, which had been made using a combination of photolithography and solid-phase chemistry.[63] The ssDNA array contained, between the linker and the variable sequence, a sequence constant across the area which was complementary to the primer they used. They could then use a polymerase to synthesize the complement to the ssDNA on the surface, creating the dsDNA probe. With a fluorescent tag on the dsDNA, digestion of the DNA by a restriction enzyme could be followed using fluorescence imaging. Another method to create a dsDNA array, which was demonstrated by O'Brien *et al.*, used the self-assembly of 5',3' disulfide-

modified dsDNA onto bare gold spots made through photolithography.[64] In this study, after the dsDNA was attached to the surface, they included a further step to remove some of the immobilized dsDNA by exposing the surface to an alkane thiol They stated that decreasing the density of the duplex was a key factor in increasing the enzyme accessibility. With AFM, they looked at the change in height of the spots after cleavage with a restriction enzyme. Smith *et al.* also used a gold surface but with a slightly more complex immobilization procedure, ultimately immobilizing thiol-modified ssDNA to maleimide groups on the surface and then hybridizing with the complement to get the dsDNA.[66] Using SPR imaging, they then studied the interactions of different dsDNA sequences with two transcription factor proteins and the behavior of these proteins in the presence of an inhibitor. Yet another example of an immobilization procedure on gold, given by Shumaker-Parry *et al.*, first uses a step self-assembling thiol-modified oligo ethyleneglycol and biotin onto gold.[65] They then either spotted streptavidin on the surface or self-assembled a film of streptavidin on the surface. Finally they spotted biotinylated-dsDNA onto the strepatividin spots or film. In their study, they followed the surface density of the dsDNA with different spotting conditions, but did not look at protein binding to the surface.

It is worth mentioning the use of dsDNAs arrays for investigation of protein-protein interactions with mass spectrometry, reported by Becker *et al.*[59] They used the DNA for DNA-directed immobilization, first by spotting 5'-amino-modified ssDNA to a succinimide functionalized surface. They could then use the complementary strand with an attached protein to specifically bind different proteins to different spots. The surface was then exposed to a second protein, which interacted with the protein immobilized on the surface. After a matrix was applied to the surface, they could use MALDI (matrix assisted laser desorption ionization) mass spectrometry to study the interaction of the two proteins.

As demonstrated in the examples given above, there are many uses for and ways to make dsDNA microarrays. Some of the key requirements of a substrate for dsDNA microarrays include that there is little non-specific binding of the protein and that the dsDNA is bound to the surface in such a way that does not inhibit the binding of the protein. Current research is underway to investigate the usefulness of our zirconium-phosphonate monolayer as a substrate for dsDNA microarrays. Our collaborators, Dr. Bruno Bujoli and the members of the Laboratoire de Synthèse Organique, in Nantes, France, performed studies analyzing the ability of a protein, ArgR, to bind to dsDNA on the zirconium-phosphonate surface. With fluorescence imaging, they looked at protein binding to dsDNA microarrays, which contained the binding site of ArgR. While they used the same probe sequence, they did, however, vary length, identity and placement of the spacer and also the placement of the phosphate linker. They found that the dsDNA sequence with a poly-G spacer and phosphate linker on both 5' ends gave the highest protein binding. In this chapter are the XPS studies of dsDNA on our zirconium-phosphonate surface, which help to explain why more protein bound to the spots of the 5'-5' phosphorylated dsDNA.

Experimental

Zirconium-phosphonate substrates were prepared as stated in the experimental section of Chapter 2 of this dissertation. To prepare the dsDNA, ssDNA was prepared in a 1 x SSC (saline sodium citrate) buffer, pH 6 at double the desired concentration. The saline sodium citrate buffer solutions are prepared from a stock solution of 20 x SSC, which corresponds to a 3.0 M NaCl and 0.30 M sodium citrate solution. Thus for a 1 x SSC solution, the concentrations are 0.15 M NaCl and 0.015 M sodium citrate, creating a solution which has an ionic strength of 0.225 M. The ssDNA was then mixed with its complement in equal volume to give the final desired concentration in a 1 x SSC buffer. The DNA was hybridized using a thermocyler, first by

heating at 98°C for 2 minutes, 65°C for 2 minutes, and finally cooling to 4°C for 4 minutes. The dsDNA was then spotted onto the slide; to create a spot large enough for XPS analysis, 30 μL of the DNA was pipetted onto the rinsed and dried zirconium-phosphonate surface. Once the DNA had been spotted, it was allowed to react with the slides overnight in Petri dishes at room temperature. Two different rinsing conditions were used. One set of conditions was performed to allow the probe coverage to be compared to the protein binding experiments, the other to allow the probe coverage to be compared to the ssDNA experiments. The rinsing conditions set to mimic those used for the protein binding experiments involved first submersion of the slide in 3.5 x SSC, 0.3% SDS (sodium dodecylsulfate) for 45 minutes with gentle rocking. Then the slide was submerged in 1 x SSC for 5 minutes with gentle rocking. Finally, the slide was rinsed in water by dipping 10 times in 5 different vials of water. The other set of rinsing conditions, which are the same as the ssDNA experiments, began with the spotted slide being immersed for 1 hour in 3.5 x SSC, 0.3% SDS at 42°C, followed by rinsing 5 times with nanopure water and spin drying. The slides then underwent a mock hybridization, which should give the true probe concentration if they were to undergo hybridization, by treatment with 25μL per spot of 3 x SSC, 0.1% SDS overnight at 42°C. Finally, the slides were rinsed in 2 x SSC, 0.1% (2 min), 1 x SSC (2 min), and 0.2 x SSC (2 times, 2 min), followed by rinsing in water 5 times. At least four spots were examined at each different rinsing condition.

Results and Discussion

Linker and Spacer Placement

The employment of dsDNA microarrays to probe different DNA-protein interactions is being seen more and more in the literature. To study how well a zirconium-phosphonate surface worked as a substrate, our collaborators, Dr. Bruno Bujoli and his group, investigated the

interaction of dsDNA, immobilized on the zirconium-phosphonate surface, with a protein. They chose to look the protein ArgR, which plays a major role in the control of certain biosynthetic and catabolic arginine genes.[70] They also looked at the influence of the identity of the spacer and the placement of the phosphate linker and spacer on the dsDNA. Relative to ssDNA the number of possible ways for attaching dsDNA to the surface increases. For ssDNA with a covalent linker, the two possibilities are to use the linker on the 5' end or the 3' end. In earlier chapters, ssDNA phosphorylated on the 5' end was used, based on earlier work which showed this effectively immobilized the ssDNA on our zirconium-phosphonate surface. For dsDNA, a number of different linker and spacer motifs were investigated by Bujoli *et al.* The corresponding fluorescent data for the protein binding experiments are shown in Figure 4-1.

To look at the protein binding to the dsDNA on the surface, first Bujoli *et al.* spotted 10 μM ds-DNA in a 1x SSC solution. The dsDNA contained a 22-bp sequence located in the middle, which is recognized by the protein. They then exposed the slide to a 0.3% α-casein, 3.5 x SSC, 0.3% SDS solution for 45 min. Casein, a protein that contains phosphate groups, binds to the area of the slide that does not contain any dsDNA. This prevents non-specific binding of the target protein, lessening the background signal. After rinsing the slide, they exposed it to the target protein, ArgR. The protein did not contain a fluorophore, but it did have what is called a histag, a sequence of 6 histidines. After rinsing again, they exposed the surface to an anti-histag antibody solution, which binds to a histag on the ArgR protein. After another rinsing, the slide is exposed to a secondary antibody, Anti-Mouse IgG, containing a fluorophore. The secondary antibody binds to the anti-histag antibody. The slide was studied with fluorescence imaging after a final rinsing. Figure 4-2 illustrates the main steps in the experiment.

Through fluorescence imaging it was seen that the dsDNA with 5',5' phosphates gave the most intense fluorescence and therefore the highest amount of protein binding. It was not clear why more protein bound to the 5'-5' phosphorylated dsDNA spots. It was surmised that it could be due to increased surface density of dsDNA, or possibly from the DNA binding on both ends using both phosphate groups creating a loop of dsDNA on the surface perhaps better exposing the segment where the protein would bind.

To determine if surface density played a role in the binding, quantitative XPS experiments were performed. Four different phosphate linker/spacer motifs, shown in Figure 4-3, were investigated. These four motifs consisted of a dsDNA sample with phosphorylation and a 9-mer guanine spacer on both 5' ends (5'G9PO4,5'G9PO4); a dsDNA sample with phosphorylation and a 9-mer guanine spacer on both 3' ends (3'G9PO4,3'G9PO4); a dsDNA sample with phosphorylation and a 9-mer guanine spacer on the 5' end of one strand and the same on the 3' end of the other strand (5'G9PO4,3'G9PO4); and finally a dsDNA sample with phosphorylation and a 9-mer random spacer on both 5' ends (5'X9PO4,5'X9PO4). The rinsing procedures used for the XPS experiments were set to mimic those used in the fluorescence experiments, before the ArgR protein binding step was performed. However, the rinsing had to be modified to prevent nitrogen contamination. For example, in the "passivation" step with the casein, the casein was not used for the XPS experiments. To immobilize the dsDNA, first it was hybridized in a thermocyler, and then spotted onto the surface. After the dsDNA had reacted with the substrate overnight, it was rinsed with gentle rocking in a 3.5 x SSC/0.3% SDS solution, followed by rinsing in a 1 x SSC solution, and finally the slide was rinsed in water and dried. XPS was then taken on the area where the dsDNA had been spotted.

The surface coverage can be calculated using a similar method to that outlined in Chapter 2. Again the N 1s peak was used with the Zr 3d peak in Equation 2-8 from Chapter 2:

$$\frac{n_N}{n_{Zr}} = \frac{I_N \sigma_{Zr} T_{Zr} t \exp\left(-t/\left(L_{Zr}^{eff} \sin\theta\right)\right)}{I_{Zr} \sigma_N T_N L_N \left(1-\exp\left(-t/\left(L_N^{eff} \sin\theta\right)\right)\right)} \qquad (2\text{-}8)$$

Equation 2-8 calculates the ratio of the nitrogen surface density to the zirconium surface density. As shown in Chapter 2, to get the DNA density from the nitrogen to zirconium ratio, the nitrogen stoichiometry is used along with known surface density of zirconium. A typical N 1s peak for the dsDNA is shown in Figure 4-4. When calculating the surface coverage of dsDNA, there are two different ways to consider the nitrogen stoichiometry. The surface coverage can be calculated as the "number of DNA strands/cm^2" or the "number of dsDNA strands/cm^2." To use the former, the average number of nitrogens per strand is taken for the dsDNA complex. For the latter, the total number of nitrogens in the dsDNA complex can be used. To compare the surface coverage among the different phosphate-linker and spacer placement experiments, the "number of dsDNA strands/cm^2" is used.

The comparison of the surface coverages is shown in Figure 4-5. The graph shows that the 3'G9PO4,3'G9PO4 DNA gave the highest surface coverage at $2.8 \times 10^{11} \pm 4.8 \times 10^{10}$ dsDNA molecules/cm^2. Then the 5'G9PO4,5'G9PO4 DNA gave the next highest surface coverage at $2.1 \times 10^{11} \pm 2.2 \times 10^{10}$ dsDNA molecules/cm^2, followed by the 5'X9PO4,5'X9PO4 DNA at $1.7 \times 10^{11} \pm 1.3 \times 10^{10}$ dsDNA molecules/cm^2. Finally the 5'G9PO4,3'G9PO4 DNA had the lowest surface coverage at $1.2 \times 10^{11} \pm 1.0 \times 10^{10}$ dsDNA molecules/cm^2. The error reported here is the standard deviation of the mean. This follows the general trend seen with fluorescence indicating that the surface coverage does play a role in the differences seen with the protein immobilization.

Based on the XPS data, it appears that having two linking groups on opposite ends of the dsDNA increases the surface coverage. The increased dsDNA density seen with 3'G9PO4,3'G9PO4 and 5'G9PO4,5'G9PO4 DNA could be due to an increased probability of binding with a phosphate group on both ends compared to two phosphate groups on a single end. This stems from the fact that with a phosphate group on both ends, binding can occur with the zirconium monolayer when either end approaches the surface. The data does not, however, indicate the orientation in how the dsDNA binds to the surface. A surface coverage of 2.85×10^{11} corresponds to 357 nm^2/dsDNA molecule. This is ample distance for the 3'G9PO4,3'G9PO4 and 5'G9PO4,5'G9PO4 dsDNA to lie down and bind with both phosphate groups. If the dsDNA binds with both phosphates, the dsDNA may be more strongly bound to the surface, which could also be a reason for higher surface coverage. The XPS data also demonstrate, based on the higher surface coverage of 5'G9PO4,5'G9PO4 over 5'X9PO4,5'X9PO4, that the poly-dG effect discussed in Chapter 3 also applies to dsDNA.

It should be noted that, although the XPS data follows a trend that corresponds slightly with the fluorescence data, the magnitudes of the differences seen in the XPS data are smaller than those seen in the fluorescence data. For example, in the fluorescence data the 3'G9PO4,3'G9PO4 DNA was 4 times more intense than the 5'X9PO4,5'X9PO4 DNA, where as the XPS data shows the 3'G9PO4,3'G9PO4 DNA has a surface coverage of only 1.7 times more than the 5'X9PO4,5'X9PO4 DNA. This may just be due to the variability of the data. On the other hand, there has also been some suggestion in the literature that larger spot sizes (2 mm spots compared to 150 μm spots) can lead to lower surface coverages.[71] Bujoli *et al.*, our collaborators performed fluorescence experiments comparing 2 mm and 8 mm spot sizes and no difference in intensity was seen between these two spots, but perhaps the 2 mm spot needs to be

smaller to see a difference. The spots necessary for XPS analysis are approximately, 1.5 cm x 1 cm. If the larger spot sizes lead to lower surface coverage, then the XPS data may not represent the surface coverages of the DNA microarrays.

Single Versus. Double Stranded DNA

Immobilizing ssDNA and dsDNA on a surface for microarrays each serve different analytical purposes. It has been shown by Peterson *et al.* that 5'-thiolated ssDNA binds at a higher surface density on gold than 5'-thiolated dsDNA.[36] A comparison of the surface coverage of ssDNA and dsDNA would help us to determine the most efficient method for making dsDNA microarrays. Would a higher dsDNA probe density be achieved for ssDNA first immobilized and then hybridized or dsDNA directly immobilized on the surface? A comparison of ssDNA and dsDNA would also help us understand further the dynamics of the DNA immobilization.

In this study, there were three different strands compared. A 5' phosphorylated ssDNA (5'PO4G9O33), a 5' phosphorylated dsDNA (5'PO4G9O33O33), and a doubly 5' phosphorylated dsDNA (5'PO4G9O37,5'PO4G9O37). The sequence of the 5'PO4G9O37,5'PO4G9O37 is different than that of the other two. In order to do this study, we wanted to use the same sequence, but for some reason when Invitrogen, the manufacturer of the DNA, tried to synthesize a 5' phosphorylated complement to 5'PO4G9O33 the sample repeatedly failed quality control. After trying the synthesis four times, they stopped trying. For this reason, the probe sequence of the doubly phosphorylated dsDNA had a different sequence than the samples. As in the other studies, the DNA was spotted on the surface with a large enough surface area to be sampled by XPS. The washing procedure is outlined in the experimental section. In brief, it begins by submerging the slide in a SSC/SDS solution, followed by water rinsing, and then treating the slide with SSC/SDS overnight. Then the slide is rinsed with water a final time and dried, after which XPS was taken.

The surface coverage results are shown in Figure 4-6. For ease of comparing surface coverage with the ssDNA, the dsDNA is reported as "number of DNA strands/cm^2" instead of the "number of dsDNA strands/cm^2." The calculated surface coverages for 5'PO4G9O33, $2.8 \times 10^{11} \pm 5.1 \times 10^{10}$ DNA strands/cm^2, and 5'PO4G9O37,5'PO4G9O37, $2.6 \times 10^{11} \pm 4.0 \times 10^{10}$ DNA strands/cm^2, are approximately the equal. While, 5'PO4G9O33O33, the singly phosphorylated dsDNA, has a lower surface coverage: $1.1 \times 10^{11} \pm 1.4 \times 10^{10}$ DNA strands/cm^2. This data shows that the bulkier dsDNA, if it has only a single phosphate like the ssDNA, binds at a lower density than the ssDNA. This is similar to what Peterson observed on gold.[36] Peterson claims in his paper that because the duplex has double the anionic charge on the backbone compared to the ssDNA, it is expected the dsDNA would bind at half the density of the ssDNA due to repulsion of the dsDNA molecules. He goes on to say that the density is even lower than half the ssDNA density indicating there are other factors coming into play such as conformation or flexibility of the DNA strands. It does not seem likely that one of the main causes of lower dsDNA density is increased electrostatic repulsion of the dsDNA strands. The charge of the dsDNA strands should be shielded by the ions in solution, minimizing repulsive forces. The most reasonable cause for the decreased surface coverage of the dsDNA is the different dynamics of the dsDNA such as decreased flexibility.

Conclusion

The surface densities of dsDNA with four different phosphate-linker/spacer motifs were calculated from the N 1s and Zr 3d XPS data. The highest surface density was achieved with the 3'G9PO4,3'G9PO4 dsDNA at $2.8 \times 10^{11} \pm 4.8 \times 10^{10}$ dsDNA molecules/cm^2 followed by the 5'G9PO4,5'G9PO4 DNA, which gave the next highest surface coverage at $2.1 \times 10^{11} \pm 2.2 \times 10^{10}$. These are also the two strands that gave the highest fluorescence in the protein binding

experiments done by our colleagues. This data indicates that the reason the protein exhibited more binding for the 5'G9PO4,5'G9PO4 and 3'G9PO4,3'G9PO4 was due to higher dsDNA surface density. In addition to a comparison of the different phosphate-linker/spacer motifs, a comparison of dsDNA vs ssDNA was made. It was seen that dsDNA with a single phosphate group on the 5' had a lower surface coverage at $1.1 \times 10^{11} \pm 1.4 \times 10^{10}$ DNA strands/cm^2 than an ssDNA strand with a single phosphate, which had a surface coverage of $2.8 \times 10^{11} \pm 5.1 \times 10^{10}$ DNA strands/cm^2. A dsDNA strand with a phosphate group on both 5' ends gave a surface coverage of $2.6 \times 10^{11} \pm 4.0 \times 10^{10}$ DNA strands/cm^2.

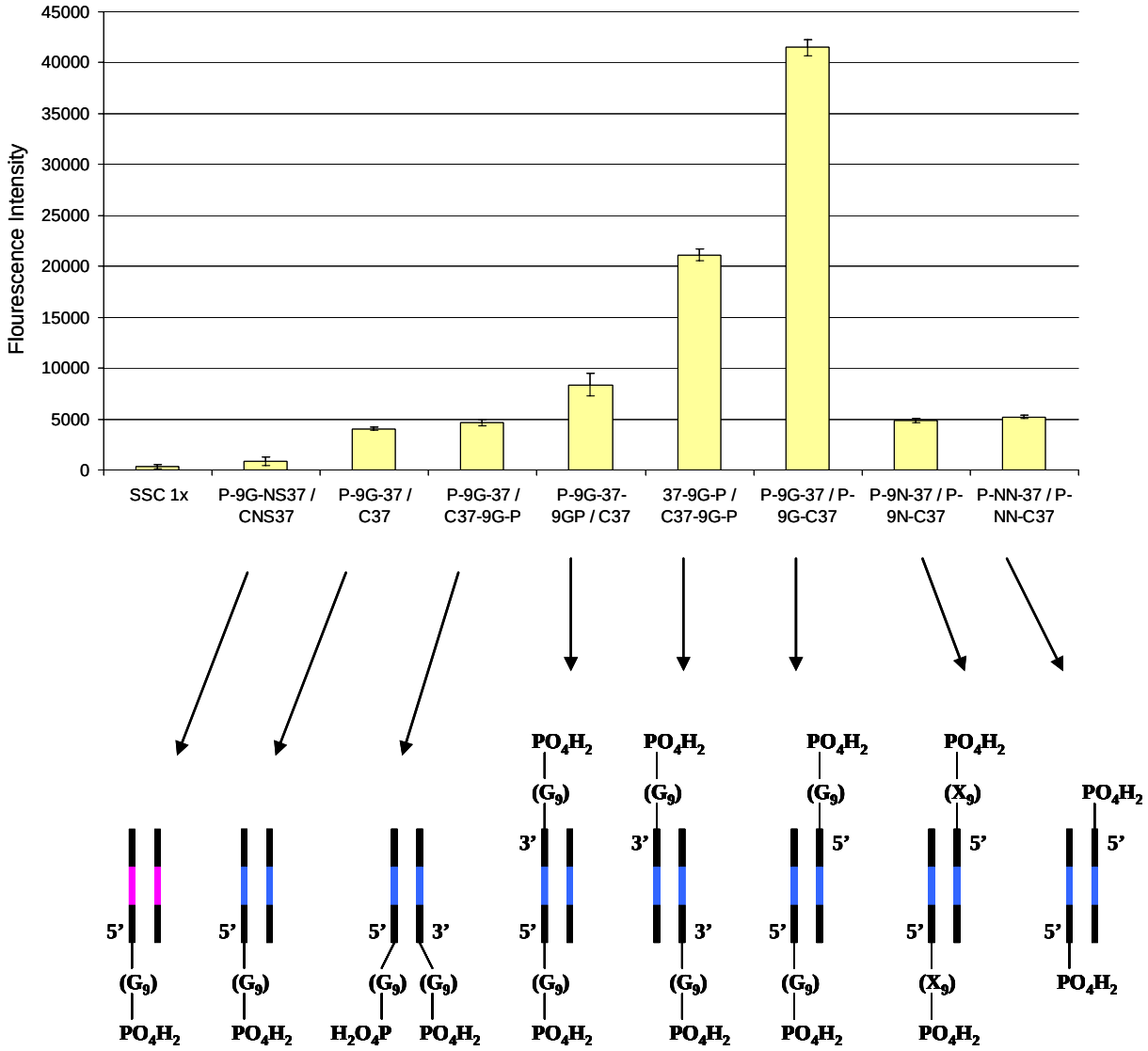

Figure 4-1. Fluorescence intensities of the spots for the protein binding to the corresponding dsDNA. The dsDNA show the different spacer and linker motifs that were used. The dsDNA with the pink band contains a random sequence which should not be recognized by the protein ArgR. The blue band is a dsDNA sequence that should be recognized by the protein ArgR. The "X" spacer is a random sequence.

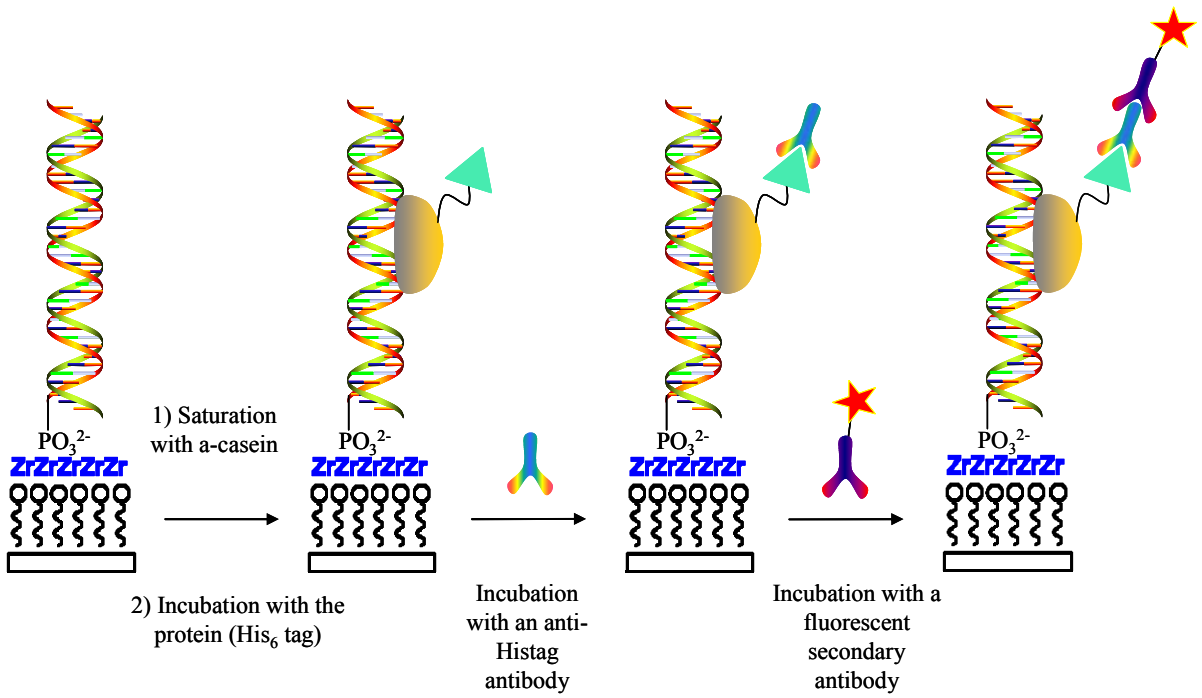

Figure 4-2. Steps used to test the binding the ArgR protein to dsDNA containing a 22 base-pair sequence. First, the dsDNA is spotted, which is followed by a surface passivation with casein. The slide is exposed to the ArgR protein containing a histag and then to an anti-histag antibody. Finally, the slide is exposed to the Anti-Mouse IgG antibody, containing a fluorophore.

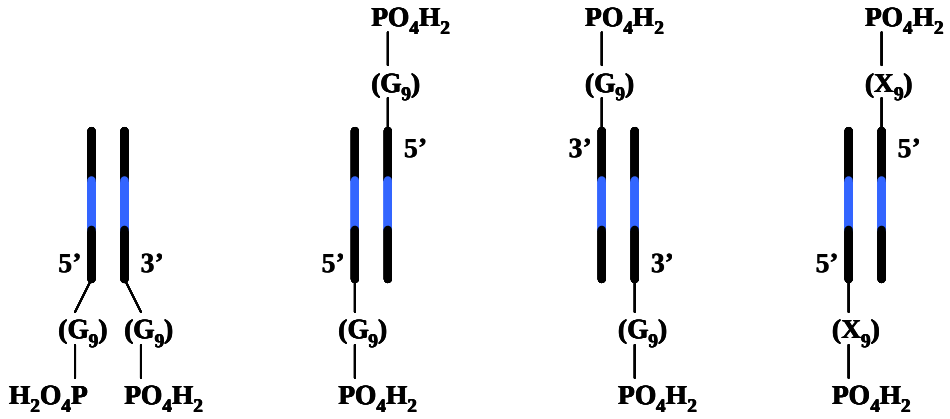

5'G9PO4,3'G9PO4 5'G9PO4,5'G9PO4 3'G9PO4,3'G9PO4 5'X9PO4,5'X9PO4

Figure 4-3. The dsDNA with the different phosphate-linker/spacer motifs that were studied with XPS.

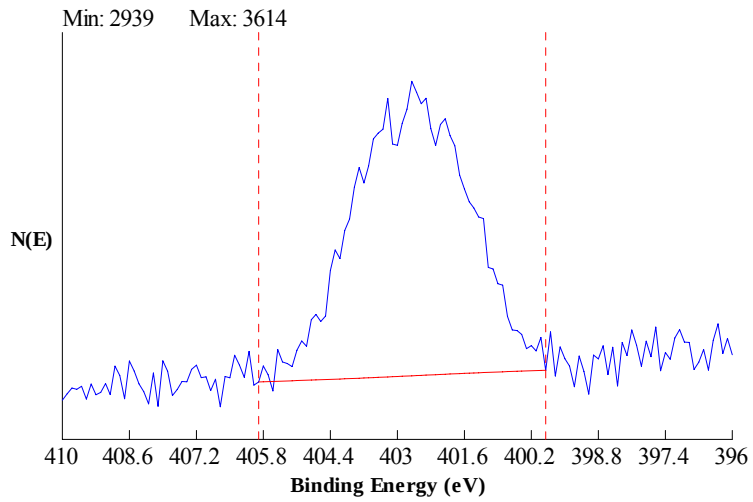

Figure 4-4. Typical XPS spectra for the N 1s peak. This peak in particular is for 3'G9PO4,3'G9PO4.

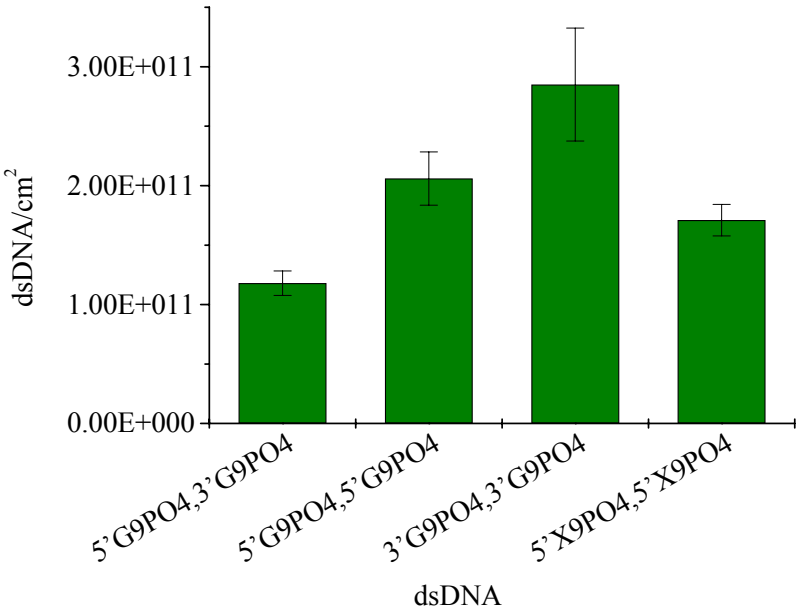

Figure 4-5. Comparison of the surface densities of the dsDNA strands.

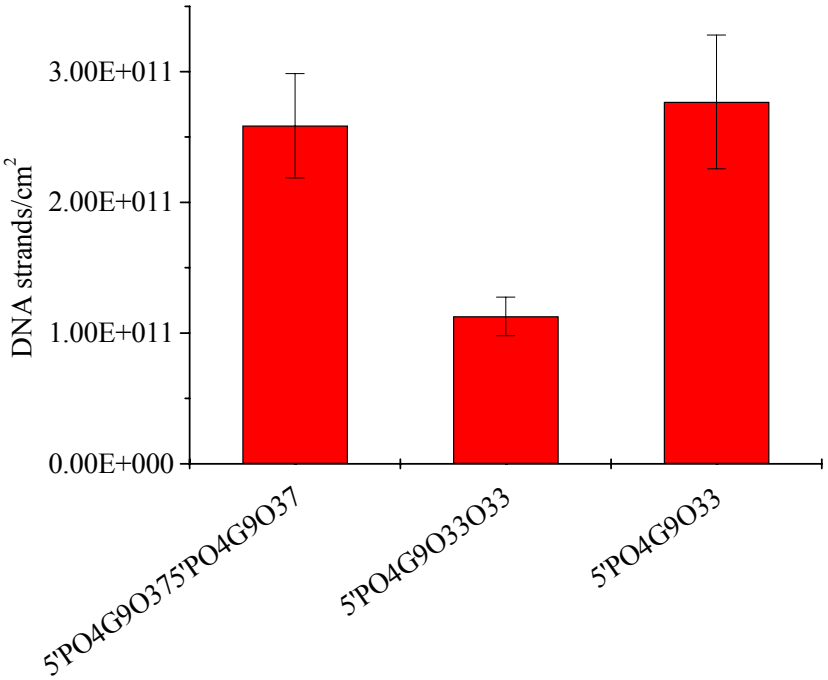

Figure 4-6. Surface density comparison of dsDNA versus ssDNA.

CHAPTER 5
HYBRIDIZATION OF DNA AT A ZIRCONIUM-PHOSPHONATE SURFACE – AN XPS STUDY

Introduction

DNA microarrays can be used for a number of different purposes. More commonly they are used to follow gene expression. To make a microarray for this purpose requires a series of complex steps including probe selection, probe spotting, target preparation (mRNA extraction, reverse transcription, and cDNA labeling), hybridization of target with probe, rinsing, scanning, and data acquisition.[30] Hybridization is a key step in the process and can affect the noise (specificity of the probe-target interaction) and the signal to background ratio. The hybridization efficiency and amount of target physisorbed to the surface where no probe is spotted determine the signal to background ratio. However, specificity and hybridization efficiency work against each other; consequently, optimization of the hybridization conditions is used to give the best results.

Optimization is facilitated by the use of fluorescence imaging with a microarray scanner. which is how the hybridization conditions were optimized for our zirconium-phosphonate support.[32] However, fluorescence imaging does not give quantitative information on the probe surface density or the hybridization efficiency. It has been shown that XPS can be used to calculate these values,[12] and in this chapter we discuss our attempt to determine the hybridization efficiency with XPS.

Experimental

The zirconium-phosphonate monolayers were prepared as stated in Chapter 2. Reagents were purchased from Aldrich and were used as received. DNA was purchased from Invitrogen, Biosource (which was bought by Invitrogen), or MWG biotech all with HPLC purification.

Confirmation of Hybridization with Fluorescence Confocal Microscopy

This fluorescence study was done on a Nikon laser confocal scanning microscope. For these experiments DNA was ordered from MWG Biotech with HPLC purity and used following sequence for the probe: 5' GGGGGGGGGGGGACCCCAGAGGTATACATACGTTGCAGT CAGGA and the following sequence for the target: 5' TCCTGACTGCAACGTATGTATACC TCTGGGGTC 3'. The target was labeled with a 5' Cy3. A 40 μM probe solution was prepared in a pH 6 1 x SSC solution. The saline sodium citrate buffer solutions are prepared from a stock solution of 20 x SSC, which corresponds to a 3.0 M NaCl and 0.30 M sodium citrate solution. Thus for a 1 x SSC solution, the concentrations are 0.15 M NaCl and 0.015 M sodium citrate, creating a solution which has an ionic strength of 0.225 M. The spots were made by dropping 5 μL on the slide with a pipetter. The slide was incubated overnight in a Petri dish. Then the slide was rinsed in 2 x SSC (saline sodium citrate), 0.1% SDS (sodium dodecyl sulfate) (2 min), 1 x SSC (2 min), 0.2 x SSC (2 times, 2 min). Following the rinsing, the slide is treated with a 1% BSA (bovine serum albumin), 3.5 x SSC, and 0.3% SDS for 1 hour at 42°C. The slide was then rinsed with water by dipping 10 times. To perform the hybridization, 40μL of the hybridization solution (5μM of target, 0.3% SDS, 3.5 x SSC, 5 x Denharts, 1 x TE buffer, and 50% formamide) was dropped onto the area containing the spots and then a 1" x 2" coverslip was placed on top. The slide was placed in a Petri dish and kept at 42°C overnight. The hybridization was followed with rinsing in 2 x SSC, 0.1 % SDS (2 min), 1 x SSC (2 min), and 0.2 x SSC (2 times, 2 min.). Finally, the slide was spun dry. After which the slide was analyzed under the microscope.

Fluorescence Comparison of Hybridization Methods

This experiment was performed with an Agilent 2-dye fluorescent microarray scanner. The probe sequence was 5'-H_2O_3PO-$(X)_9$-CCGCCGGTAACCGGAGGTTAAGATCGAGA-TCCA and the target sequence was 5'-TGGATCTCGATCTTAACCTCCGGTTACCGGCGG with a Cy3 fluorophore on the 5' end. Both a poly-adenine and guanine spacer on the probe was studied. A 40μM solution of the two probes were prepared in a 1 x SSC, pH 6 buffer. These were spotted on the slide by dropping 4, 2.5 μL spots, which coalesced to form one large 10 μL spot. The slide was then incubated overnight at room temperature. Following incubation, the slide was submerged in a 3.5 x SSC, and 0.3% SDS for 1 hour at 42°C, after which it was rinsed by dipping 10 times in water. Two different hybridizations were performed on the slide. On one half of the slide – 2 spots of the probe containing poly-A and 2 spots of the probe containing poly-G – it was subjected to the normal hybridization, where 20 μL of the hybridization solution (5 μM target, 0.3% SDS, 3.5 x SSC, 5 x dernhardt's, and 50% formamide) is dropped on the spotted area and a 1" x 1" coverslip is placed on the drop. On the other half of the slide, where there was also 2 spots of the poly-A containing and poly-G containing probe, was dropped 15μL of the "nitrogen-free" hybridization solution (5 μM target, 3 x SSC, 0.1% SDS) on each area where the probe was. After sitting overnight in a humid Petri dish at 42°C, the slide was rinsed 2 x SSC, 0.1 % SDS (2 min), 1 x SSC (2 min), and 0.2 x SSC (2 times, 2 min.). Finally the slide was spun dry and the fluorescence imaging was performed.

Determination of Nitrogen Contamination from Hybridization Solution with XPS

Blank hybridization experiments were performed by first spotting a mock probe solution of 1 x SSC, pH 6 (contained no probe) onto a zirconium phosphonate substrate. The slide was then submerged in a 3.5 x SSC, and 0.3% SDS for 1 hour at 42°C. After rinsing 5 times with water,

the slide was treated with one of two mock hybridization solutions (contained no target). One solution was composed of 0.3% SDS, 3.5 x SSC, 5 x Dernhardts, and 50% formamide. The other solution was 0.3% SDS, 3.5 x SSC, and 50% formamide (the same as the first except without the Dernhardts). The 20 μL of the mock hybridization solution was dropped on the slide and a 1" x 1" was placed over the drop. The slide was then placed in a humid chamber and left overnight at 42°C. After which, the slide was rinsed with 2 x SSC, 0.1 % SDS (2 min), 1 x SSC (2 min), and 0.2 x SSC (2 times, 2 min.), followed by rinsing 5 times with water. The slide was spun dry and XPS analysis was performed on the area where the 1 x SSC had been spotted.

Hybridization Study with XPS

Real hybridization experiments were performed using the probe sequence, 5'-H_2O_3PO-$(X)_9$-CCGCCGGTAACCGGAGGTTAAGATCGAGATCCA, and the target sequence: 5'-TGGATCTCGATCTTAACCTCCGGTTACCGGCGG . A 40μM solution of the probe DNA was prepared in a 1 x SSC buffer, pH 6. The DNA was spotted on the slide to cover an area large enough for XPS analysis. The slide was then allowed to incubate overnight at room temperature, followed by submersion in a 3.5 x SSC, and 0.3% SDS solution for 1 hour at 42 °C. A 5 μM target solution was prepared in a 3 x SSC, 0.1% SDS buffer. 25μL of the target solution was spotted on the slide, covering the area where there was probe. The slide was placed in a humid Petri dish overnight at 42 °C. Then the slide was rinsed with 2 x SSC, 0.1 % SDS (2 min), 1 x SSC (2 min), and 0.2 x SSC (2 times, 2 min.), followed by either dipping 2 times in 5 vials of water or 10 times in 5 vials of water. After this, XPS was taken.

Results and Discussion

The basis of the DNA microarray is the specific hybridization of each probe to a labeled complementary target. There are many parameters that affect the efficiency of hybridization of a

probe with its complementary target at a surface. These parameters include the identity of the probe and target, the probe environment, the buffer conditions and the temperature.[36, 37, 52, 72, 73] Some of these parameters can easily be changed and are adjusted to give the optimum result, which is generally high specificity and a high signal to background ratio. A high signal to background ratio is obtained with a high probe surface density, high hybridization efficiency, and low physisorption of the target to non-probe containing regions. The specificity of each probe is associated with its melting temperature. To help optimize the specificity there is an equation, which was first proposed by Howley *et al.*, that relates the melting temperature of the DNA on a surface to the conditions of the hybridization:[74]

$$T_m = 81.5 + 16.6\left(\log\left[\mathrm{Na}^+\right]\right) + 0.41(\%GC) - 0.61(\%\mathrm{form}) - 500/\mathrm{bp} \qquad (5\text{-}1)$$

where [Na+] is the concentration of sodium ions; %GC is the percentage of guanine and cytosine in the probe and target; %form is the percentage of formamide in the hybridization solution; and bp is the number of base pairs. The equation was developed for DNA 50 base pairs or longer. Nevertheless, the equation shows the important relationship of two components which are often included in a hybridization solution: Na^+ and formamide. The Na^+ increases the melting temperature and the formamide decreases it. Thus, to increase specificity, the formamide can be increased, but this will also lower hybridization efficiency. On the other hand, to increase specificity [Na^+] can be decreased, but again this can lead to lower hybridization efficiency.

As mentioned above the probe environment can affect the hybridization efficiency. For example, if the density of the probe is too high this will lead to low hybridization efficiency.[36] Of course, if the probe density is too low, then only a small amount of target will be hybridized onto the surface, which may result in low signal to background. It has also been shown that a

spacer placed between the linker and probe sequence can increase hybridization efficiency supposedly by bringing the probe sequence closer in contact with the solution phase.[37, 52] Furthermore, there is evidence that the charge on the surface can affect hybridization.[73]

For the ssDNA arrays made on our zirconium-phosphonate surface, the spotting and hybridization conditions were optimized by our colleagues in France using fluorescence imaging.[32] These optimized conditions begin with spotting the ssDNA (10 – 40 μM) prepared in a pH 6, 1 x SSC buffer. The slide is then incubated overnight in 50% humidity. Then, the slide is subjected to a passivation step, where it is submerged in 1% BSA (bovine serum albumin), 3.5 x SSC, and 0.3% SDS for 1 hour at 42°C, which is followed with rinsing 5 times with water. The next step is hybridization where the 20 μL of the hybridization solution (5 μM target, 0.3% SDS, 3.5 x SSC, 5 x Denhardts, 1 x TE (tris(hydroxymethyl)aminomethane/EDTA) buffer, and 50% formamide) is dropped onto the surface and a coverslip is placed on this drop so that it spreads out over the array area. The slide is then place in a humid sealed chamber in an oven overnight at 42°C. Finally the slide is washed with 2 x SSC, 0.1 % SDS (2 min), 1 x SSC (2 min), and 0.2 x SSC (2 times, 2 min.). This experiment was tried – with larger spots – in our lab to confirm we were using the correct techniques. The spots, which were about 2 mm in diameter, were analyzed with confocal fluorescence microscopy (Figure 5-1). The spotting and hybridization in our lab appeared successful.

To determine the hybridization efficiency, the XPS experiments simply looked at the increase in the N 1s signal after hybridization. Several modifications had to be made in order to make the experiments viable with XPS. One simple modification made was that the slides had to be rinsed water to remove salts after the final SSC rinsings. This was because the salts could attenuate the signals from the DNA and zirconium layers. Also, the hybridization solution had to

be modified so that the nitrogen containing solution components, other than the target, would not contaminate the surface giving a false increase in nitrogen signal. The nitrogen containing constituents that might cause contamination were formamide, Denhardt's solution, and Tris E buffer. Denhardt's is a mixture of ficoll (a sucrose polymer), polyvinylpyrrolidine, and BSA, of which the latter two contain nitrogen. Thus before the real hybridization experiments took place blank experiments were performed to determine which components might cause nitrogen contamination. This was done using spotting solutions and hybridization solutions containing no DNA and varying the nitrogen containing additives. The TE buffer was eliminated without testing simply because our French collaborators changed the hybridization solution such that the TE buffer was no longer used. The blank spotting solutions were spotted onto the zirconium-phosphonate surface. Then the slides were rinsed as outlined in the Experimental section. Then the slides were subjected to one of two blank hybridization solutions overnight at 42°C. One contained SDS, SSC, Denhardt's reagent, and formamide (Blank 1). The other solution contained SDS, SSC, and formamide (Blank 2). Following the blank hybridization, the slide was rinsed with several SSC solutions and then water. The XPS survey scans (Figure 5-2) both contain a considerably large N 1s peak, giving evidence that both solutions produced nitrogen contamination with Blank 1 (the Denhardt's-containing solution) giving more nitrogen contamination. From these results came the decision to use a hybridization solution containing only SSC, SDS, and the target DNA. Eliminating formamide and Denhardt's solution may actually increase the apparent hybridization since both are in the hybridization solution to prevent nonspecific interactions.

The hybridization solution containing only SSC, SDS, and target was compared using fluorescence detection along side the hybridization solution containing SDS, SSC, Denhardt's

reagent, and formamide and target. To do this the ssDNA was spotted onto a slide. After the slide was rinsed, on one half of the spots, the 20μL of the latter hybridization solution was dropped and then a coverslip was placed over it. On the other half, the former hybridization solution was dropped onto the probe areas just enough to cover the spot. The slide then underwent the routine SSC rinsings, which were followed by water rinsings. Scanning fluorescence imaging was then used to analyze the spots (Figure 5-3). From these results it was seen that there was little difference in the intensities from the spots using the two different hybridization methods. This validated the use of the "nitrogen-free" hybridization solution.

After the nitrogen-free hybridization buffer was tested with fluorescence, hybridization using this buffer was followed with XPS. This was done by spotting the probe, rinsing the slide, and then spotting the target, prepared in the nitrogen-free buffer, in the area of the probe. The slide was incubated overnight and with the target then a final rinsing with SSC buffers was performed. As mentioned before, it is necessary to rinse the slides with water before taking XPS. This removes excess salt from the buffers, which can cause attenuation of the N 1s and Zr 3d XPS peaks. There was concern that the water rinsings may cause denaturation – as seen in Equation 5-1, DNA needs salt to hybridize. For this reason, two water rinsing conditions were explored. One used 10 dips in 5 different vials of water and the other used 2 dips in 5 different vials of water. Using the N 1s and Zr 3d peak intensities, the surface coverage (reported in DNA strands/cm^2 – not dsDNA/cm^2 molecules) were calculated using the methods outlined in Chapter 2 and 4.

The DNA surface coverage calculations are shown in Table 5-1. The surface coverage of the poly-G containing probe and poly-A containing probe are $2.8 \times 10^{11} \pm 5.1 \times 10^{10}$ ssDNA molecules/cm^2 and $1.4 \times 10^{11} \pm 3.3 \times 10^{10}$ ssDNA molecules/cm^2, respectively. These values are

also given in Chapter 3, and the procedure for immobilizing the probe is also in Chapter 3. After Hyb-1, the surface coverages for the poly-G containing probe and poly-A containing probe are $2.1 \times 10^{11} \pm 5.2 \times 10^{10}$ DNA strands/cm^2 and $1.2 \times 10^{11} \pm 2.0 \times 10^{10}$ DNA strands/cm^2, respectively. After Hyb-2, the surface coverages for the poly-G containing probe and poly-A containing probe are $1.7 \times 10^{11} \pm 1.8 \times 10^{10}$ DNA strands/cm^2 and $0.7 \times 10^{11} \pm 2.8 \times 10^{10}$ DNA strands/cm^2, respectively.

As the data show, no increase in DNA surface coverage could be seen with XPS after hybridization; conversely, there appears to be a decrease in the surface coverage. However to determine the probe surface coverage, a mock hybridization was included, so that the probe was subjected to the same conditions as hybridization except no target was present. For this reason, it makes the decrease in coverage seen very puzzling. There are several possible explanations for this. One is that the water rinsings, which are necessary to remove salts before XPS analysis, are causing denaturation of the dsDNA (and possibly more desorption of the probe). However, our French colleagues sometimes rinse their dsDNA slides in water briefly, but do not experience denaturation. Unfortunately, there are no studies that investigate water rinsings of dsDNA immobilized on a surface. If the hybridization is occurring, which seems to be the case based on the fluorescence data, unless the hybridization efficiency was above around 20%, it would be difficult to detect with XPS based on the experimental error of the probe data. A low hybridization efficiency is likely related to the low probe surface coverage, where the ssDNA strands are able to lie down on the zirconium-phosphonate surface. The positive potential (as shown in Chapter 3) of the surface attracts the negatively charged phosphodiester backbone. Others have reported low or zero hybridization if the probe was too close to the surface. For example Guo *et al.*, reported that when they did not use a spacer between the linking group and

the probe sequence no hybridization was seen.[52] Perhaps with our surface, when the probe is close to the surface, the target is sterically hindered from hybridizing with probe. Overall, considering the XPS experiments and the fluorescence experiments, hybridization is occurring, but not at a high enough efficiency to be detectable with XPS. However, why a decrease is seen in the DNA surface coverage is puzzling. Perhaps, after hybridization, probes that are not bound with sufficient strength, as a duplex the DNA rinses off more easily.

Conclusion

In conjunction with fluorescence imaging experiments, XPS experiments were performed in order to determine the hybridization efficiency. Hybridization was observable with the fluorescence, but not with XPS. This indicates that the extent of hybridization is too little to observe with XPS. Even though, when determining the probe surface coverage, a mock hybridization was used, a decrease was seen in the overall DNA surface coverage during the real hybridization experiments, making the data more difficult to interpret.

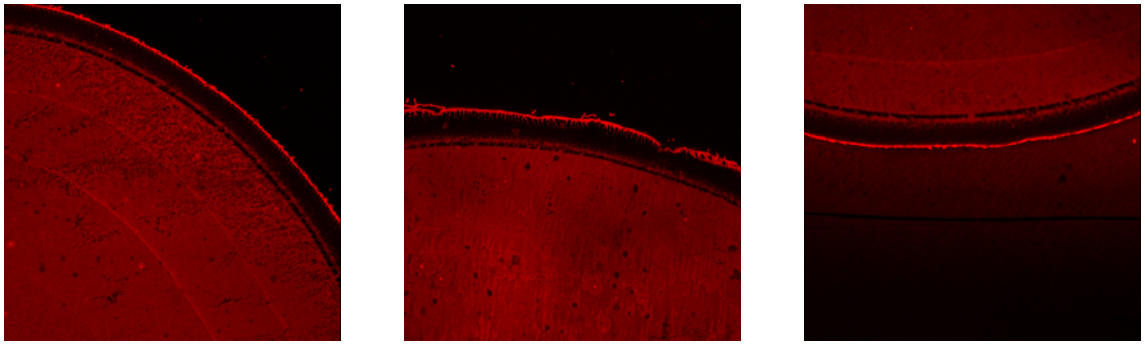

Figure 5-1. Fluorescence confocal microscopy image of hybridized spots. The total spot (about 2mm in diameter) would not fit in the whole image.

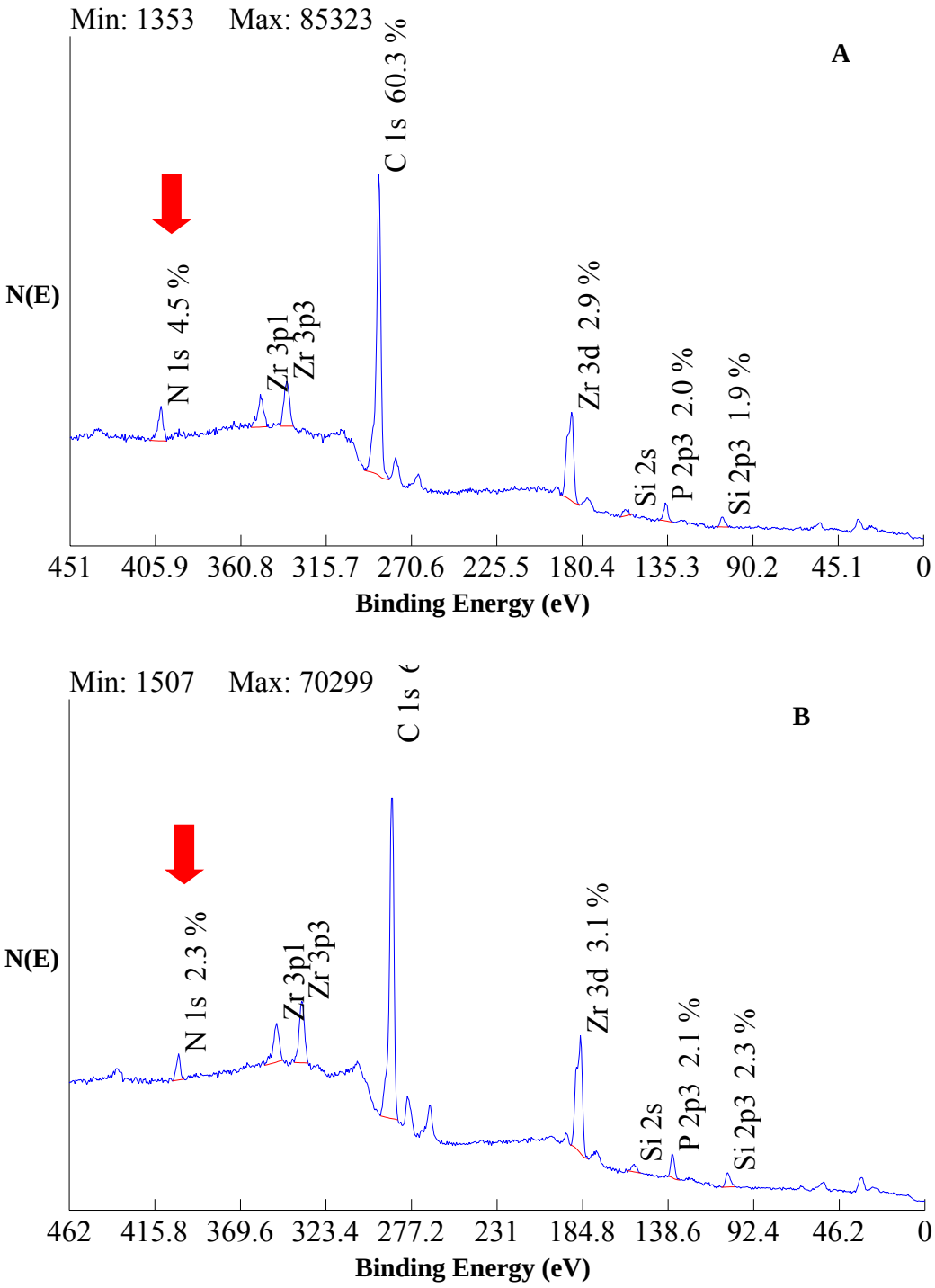

Figure 5-2. XPS spectra of blank hybridization taken to determine if nitrogen contamination would occur by following the N 1s peak. Only the significant region is shown, for this reason the percentages do not add up to 100. A) XPS spectrum of slide prepared using Denhardt's and formamide, which shows a higher N 1s signal, an indication that both formamide and Denhardt's physisorb. B) XPS spectrum of slide prepared using only formamide.

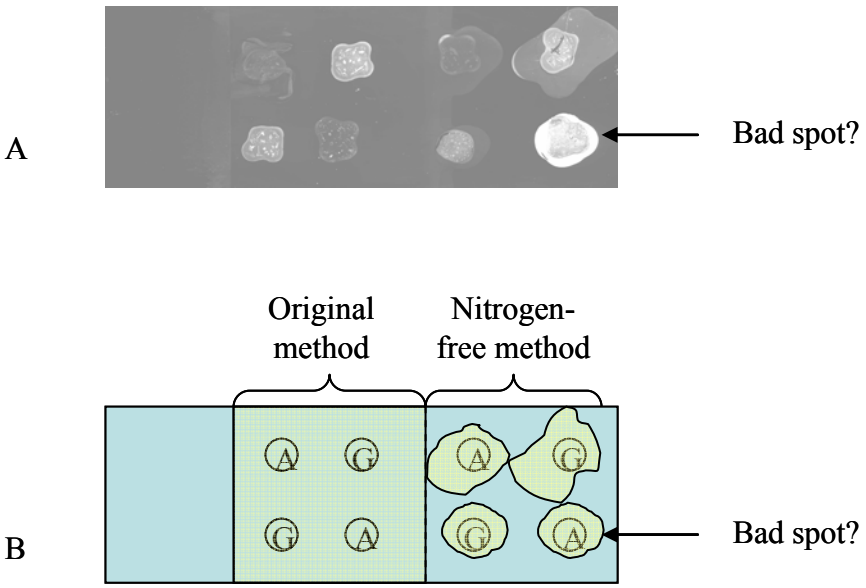

Figure 5-3. Fluorescence image of hybridized spots comparing two hybridization methods. A) Fluorescence image comparing the two hybridization methods. B) Drawing indicating which part of the slide corresponds to which method and which spots correspond to either the probe with poly-A spacer or poly-G spacer. The 4 spots on left were hybridized with the original method, with the Denhardt's solution and formamide and the 4 spots on the right are the nitrogen-free method. As the illustration shows, in the nitrogen free method, the target solution does not cover the whole slide, just the area where the spot is. Also there appears to be a bad area in the zirconium-phosphonate film, which led to strong adsorption of the target.

Table 5-1. Comparison of surface coverage of the DNA before hybridization, after hybridization with fewer water rinsings (After Hyb-1) and after hybridization with more water rinsings (After Hyb-2) for probe containing either a poly-A spacer or poly-G spacer.

	Before Hyb (DNA strands/cm^2)	**After Hyb-1** (DNA strands/cm^2)	**After Hyb-2** (DNA strands/cm^2)
Poly-A	$1.4 \times 10^{11} \pm 3.3 \times 10^{10}$	$1.2 \times 10^{11} \pm 2.0 \times 10^{10}$	$7.0 \times 10^{10} \pm 2.8 \times 10^{10}$
Poly-G	$2.8 \times 10^{11} \pm 5.1 \times 10^{10}$	$2.1 \times 10^{11} \pm 5.2 \times 10^{10}$	$1.7 \times 10^{11} \pm 1.8 \times 10^{10}$

CHAPTER 6
LANTHANIDE MONOLAYERS AS SUBSTRATES FOR PROTEIN MICROARRAYS – PART 1: PREPARATION OF A ROBUST LANTHANIDE MONOLAYER

Introduction

With the success of DNA microarrays, many scientists are trying to expand this technology to other biomolecules, such as carbohydrates or proteins. Protein microarrays work similarly as DNA microarrays, in that there is a probe molecule immobilized on a surface and a fluorescently labeled target interacts with some of the probes.[75] Thus, the probe target interaction can be followed using fluorescence imaging. The possible uses for protein arrays cover a wide area including antibody-based therapeutics and general laboratory research investigating protein-biomolecule interactions.[76] While the use of DNA microarrays is well established in the laboratory, the science of protein microarrays is still being developed. There are several differences between DNA and proteins that hinder the construction of a universal, protein microarray. Proteins are more complex and diverse than DNA; where one substrate may work with one type of protein, it may not work with another.

In the literature, there are a wide variety of substrates proposed for protein microarrays. These include glass-, gold-, and polymer-based substrates; each has their advantages and disadvantages. Glass slides are generally modified with an alkylalkoxysilane (siloxane), which should provide binding sites and stability from protein denaturation. There are various methods of coupling the proteins on a glass microarray platform, for example, an amine coated slide, which electrostatically binds proteins, or an epoxy coated slide, which covalently binds with Lys, Gln, or Arg in the protein.[76] These examples do not control the orientation of the protein on the surface, which has been shown to play a considerable role in the protein's functionality.[77] To get around this problem, a Ni-NTA (nitrilotriacetic acid) surface has been developed.[78]

The Ni-NTA support binds the protein through a 6-histdine oligomer called histag. With this system, all proteins should be oriented in one known direction. Also, the Ni-NTA surface is very selective for the histagged proteins. There are still some drawbacks with the Ni-NTA surface. One being that the binding of the histag to the nickel is easily reversible; with minor changes in pH or additives, bound protein can wash away.[79]

The chapter describes work towards a proposed new metal-organic substrate and binding tag system to be used for protein microarrays. The substrate will consist of a lanthanide, Tb^{3+}, Eu^{3+}, or Sm^{3+}, monolayer. The probe molecule will then bind to the lanthanide through a sensitizing, binding tag consisting of amino acids. The optimum sequence of amino acids will be determined in the course of the experiments, but will contain tryptophan, which will act as the fluorescence sensitizer to the lanthanide, and either aspartic acid or glutamic acid, which will bind strongly to the lanthanide.

Two different approaches were taken in the development of the lanthanide monolayer. One approach, the Langmuir-Blodgett method, used an alkyl-phosphonate surfactant, which creates a lanthanide-phosphonate network on the surface. The other approach investigated uses self-assembly on a glass surface and a covalent linkage between a siloxane-containing lanthanide-binding ligand (N-trimethoxysilylpropyl)ethylenediamine triacetic acid trisodium salt (EDTA-siloxane) and the glass surface. These concepts are demonstrated in Figure 6-1. There is one report in the literature of using the EDTA-siloxane as a gadolinium chelator in silica nanoparticles.[80]

Lanthanides can be sensitized by a large number of different ligands. In general the ligand is excited and energy transfer occurs from the triplet excited state of the organic ligand to the lower level excited states of the lanthanide, as represented in Figure 6-2. The sensitization of the

lanthanide fluorescence by polypeptides is based on recent literature of lanthanide binding tags. These tags are highly fluorescent and bind strongly to lanthanides.

This microarray system would have several advantages over those currently used. First, each probe molecule will contain this tag, which will give rise to fluorescence once it is bound to the lanthanide, confirming the orientation of the protein on the surface. Second, using the fluorescence of the lanthanide and that of the target fluorophore a ratio can be taken for all spots of the microarray. This will give a ratiometric account of the probe-target interaction strength. Third, the polypeptide tag will be developed to bind strongly to the lanthanides, unlike the Ni-histag system. Finally, because the tag will consist of natural amino acids, the tagged proteins can be synthesized using DNA containing the code for the tag sequence.

Experimental

Materials

The reagents were purchased through commercial sources, except the octadecylphosphonic acid (ODPA) which was synthesized by our collaborators in Dr. Bujoli's laboratory in Nantes, France. (N-trimethoxysilylpropyl)ethylenediamine triacetic acid trisodium salt was purchased from Gelest. To form samarium chloride, HCl was simply added to samarium oxide (Sm_2O_3) and any excess HCl was evaporated off. To form the terbium chloride, terbium oxide (Tb_4O_7) was refluxed in HCl, and any excess HCl was evaporated off.

Lanthanide Phosphonate Langmuir-Blodgett Films

Substrate preparation. Glass microscope slides were used as the supports for most of the experiments. The glass slides were cleaned with piranha etch and the RCA method, and made hydrophobic by treating with a 5mM solution of octadecyltrichlorosilane (OTS) in bicyclohexyl for 2 minutes, rinsing with toluene for 30 seconds, and then drying with N_2. The slides were treated again with the OTS, rinsed with toluene, and finally dried with N_2.

LB film formation. A KSV 2000 LB double-barrier Teflon trough, purchased from KSV Instruments (Stratford, CT), was used to form the ODPA monolayers at the air-water interface. A filter-paper Wilhelmy balance attached to a KSV microbalance was used to measure surface pressure.

The lanthanide-phosphonate films were made by first spreading a 0.3 mg/mL solution of ODPA in chloroform on a 2.6 mM aqueous $CaCl_2$ subphase, which had a pH adjusted to 7.8 using a KOH solution. The ODPA was compressed at the rate of 10 mm/min to a pressure of 20 mN/mm. Once the target pressure was reached, a hydrophobic glass slide was dipped 50mm into the subphase at a rate of 8 mm/min. The slide was then lowered into a glass vial in the trough. A volume of the lanthanide chloride solution was added to the vial with the OPDA coated slide to reach a concentration of 1.5 mM of Ln^{3+} in the vial with the slide. The slides sat for at least 7 days in the Ln^{3+} solution. If the slides were not used right away, they were stored in a 1.5 mM, pH 6 Ln^{3+} solution until later use. Before this previous procedure was tried, we also attempted to make the films by incorporating the lanthanide ion in the subphase, but we did not find much success with this method.

Self-Assembled Lanthanide Films

Glass supports were cleaned using the RCA cleaning method and piranha etch. They were then submerged in a solution containing 4% EDTA-siloxane, 0.086 M Tb^{3+}, and 0.02% acetic acid. The slides were heated overnight at 90°C. The EDTA-siloxane solution was poured out. The slides were rinsed 2 times with water and then sonicated with more fresh water and finally rinsed 2 more times with water. The slides were stored in water until later use.

To test the stability of the film, when exposed to different chelating ligands, the slides were submerged in either a 1 mM, pH 10 dipicolinic acid solution; 1 mM, pH 7.5 picolinic acid; 1 mM, pH 9.5 picolinic acid.

Analysis

XPS was performed using a UHV XPS/ESCA PHI 5100 system. Survey scans were taken with either a Mg or Al Kα X-ray source using a power setting of 300 W, a pass energy of 89.4 eV and a take off angle of 45° with respect to the surface. Using commercial XPS analysis software and Shirley background subtraction, the peak areas were determined. The elemental percentages were determined using the peak areas and sensitivity factors given by the maker of the XPS instrument. Tapping-mode AFM was carried out on air-dried samples using a Multimode AFM with a Nanoscope IIIa controller (Digital Instruments, Santa Barbara, CA) and commercially available silicon cantilever probes (Nanosensors, Phoenix, AZ).

Results and Discussion

Langmuir-Blodgett Lanthanide Monolayers

The general procedure for making the lanthanide LB films is shown in Figure 6-3. The transfer ratios of ODPA onto the OTS coated slides were always around unity. After one week of sitting in the Ln^{3+} solutions, the slides were taken out of the solution and were observed for hydrophilicity. If a slide did not appear hydrophilic over the entire 5 cm where the film was supposed to be, it was considered "bad" and the slide was discarded. Both the samarium films and terbium films exhibited hydrophilicity where the film should have been. This was the first indication that the terbium and samarium had formed metal-phosphonate monolayers. Only the films that were continuously hydrophilic were analyzed further.

The purpose of the Ca^{2+} in the subphase is to supply stability by forming a weak network with the phosphonate groups, which aids the transfer of the ODPA onto the slide. The Ca^{2+}

should be replaced by the other metal ion, *i.e.* samarium, or terbium, while the slide sits in the metal ion solution. In the analysis of the samarium and terbium-phosphonate monolayers, the XPS data provides information into whether there is residual Ca^{2+} in the film and whether there is an equal elemental percentage of phosphorus and lanthanide. The XPS images in Figure 6-4 give the elemental percentages for the samarium-phosphonate and terbium-phosphonate films. First, the samarium-phosphonate film does not appear to have any calcium, which would give rise to a Ca 2p3 peak around 346-347 eV. Furthermore, the XPS results for the samarium-phosphonate film give the ratio of samarium to phosphorus at 1.2:1. These results are based on the Sm 4d peak and the P 2s peak.

For the terbium-phosphonate films, first, there is no Ca 2p peak around 346 eV. On the other hand, the terbium to phosphorous ratios are about 43:1 calculated using the Tb 3d5 and P 2p3 peaks. The high percentage of terbium is an indication that there is more than just a monolayer of it. There are other indicators of this including the attenuation of the Si 2p3 peak from the glass support in the terbium films as compared to the Si 2p3 peak in the samarium-phosphonate films. The peaks from silicon will be more attenuated as the terbium overlayer thickness increases. Overall, this indicates that the film does not consist only of a terbium-phosphonate monolayer. Most likely, there is a precipitation of terbium oxide/hydroxide on the surface. Whether there is a terbium-phosphonate layer underneath the terbium oxide/hydroxide is unclear from the XPS results.

The AFM images (Figure 6-5) support the XPS results. An AFM image of a zirconium-phosphonate film is shown for reference. The film is smooth with some holes, which allow depth analysis. The holes in the zirconium-phosphonate film have a depth of 25 Å. This corresponds to the height of the ODPA and zirconium layer. The samarium-phosphonate film is

not as smooth as the zirconium-phosphonate film, but does have the same topography as seen with the zirconium-phosphonate films and does have a film height of approximately 25 Å. The terbium film appears smooth, but it does not have the typical topography that the samarium and zirconium-phosphonate films have, which not only makes it difficult to measure the height of the film. The topography and XPS results indicate that a monolayer of terbium is not being achieved, but most likely a terbium oxide/hydroxide film is forming on the slide.

Currently, samarium and terbium are the only lanthanides that have been investigated for forming a metal-phosphonate monolayer. Because the lanthanides exhibit similar chemical properties, the binding behavior of the lanthanides should be similar. For this reason, if a method to make a lanthanide-phosphonate monolayer works with one lanthanide, it should work with the other lanthanides.

The zirconium-phosphonate films are stored in water after the formation of the film, but the samarium-phosphonate films do not appear to be stable in water. Although, there is no data to quantify this, it is obvious that the samarium-phosphonate films loose their hydrophilicity after sitting in water for several hours. This suggests that the samarium is dissolving off the phosphonate headgroup. Without the network of metal ions at the surface, the monolayer is no longer as robust and washes off the OTS coated support. The samarium-phosphonate films do appear stable, *i.e.* they do not loose their hydrophilicity, if they are sitting in a 3 mM, pH 6 Sm^{3+} solution.

Self-Assembled Lanthanide Films on Glass

Based on the lanthanide-phosphonate films, a more stable system was needed that would not dissolve in water. One way to resolve this problem was to use a ligand covalently linked to the glass support that could also bind the lanthanide. The commercially available EDTA-siloxane was a relatively inexpensive and convenient answer to this problem. Also, the

preparation of the EDTA-lanthanide coated slide was a simple process. There were two possible methods for immobilizing the EDTA-lanthanide complex. The EDTA-siloxane could first be immobilized on the surface and then the surface could be exposed to a lanthanide solution. The other possibility is to first prepare the EDTA-lanthanide complex in solution and then immobilize this on the surface. The latter method was used, even though there might be a possibility of having more than one EDTA-siloxane per lanthanide, because it was thought a higher lanthanide surface concentration would be obtained this way. Terbium was used in these experiments.

The XPS survey spectrum of the lanthanide-EDTA siloxane complex immobilized on glass is shown in Figure 6-6. The XPS spectra are labeled with elemental percentages. In the lanthanide-EDTA film the elemental percentages that give information about the film are the nitrogen: 2.6%, carbon: 28.1%, sodium: 0.5%, terbium: 11.1%, and silicon: 10.7%. An XPS survey spectrum of bare glass, gives a silicon percentage of 25.5 % and carbon percentage of 8.6%. The attenuation of the silicon peak with the lanthanide-EDTA film is one of the first indications that film formation was successful. The carbon on bare glass is due to adventitious carbon contamination. If the carbon contamination is taken into account, the nitrogen to carbon works out to be approximately 1:7, the expected ratio of the EDTA-siloxane based on the molecular formula. However, the terbium to nitrogen ratio is higher than expected. We would expect the terbium to nitrogen ratio to be about 1:2, but ratio turns out to be around 4:1. It is possible this is due to a formation of a thin layer of terbium oxide on surface.

Three different solutions were investigated to determine robustness of the lanthanide film to the chelators dipicolinic and picolinic acid (Figure 6-7). These three solutions were 1 mM, pH 10 picolinic acid; 1 mM, pH 9.5 picolinic acid; and 1 mM, pH 7 picolinic acid. Based on the

literature, dipicolinic acid binds strongly to terbium in a wide pH range, but more strongly at a higher pH, around 10 or 11.[81] Picolinic acid binds less strongly to terbium and in a narrower pH range, with a maximum around 7 or 8.[81] After the lanthanide-EDTA surface is treated with pH 10, 1 mM picolinic acid, it can be seen that the terbium peaks are no longer present in the XPS spectrum (Figure 6-8). It appears that the dipicolinic acid is pulling the terbium off the surface. After the lanthanide-EDTA surface is treated with 1 mM, pH 9.5 picolinic acid, a good portion of the terbium remains on the surface, with the terbium to nitrogen ratio at 1:1 (Figure 6-9). Again, this ratio is still higher than the expected ratio of 1:2. When 1 mM, pH 7 picolinic acid is used, a larger decrease in terbium is seen, with the terbium to nitrogen ratio at 1:1.5 (Figure 6-10). However, the terbium to nitrogen ratio is still higher than the expected 1:2. At pH 7, the literature shows that the terbium-picolinic acid interaction is much greater than at pH 9.5.[81]

The XPS data shows that when the lanthanide-EDTA slide is placed in a solution of an efficient chelator, such as dipicolinic acid, the terbium is stripped off the surface. When a weaker chelator is used, picolinic acid, pH 9.5, more of the terbium stays on the surface. Also, a slight decrease in the nitrogen signal is seen after treatment with the two more efficient chelators. The terbium-EDTA film has a nitrogen percentage of 2.6%, after treatment with pH 7 picolinic acid the nitrogen decreases to 1.8% and after treatment with the dipicolinic acid the percentage decreases to 1.1%. This shows that with the terbium some of the EDTA-siloxane is coming off, which may inidicate that the terbium is binding more than one EDTA-siloxane. If the terbium binds more than one EDTA-siloxane, it is unlikely that more than one EDTA-siloxane is bound to the glass. Therefore, the EDTA-siloxane which is not bound to the glass, comes off with the terbium.

These studies demonstrate that a terbium EDTA-siloxane surface was prepared on a glass support. The terbium EDTA monolayer is stable in water and some weakly chelating solutions. However, when the surface is placed in a solution of a ligand which binds efficiently to the terbium, the ligand strips the terbium from the EDTA. Most likely, the EDTA ligand is a stronger chelator than dipicolinic acid, but because there is so much more of the dipicolinic acid, the terbium is taken off the slide by the dipicolinic acid. It would be interesting to try a chelating ligand, such as dipicolinic acid, at a much smaller volume and concentration, similar to that used when spotting proteins for microarrays. It should be mentioned that preliminary fluorescence spectroscopy was attempted with the picolinic and dipicolinic treated slides. However, no appreciable luminescence was seen. It is possible to try an even stronger chelating ligand to hold the terbium on the surface. Nevertheless, the lanthanide needs binding sites left available for the lanthanide binding tag on the protein.

Conclusion and Remarks

A method for making samarium phosphonate monolayers was developed, which with minimal changes should be applicable to other lanthanides. Preliminary experiments were tried with terbium, but it appears to be forming more than a monolayer. Most likely with the right conditions a terbium-phosphonate monolayer should form. The samarium films appear to have inferior stability, they dissolve in water, compared to the zirconium-phosphonate films, but do appear stable in a Sm^{3+} solution.

More stable lanthanide films were made using terbium and an EDTA-siloxane. These films proved stable in water, but when placed in a solution of an efficient chelating ligand, the terbium was removed from the film. It would be interesting to investigate the stability of the terbium, when a much smaller volume and concentration, similar to that used with the microarray spotting of proteins.

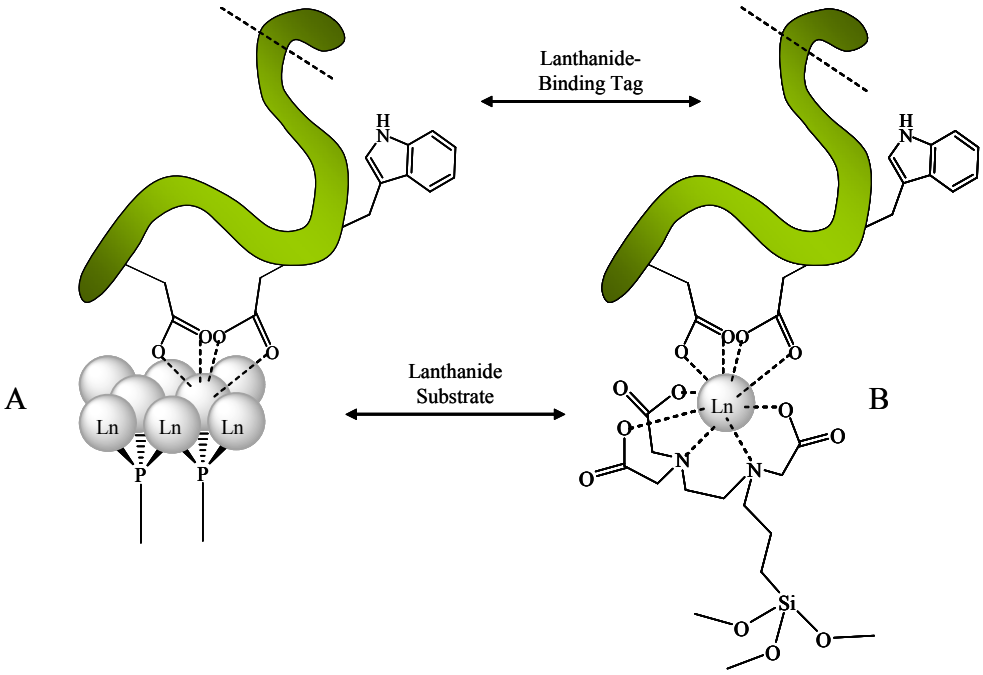

Figure 6-1. Two approaches explored here to prepare a lanthanide substrate for protein binding microarrays. A) The Langmuir-Blodgett method for preparing the substrate. B) The self-assembly method using a siloxane-containing lanthanide-binding ligand. The molecule binding to the lanthanide is a hypothetical illustration of a polypeptide binding to the lanthanide substrate.

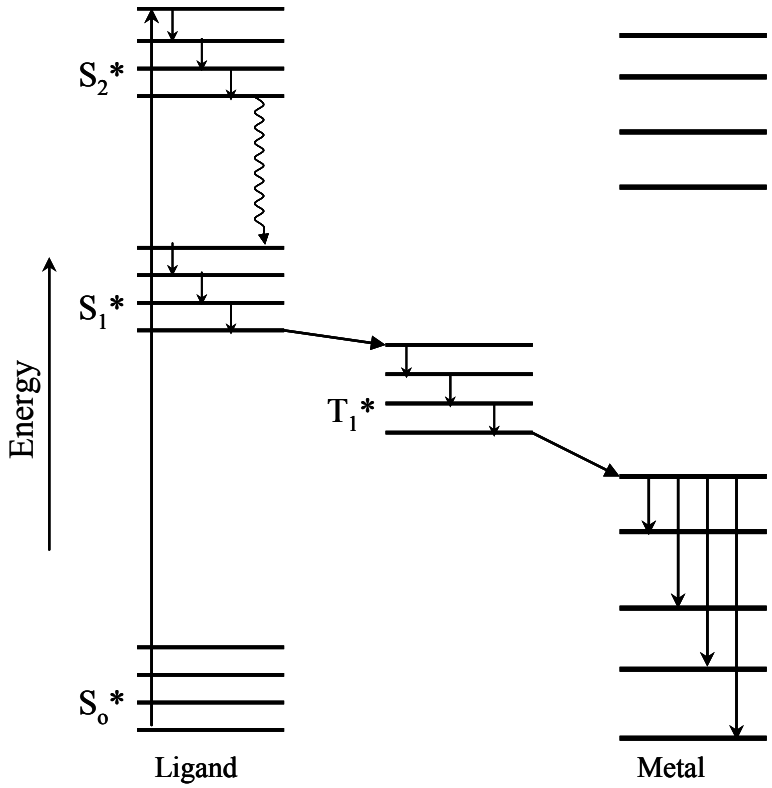

Figure 6-2. The intramolecular energy transfer that can occur between a ligand and lanthanide.

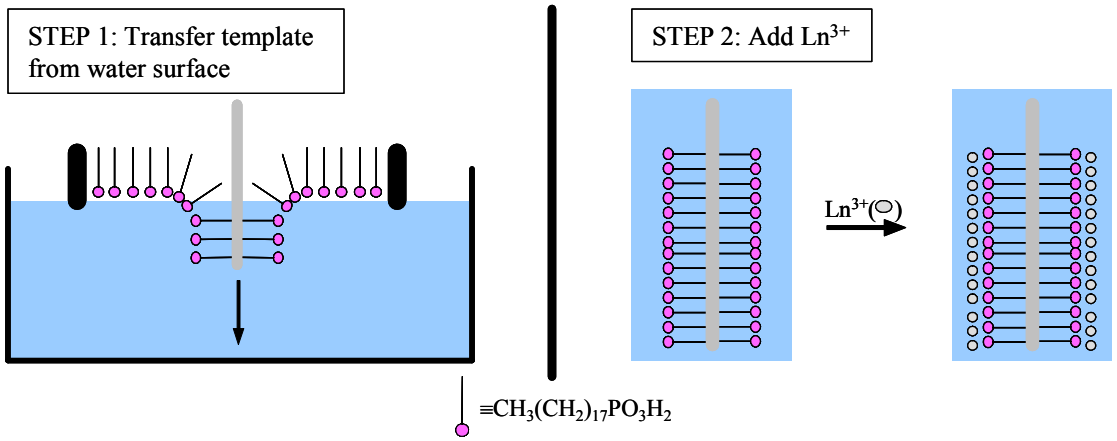

Figure 6-3. Procedure of the Langmuir-Blodgett method used to make the metal-phosphonate monolayers. Note that for clarity the Ca^{2+} in the subphase is not shown in the figure.

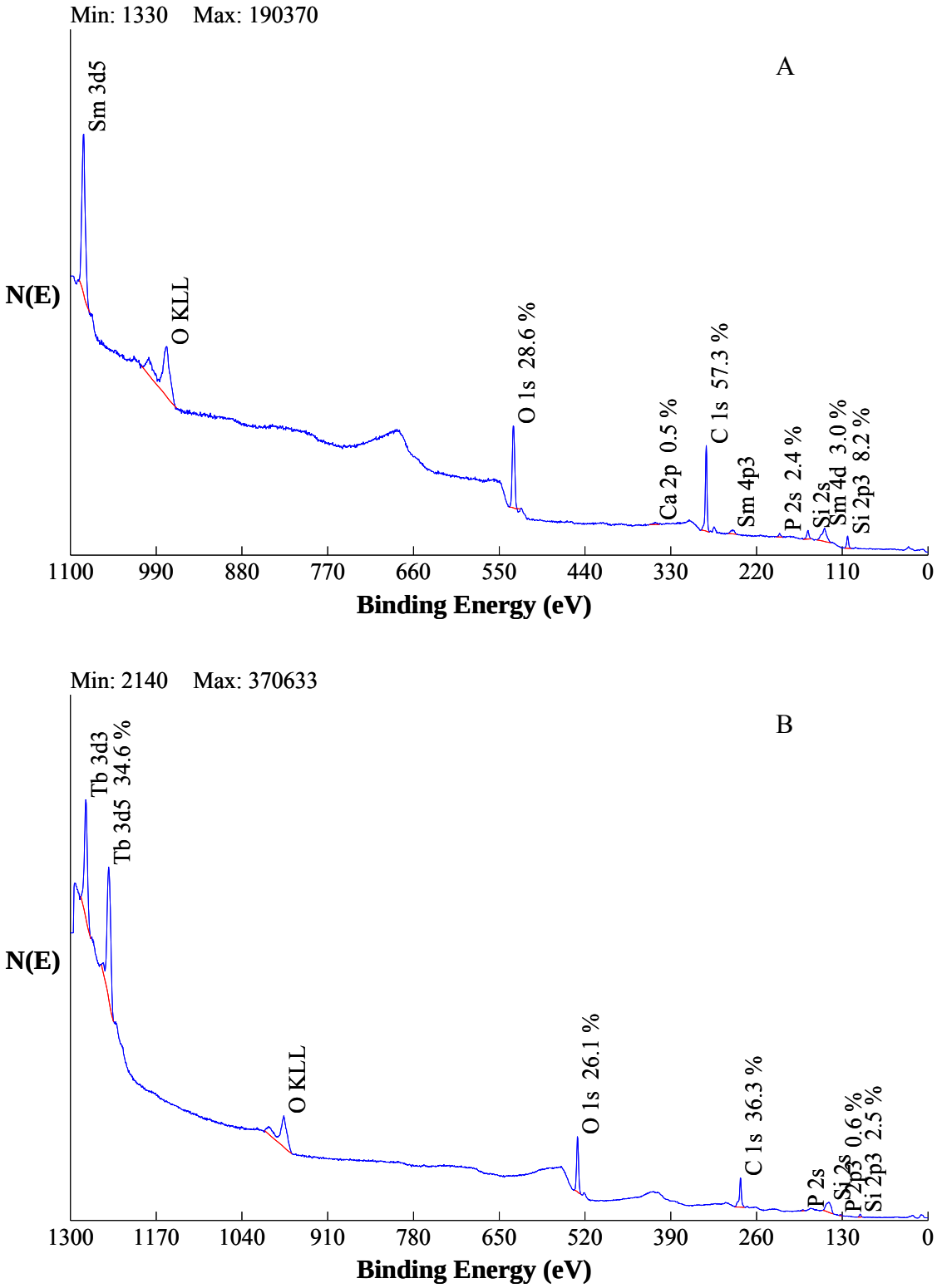

Figure 6-4. XPS survey scan of lanthanide phosphonate films. A) Samarium-phosphonate film. B) Terbium-phosphonate film.

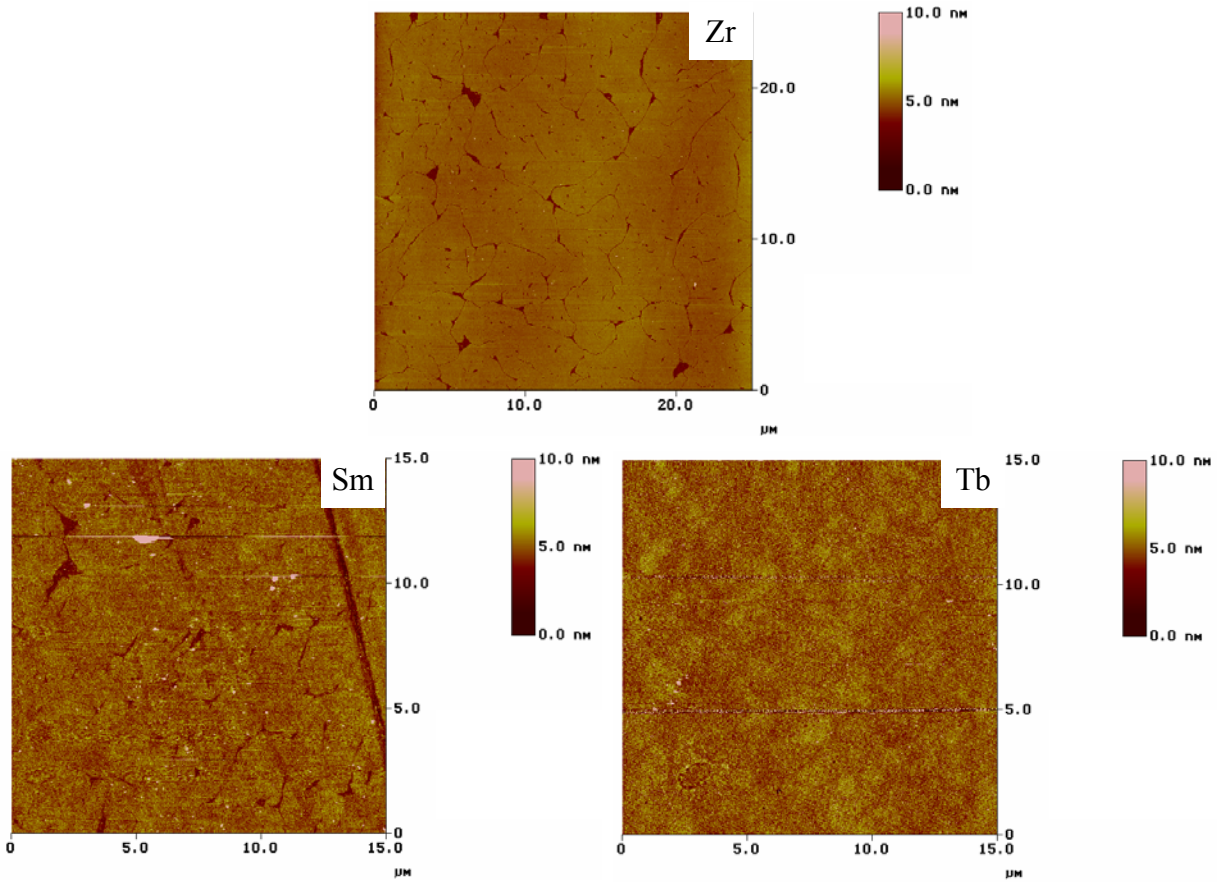

Figure 6-5. AFM images of zirconium, samarium, and terbium phosphonate films

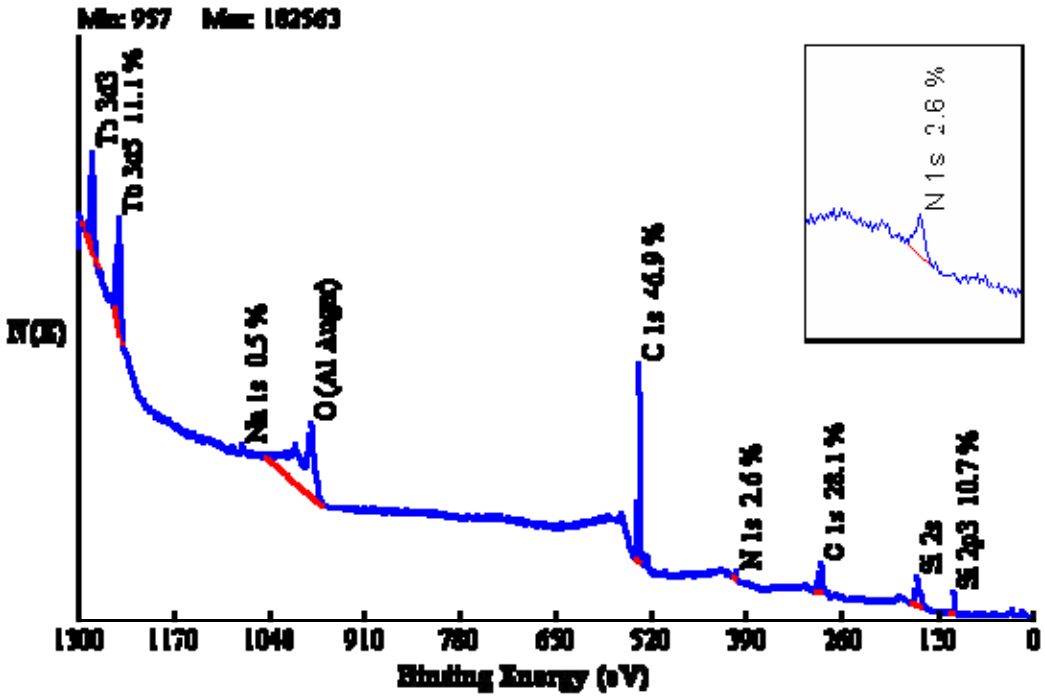

Figure 6-6. XPS spectrum of self-assembled EDTA-siloxane lanthanide film. The insert is a magnification of the N 1s region.

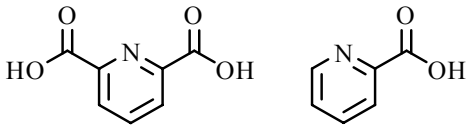

Dipicolinic Acid Picolinic Acid

Figure 6-7. Molecular structure of dipicolinic acid and picolinic acid.

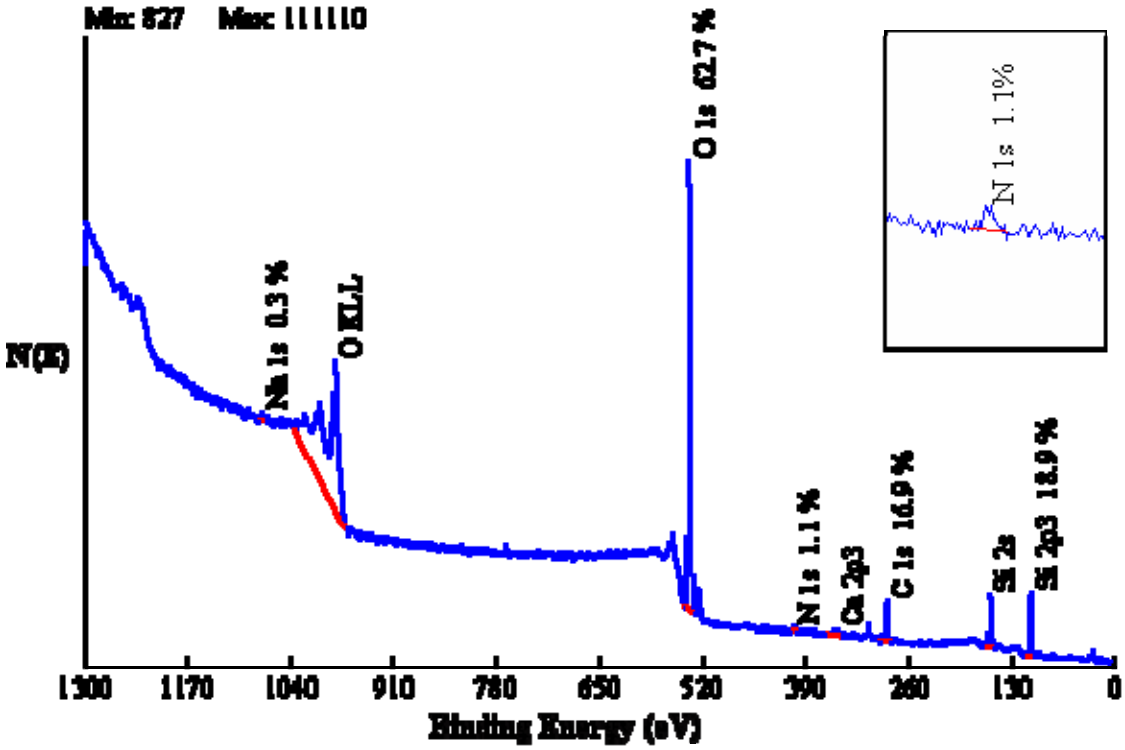

Figure 6-8. XPS spectrum of self-assembled EDTA-siloxane lanthanide film after treatment with dipicolinic acid. The insert is a magnification of the N 1s region.

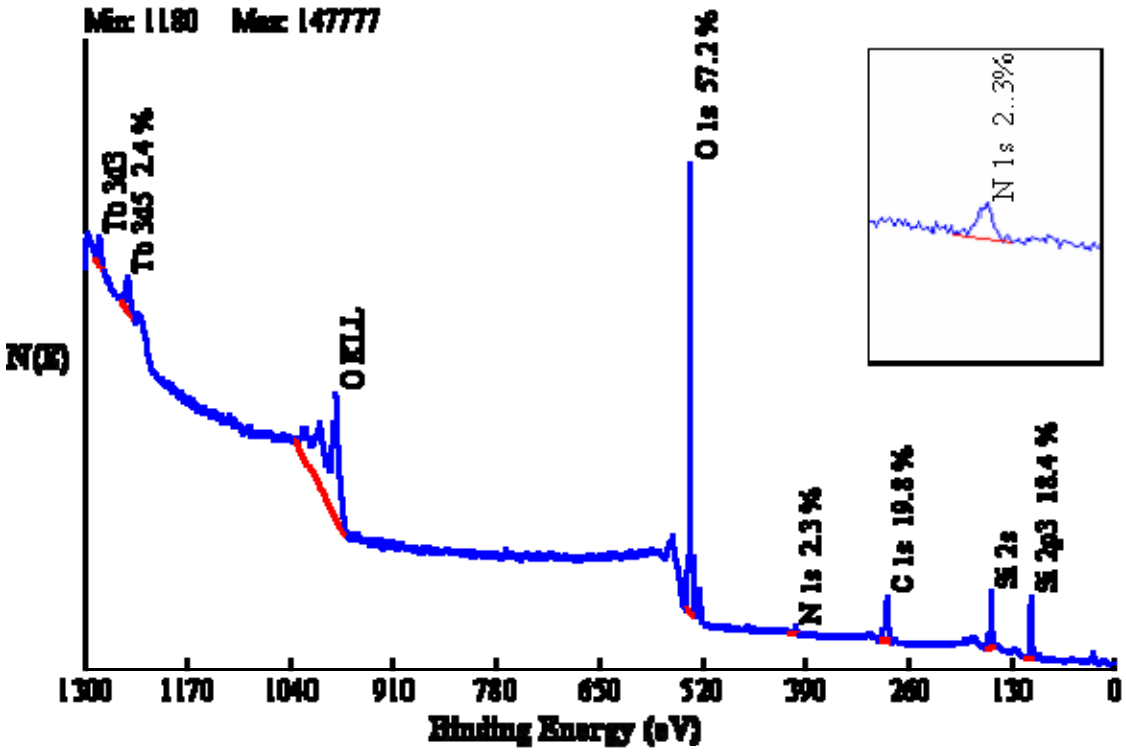

Figure 6-9. XPS spectrum of self-assembled EDTA-siloxane lanthanide film after treatment with pH 9.5 picolinic acid. The insert is a magnification of the N 1s region.

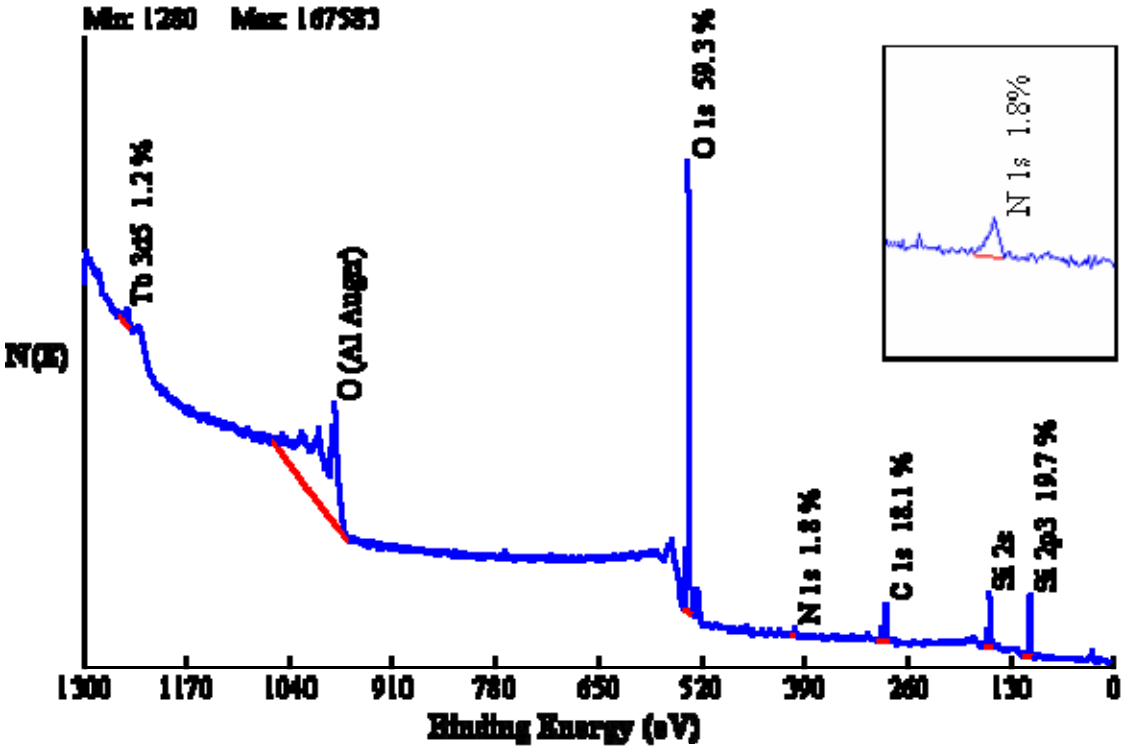

Figure 6-10. XPS spectrum of self-assembled EDTA-siloxane lanthanide film after treatment with pH 7 picolinic acid. The insert is a magnification of the N 1s region.

CHAPTER 7
LANTHANIDE MONOLAYERS AS SUBSTRATES FOR PROTEIN MICROARRAYS – PART 2: A MODEL STUDY

Introduction

It has been known for quite some time that certain ligands can bind to lanthanides and through an intramolecular energy transfer from the ligand to the lanthanide, a dramatic increase in luminsence from the lanthanide can be seen.[82] This energy transfer occurs from the triplet excited state of the organic ligand to the lower level excited states of the lanthanide, as represented in Figure 6-2. The possible use of lanthanides as luminescent indicators of protein binding to surfaces, as shown in Chapter 6, brought up the question of the luminescent behavior of lanthanides in a monolayer. A project was developed to study the ligand-enhanced luminescent behavior of lanthanides at the air solid interface.

The aim of this project was to investigate the luminescent behavior of a monolayer of sensitized lanthanides on a glass surface. Specifically, we wanted to study the intermolecular energy transfer from one lanthanide to a different lanthanide, such as from terbium to europium. One of the first studies of lanthanide intermolecular transfer was done in dimethyl sulfoxide between europium and terbium.[83] It is thought that in solution it is necessary for the lanthanides to form polymeric structures, or in other words to share ligands, in order for the intermolecular lanthanide energy transfer to occur.[81] However, there has been one group to study this intermolecular lanthanide ion energy transfer in multilayer LB (Langmuir-Blodgett) films, where the lanthanides are not apparently sharing ligands.[84] To perform this study they used films of different molar percentages of $Eu(TTA)_3Phen$ (TTA=2-thenoyltrifluoroacetone; Phen=1,10-phenanthroline) with $Gd(TTA)_3Phen$ coexisting with arachidic acid. They developed a model of their system called "active enhancement circle," which showed that there is must be a minimum distance between the donor and acceptor for the energy transfer to occur. In the case of

gadolinium and europium, they found this distance to be 1.2 nm. From previous research it was already known that the energy was transfer from the donor to the acceptor ion through a triplet excited state of TTA.[85] In addition to this energy transfer study, there have been a number of other studies that have looked at the luminescence of lanthanides in LB monolayers and thin films.[86, 87]

In this project, we are attempting a similar study, but using self assembly on a glass surface to make the lanthanide monolayer and also using a different ligand system. The first part of the project involved the development of a ligand that would hold the lanthanides on a surface and sensitize the luminescence through an intramolecular energy transfer from the ligand to the lanthanide ion. The second part of the project would be studying the luminescence behavior of mixed lanthanide monolayers made various ways. The lanthanide ratios would be varied as well as the surface density. The surface modification and lanthanide ratios would be followed with XPS. The ligand that was chosen for this system contains a chelidamic acid moiety (4-hydroxypyridine-2,6-dicarboxylic acid) which closely resembles the well known sensitizer of lanthanides, dipicolinic acid (pyridine-2,6-dicarboxylic acid) (Figure 7-1).[81] Several different routes, as shown in Figure 7-2, were explored to find a suitable ligand, which contained the chelidamic acid moiety and would react with an amine-reactive modified glass surface or directly with a glass surface. Unfortunately, this ligand in pure form has not yet been synthesized. This rest of this chapter outlines the procedures for the reactions that were attempted and a short explanation of the different synthetic routes.

Experimental

Reagents were ordered from Acros or Aldrich and used without further purification, except when stated. Samarium oxide was converted into the chloride by treating with concentrated HCl.

Diethyl 2,4,6-trioxoheptanedioate (1). The synthesis for **1** and **2** was taken from Riegel *et al.*[88] 250 mL of ethanol was distilled over Na into a 3-neck round bottom flask under argon. A condenser under argon was added to the 3-neck flask and then 16.2 g (0.7 moles) of sodium was added slowly to the ethanol. The sodium and ethanol were allowed to react to completion with heating at the end. Using a large graduated pipet, 100 mL of the sodium ethoxide solution was transferred to another 3-neck round bottom under argon. The remaining 150 mL was kept warm. To the 100-mL sodium ethoxide, 50 g (0.34 moles) of diethyl oxalate and 19.7 g (0.34 moles) of acetone was added with stirring, which resulted in rapid precipitation of a very thick yellow solid. Then, 50 g (0.34 moles) of diethyl oxalate was added with stirring to the remaining 150 mL of the sodium ethoxide solution and finally this solution was added to the sodium ethoxide/acetone/diethyloxalate flask. This thick mixture was stirred for 1 hour and then the ethanol was taken off under vacuum until dry. To the dark greenish-yellow solid was added ~350 g of ice and 100 mL of concentrated HCl. This yellow slurry was stirred so that all the clumps were broken up and then the yellow paste was filtered, washed several more times with ice water until a pale yellow paste was obtained and then dried under vacuum. These procedures gave 70 g of crude product (~ 80% yield). ^{1}H (300 MHz, $CDCl_3$) δ_H: 6.9 (s). ^{13}C (75 MHz, $CDCl_3$) δ_C: 14.51, 63.24, 104.46. 162.34.

4-Oxo-4H-pyran-2,6-dicarboxylic acid (chelidonic acid) **(2)**. In a 200mL round bottom flask, with an attached reflux condenser, was added 70 g (0.27 moles) of **1** and 100 mL of concentrated HCl. This mixture was refluxed at 100°C for 20 hours. The reaction was allowed to cool to room temperature and 100 g of ice was added. The precipitate was filtered and washed several times with 30 mL of cold water. The pink solid was dried under vacuum. 29 g (56%

yield). ^{1}H (300 MHz, DMSO-d_6) δ_H: 6.9784. ^{13}C (75 MHz, DMSO-d_6) δ_C: 119.71, 154.71, 161.55, 180.11.

4-Hydroxypyridine-2,6-dicarboxylic acid (chelidamic acid) **(3)**. The synthesis for 3 was taken from King *et al.*[89] In a 250-mL round bottom flask was added 29 g of 2 and 155 mL of 10% NH4OH was added. This solution was allowed to reflux for 4 hours and with each hour, 8.5 mL of concentrated NH4OH was added. The water was removed under vacuum, followed by the addition of 150 mL of cold water and 25 mL of concentrated HCl. The beige precipitate was filtered and washed several times with cold water. ^{1}H (300 MHz, DMSO-d_6) δ_H: 7.60 (s). ^{13}C (75 MHz, DMSO-d_6) δ_C: 110.91, 145.33, 161.47, 162.67.

Diethyl 4-hydroxypyridine-2,6-dicarboxylate (4). The synthesis for **4** and **5** were taken from Cooper *et al.*[90] In a 100-mL flask with an attached reflux condenser was added 25mL 100% ethanol at 0°C under N_2. To the same flask was slowly added 6.2 mL (85 mmol) of thionyl chloride with stirring. Then 2.5 g (13.7 mmol) of **3** was added. This solution was stirred at room temperature for 18 hours and then refluxed for 2 hours. The solvent was removed under reduced pressure, followed by the addition of 20 mL cold water. The solution was neutralized with 5 mL of cold 10% aqueous Na_2CO_3, upon which a light beige precipitate formed, and then 5 mL of cold 50% aqueous ethanol. The solution was allowed to stir overnight, so that the precipitate was less clumpy. 3.24 g (96% yield). ^{1}H (300 MHz, $CDCl_3$) δ_H: 1.42 (t, 6H), 4.47 (q, 4H), 7.34 (bs).

Diethyl 4-(10-bromodecyloxy)pyridine-2,6-dicarboxylate (5). 100 mL of acetone was distilled over anhydrous K_2CO_3 into a 250-mL flask containing 2.5 g (10.4 mmol) of **4** and 6.3 mL of 1,10-dibromodecane. To this solution was added 2.32 g of K_2CO_3. This solution was allowed to reflux for 40 hours under argon while following with TLC, after which the solvent

was removed under reduced pressure. The oil was purified using a column chromatography with silica as the stationary phase. Hexane was used to elute the excess 1,10-dibromodecane, which was followed with methylene chloride to elute the product. The solvent was removed with rotary evaporation to give a pale yellow oil. 2.5 g (53% yield). ^{1}H (300 MHz, $CDCl_3$) δ_H: 1.39 (m, 18H), 1.85 (m, 4H), 3.41 (t, 2H), 4.13 (t, 2H), 4.47 (q, 4H). ^{13}C (75 MHz, $CDCl_3$) δ_C: 14.40, 26.01, 28.36, 28.92, 29.38, 29.51, 29.56, 62.57, 69.20, 114.59, 150.23, 165.01, 167.23.

Diethyl 4-(10-cyanodecyloxy)pyridine-2,6-dicarboxylate (6). The synthesis for **6** was adapted from information given by Vogel.[91] Into a 3-neck flask, was distilled under reduced pressure 15 mL of DMF dried over anhydrous $MgSO_4$. To the same flask was added 1.5 g (3.3 mmol) of **5**, which was followed with the addition of 0.7 g (10.75 mmol) of potassium cyanide. This solution was allowed to stir for 2 hours. To the DMF solution was added 10 mL of water and then this solution was extracted 3 times with 20 mL of a 1:1 mixture of diethyl ether and petroleum ether. The organic phase was washed 2 times with 30 mL of brine and then dried with $MgSO_4$. The organic phase was retained and the solvent was removed by rotary evaporation. 0.25 g (18% yield). ^{1}H (300 MHz, $CDCl_3$) δ_H: 1.40 (m, 18H), 1.65 (m, 2H), 1.83 (m, 2H), 2.34 (t, 2H), 4.13 (t, 2H), 4.47 (q, 4H), 7.77 (s, 2H). ^{13}C (300 MHz, $CDCl_3$) δ_C: 14.43, 26.05, 28.34, 28.95, 29.40, 29.54, 29.59, 33.03, 34.24, 62.60, 69.21, 114.55, 150.27, 165.05, 167.26.

Diethyl 4-(11-aminoundecyloxy)pyridine-2,6-dicarboxylate (7). The synthesis for **7** was adapted from a procedure shown by Borkowski *et al.*[92] The reduction of the nitrile was attempted using a Co^{2+} and $NaBH_4$ mixture. In 21 mL of 100% ethanol, 0.25 g (0.62 mmols) of **6** was dissolved. To the solution was added 0.24 g of $CoCl_2 \cdot 6H_2O$. The cobalt was allowed to dissolve and then 0.21 g of $NaBH_4$ was added to the solution. After the reaction had stirred for 3 hours, 3 M HCl was added until all of the solid dissolved. The solution was extracted twice with

10 mL of diethyl ether. The aqueous phase was basified with concentrated NH_4OH and then extracted with 4 10-mL portions of diethyl ether. After extracting the organic phase with an equal volume of brine, it was dried with $MgSO_4$. Finally, the solvent was removed under reduced pressure. Only a small amount of a residue was obtained as a product, and an NMR taken in $CDCl_3$ showed significant degradation of the parent molecule.

Diethyl 4-(10-azidodecyloxy)pyridine-2,6-dicarboxylate (8). The synthesis for **8** was adapted from a procedure written by Roy *et al.*[93] In a round bottom flask under argon, 1.5 g (3.3 mmols) of **5** was dissolved in 30 mL of dry DMF. To this was added 0.29 g (4.4 mmols) of sodium azide and the flask was heated at 90°C for 14 hours. After the reaction had cooled to about 50°C, the DMF was removed under vacuum. To the residue was added 15 mL of diethyl ether and 20 mL of water. The aqueous portion was extracted twice with 15 mL of diethyl ether and then the combined diethyl ether extractions were extracted once with 30 mL of water and once with 30 mL of brine. After which, the organic portion was dried with $MgSO_4$, filtered, and rotary evaporated. This gave 1 g (75% yield) of a viscous oil. ^1H (300 MHz, $CDCl_3$) δ_H: 1.37 (m, 18H), 1.58 (m, 2H), 1.82 (m, 2H), 3.24 (t, 2H), 4.12 (t, 2H) 4.46 (q, 4H), 7.76 (s, 2H). ^{13}C (300 MHz, $CDCl_3$) δ_C: 14.44, 26.06, 26.93, 28.96, 29.05, 29.33, 29.41, 29.58, 51.67, 62.59, 69.21, 114.83, 150.34, 164.81, 167.30.

Diethyl 4-(10-aminodecyloxy)pyridine-2,6-dicarboxylate (9). Several methods were explored for the reduction of the azide to an amine. The first method employed H_2 gas and 10% palladium on carbon catalyst, which was adapted from a procedure written by Roy *et al.*[93] To use this method, a 3 neck flask containing 0.06 g of 10% Pd/C with a glass tube to disperse the H_2 was evacuated and purged with N_2 several times. Then, it was evacuated and filled with H_2, which was followed with the injection of 0.5 g (1.3 mmols) of **8** and 1 mole equivalent of HCl

dissolved in 20 mL of methanol. The reaction was stirred with H_2 bubbling for 45 minutes. The material was filtered over celite and the solvent was removed using rotary evaporation. ^{1}H NMR was taken in $CDCl_3$, and although an α-NH_3 peak with a δ_H of 2.94 ppm was seen, degradation of parent compound could be observed by the appearance of multiple aromatic groups.

The second method used the Staudinger procedure, which was adapted from a procedure written by Somfai *et al.*[94] For this method, 0.50 g (1.3 mmols) of **8** was dissolved in 20 mL of 10:1 THF and water and then 382 mg (1.4 mmoles) of triphenylphosphine was added. The solution was allowed to stir overnight, after which the solvent was removed under reduced pressure. Purification was attempted using a minicolumn made with a small glass frit funnel and silica gel. First 150 mL of ethyl acetate was run through the column, followed by a mixture of 10:0.1 methanol:NH_4OH. A very sticky residue was obtained. By ^{1}H NMR, taken in $CDCl_3$, it was seen to contain a significant amount of the triphenylphosphine.

The third method, which used zinc powder, was adapted from a procedure written by Lin *et al.*[95] First, 1.0 g (2.4 mmols) of **8** was dissolved in 3:1 ethanol:water solution. To this solution was added with stirring, 0.29 g of ammonium chloride, which was followed by the addition of 0.300 g of zinc powder. The solution was refluxed for 15 minutes and then filtered to remove the remaining zinc powder. Extraction with dichloromethane was attempted, but at this point a gooey precipitate had formed. This precipitate was washed with HCl and H_2O extensively. The precipitate was dried under vacuum to form a white powder. ^{1}H (300 MHz, D_2O) δ_H: 1.21 (m, 13H), 1.81 (m, 2H), 2.61 (t, 2H), 4.22 (t, 2H), 7.54 (s, 2H)

Diethyl 4-(10-(3-triethoxysilyl)propylamino)decyloxy)pyridine-2,6-dicarboxylate (10). In 30 mL of dry dichloromethane, 0.5 g (1.2 mmoles) of **5** and 0.179 g (1.0 mmoles) of 3-aminopropyltriethoxysilane (APTES) was added under N_2. The solution was allowed to reflux

for 3 days, after which, 10 mL more dichloromethane was added and it was filtered 3 times over celite. The solvent was then removed using rotary evaporation. An ^{1}H NMR was taken which showed that there was likely the desired product mixed with a single by-product.

Diethyl 4(3-(trimethoxysilyl)propylcarbamoyloxy)pyridine-2,6-dicarboxylate (11). To make this molecule two different methods were explored. The first method, adapted from Lenaerts *et al.*,[86] used 0.25 g of **4** and 5 mL of triethoxy(3-isocyanatopropyl)silane. The reaction was performed neat with heating at 85°C for 72 hours. Precipitation was attempted out of cold hexane, heptane, and petane, but none of these solvents resulted in precipitation.

The other condition tried, which was adapted from Cui *et al.*,[96] used 0.30 g (1.25 mmoles) of **4** and 0.34 mL (1.375 mmols) of triethoxy(3-isocyanatopropyl)silane and 1 drop of triethylamine in THF. The solution was reluxed at 80°C for 48 hours. The material was filtered through celite and the solvent was removed with rotary evaporation. An ^{1}H NMR in $CDCl_3$ was taken which showed many by products and no clear product.

Diethyl 4-(3-(trimethoxysilyl)propoxy)pyridine-2,6-dicarboxylate (12). For this reaction 1.5 g (5.2 mmols) of (3-iodopropyl)trimethoxysilane and 0.5 g (2.1 mmols) of **4** was dissolved in 30 mL of dichloromethane with 0.37 g of anhydrous K_2CO_3. This was refluxed for 2 days, after which, it was filtered through celite using dichloromethane. An ^{1}H NMR was taken in $CDCl_3$ which showed no real product.

Slide modification. Epoxide coated slides were made using glass slides freshly cleaned with the RCA and then piranha cleaning solutions (See the Experimental section of Chapter 2). The glass slides were placed in a 10% v/v solution of glycidyloxypropyl trimethoxysilane and toluene. The slides sat in this solution overnight after which they were washed twice with toluene, sonicated in toluene for 15 minutes and then washed again two times more with toluene.

Immobilization of **9** complexed with Sm^{3+} was performed on an epoxide modified slide. To do this a 6.0×10^{-4} M and 2.0×10^{-4} M solution of **9** and Sm^{3+}, respectively was prepared at pH 11. The epoxide slide was then submerged in this solution overnight at 42°C. The slide was then washed repeatedly with water, however, a solid could still be see on the surface of the glass.

Results and Discussion

The first area of synthesis focused on making an amine modified chelidamic acid, which would chelate lanthanides and sensitize their fluorescence. As shown in Figure 7-3, this could then react with a glass surface which has been modified with an amine-reactive molecule, such as an epoxide. Several different synthetic routes were tried. One route investigated a nitrile modified chelidamic acid which could then be reduced to the amine. The synthesis of the nitrile gave very low yield. When the reduction was attempted using a cobalt borohydride mixture, which is supposed to be a mild procedure, degradation of the parent molecule occurred.

In a second route, an azide modified chelidamic acid was made, which could then be reduced to the amine. The facile synthesis of the azide gave a good yield and thus our efforts shifted from the nitrile to the azide. Several different methods were investigated for the reduction of the azide. These methods included the Staudinger procedure, where the azide is reduced using tryphenylphosphine; a classic reduction in the presence of H_2 gas and a palladium catalyst; and a lesser known method of using zinc powder. The Staudinger procedure, considered a mild reduction route, resulted in some degradation of the parent compound. Saponification of the ester protecting the carboxylic acid groups of the chelidamic acid occurred with this procedure as well as with the other azide-reduction procedures. The saponification of the ester greatly decreased the solubility of the molecule making purification difficult in general. This further complicated the removal of the triphenylphosphine oxide by-products of the

reaction. When using the H_2 gas and a palladium catalyst, there seemed to be a tradeoff which could not be perfected. When the hydrogenation was performed, degradation of the parent compound occurred. The degradation could be lessened by decreasing the reaction time, but then this led to only partial reduction of the azide. Again saponification of the ester was seen which complicated the purification. In the zinc reduction, full reduction of the azide could be achieved with little to no degradation of the parent compound, there was however saponification of the ester. Saponification of the ester left the molecule sparingly soluble in basic water making it difficult to wash. However, based on the NMR, the material appeared to be fairly pure and it was decided to use this product for the next phase of the project: immobilization on a surface and subsequent luminescence studies.

The product from the zinc reduction was mixed with either samarium or terbium and then reacted with epoxy coated glass slides. However when XPS was taken of this slide, it showed there was still contamination with zinc (Figure 7-4). Preliminary fluorescence spectroscopy of a terbium slide did show a typical emission picks of terbium. However, because of the poor solubility of the material, it could not be certain if all the material that was not bound to the glass had washed off. Because of the difficulty in obtaining **9** in pure form and the apparent poor solubility after ester saponification, it was decided that a different approach to forming these luminescent lanthanide films should be explored.

The next possibility explored was the preparation of a chelidamic acid containing a siloxane so that it could be immobilized directly onto bare glass. Three different synthetic approaches were explored, which tried to make compounds **10**, **11**, or **12**. One difficulty in preparation of silanes is that they cannot be purified through column chromatography. Many of the papers that report the preparation of siloxanes use either precipitation or distillation for

purification, but neither of these methods proved successful in these reactions. NMR of the material from the reactions for **11** and **12** after it had been filtered through celite showed many side products. The reaction that showed the most promise was that for **10**. In the ^{1}H NMR of the material, it showed mostly the product. However, the integration of the NMR indicated that there is a mixture of APTES with two of **5** added onto the amine and APTES with a single **5** added onto the amine, which is to be expected, but because the siloxane purification with column chromatography is not feasible, separation of the two would be difficult.

Future Work

This project is not yet finished. The target molecule, **9**, was apparently synthesized, but was contaminated with zinc. Also, the molecule exhibited poor solubility which would make its immobilization as a monolayer on glass difficult. A different approach was taken, which focused on synthesizing chelidamic acid modified silanes, but little progress was made. There are still many routes that can be tried for making a siloxane modified chelidamic acid. There are also different coupling schemes besides the amine-epoxide method shown in Figure 7-3. Once the chelidamic-lanthanide monolayer is constructed, the fluorescence experiments would still need to be conducted.

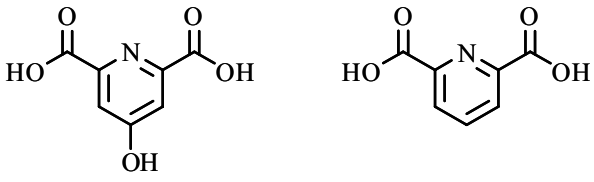

Chelidamic acid Dipicolinic acid

Figure 7-1. Two common sensitizers of lanthanides are chelidamic acid and dipicolinic acid.

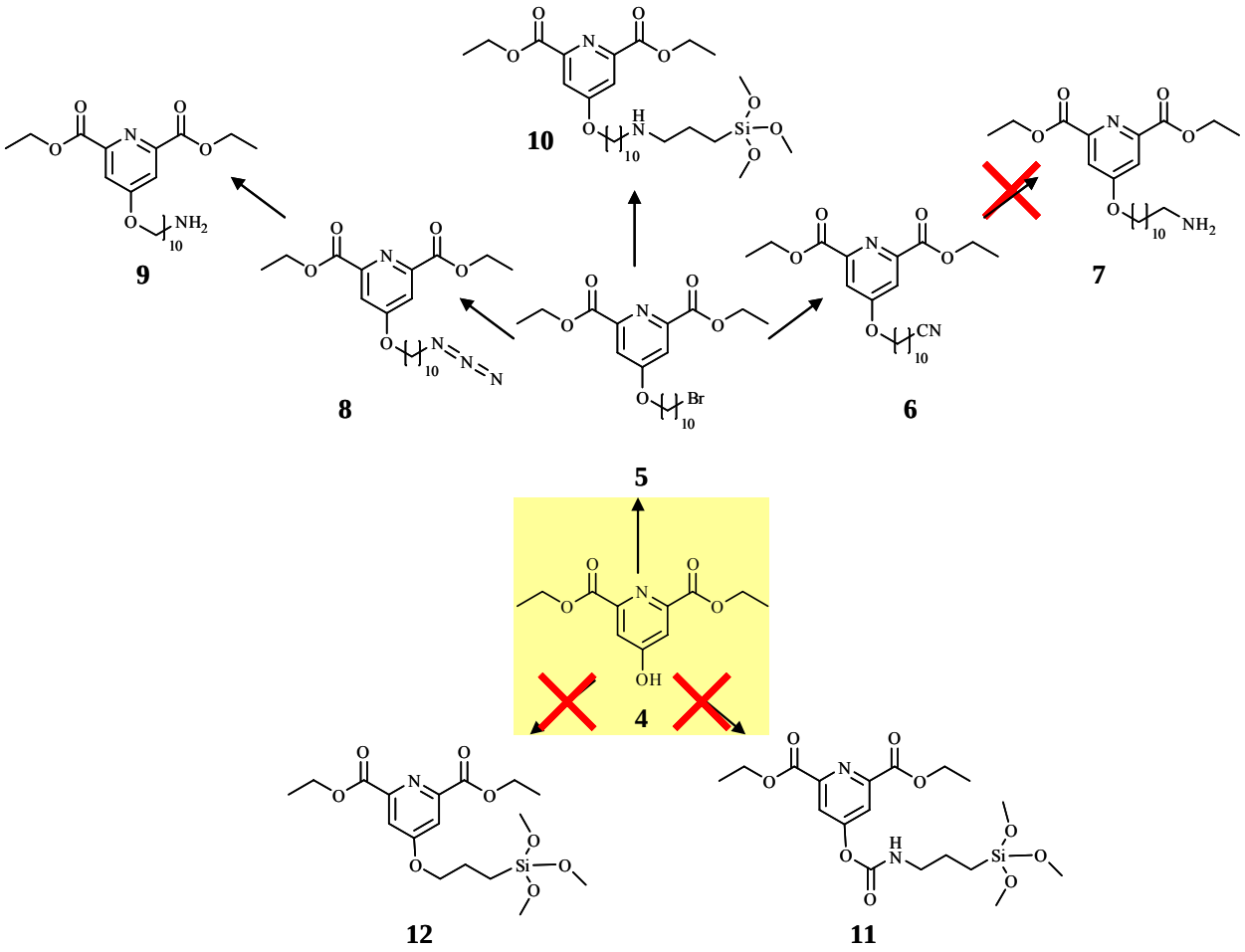

Figure 7-2. Scheme of different routes for a surface reactive chelidamic acid. The procedures used to prepare these compounds are shown in the experimental section.

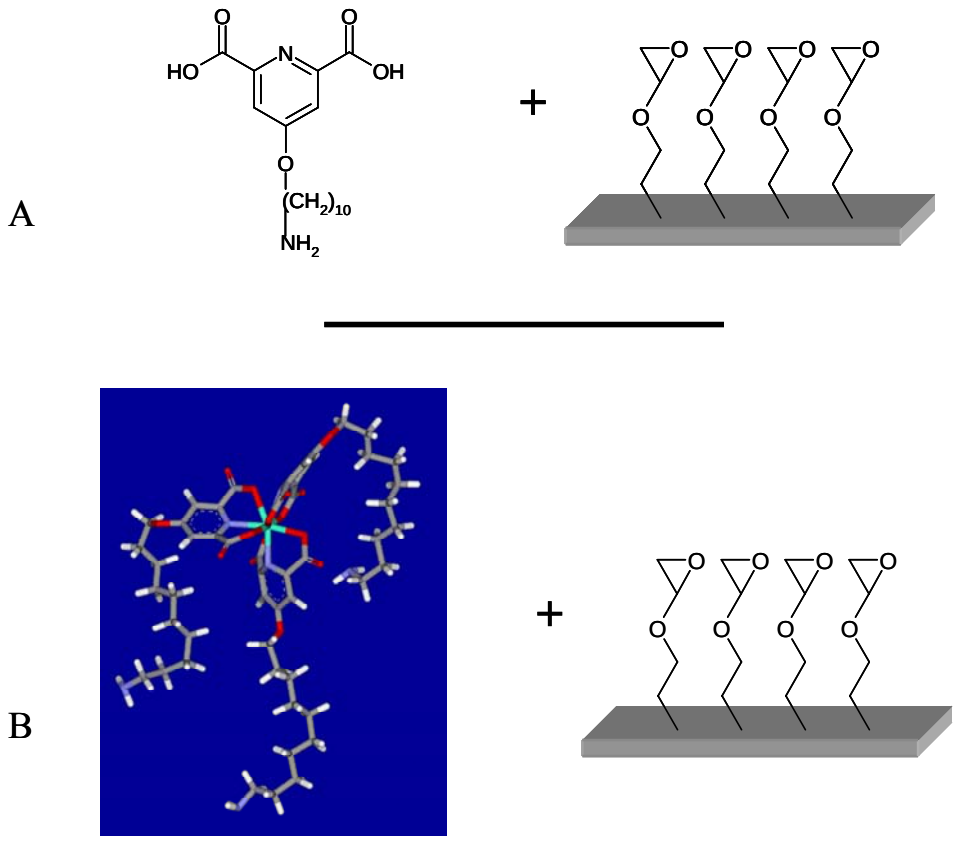

Figure 7-3. Two possible routes of immobilizing the chelidamic acid/lanthanide complex onto a surface. A) Method involves the reaction of the chelidamic-containing ligand with the surface and then this surface with the lanthanide solution. B) The route other involves first the reaction of the lanthanide with the ligand and then immobilization of this complex on the surface.

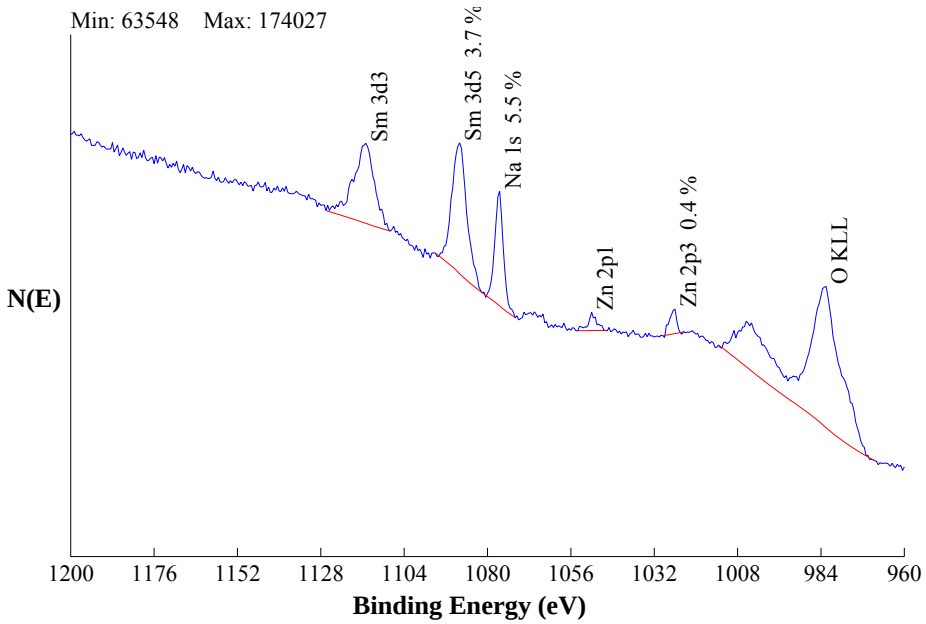

Figure 7-4. Portion of an XPS spectrum where ligand **9** was allowed to react with Sm^{3+} and then the resulting complex was allowed to react with an epoxide surface. The XPS spectrum shows that **9** was contaminated with zinc, coming from the reduction process of the azide.

CHAPTER 8
CONCLUSIONS

XPS has proven to be a powerful tool to study DNA on zirconium-phosphonate surfaces. A model was developed, based on the substrate-overlayer model, for the quantitative calculation of the DNA surface coverage on zirconium-phosphonate monolayers. This model could also be used for the calculation of surface density of other substances immobilized on a zirconium-phosphonate monolayer. With this model the surface coverage of ssDNA was found to be around 2.8×10^{11} DNA molecules/cm^2 for a probe molecule containing a phosphate linker and poly-dG spacer on the 5' end. For a probe with a poly-dA spacer, the surface coverage was calculated as 1.4×10^{11} DNA molecules/cm^2; however, this surface coverage was found to be highly dependent on the rinsing conditions. The surface coverage of dsDNA was also investigated. The highest surface coverage, 2.8×10^{11} dsDNA molecules/cm^2, was obtained for dsDNA which had a poly-dG spacer and phosphate linker on both 3' ends. A lower surface coverage, 2.1×10^{11} dsDNA molecules/cm^2, was found for dsDNA which had a poly-dG spacer and phosphate linker on both 5' ends. The lowest surface coverages were obtained for dsDNA with a random spacer and phosphate linker on both 5' ends (1.7×10^{11} dsDNA molecules/cm^2) and for dsDNA with a poly-dG spacer and phosphate linker on the 3' end and 5' end (1.2×10^{11}dsDNA molecules/cm^2). XPS was also used to follow the hybridization efficiency of immobilized ssDNA probes with a target of complementary sequence, but no increase in the N 1s signal could be seen after hybridization, indicating that the amount of target hybridized was too low to be seen with XPS.

Finally, the synthesis and immobilization of several lanthanide-chelating ligands was explored. A robust lanthanide monolayer was developed using an ethylenediamine triacetic acid ligand with a siloxane moiety. It would be interesting to test this surface as a substrate for

protein microarrays. The synthesis of a ligand which would sensitize the luminescence of lanthanides as well as immobilize the lanthanide on a surface was also explored. A molecule containing a chelidamic acid moiety and an amine group was synthesized, but the purification and use of this molecule was hindered by its poor solubility. Again, XPS played a key role in developing and studying the lanthanide monolayers.

LIST OF REFERENCES

(1) Alivisatos, A. P.; Johnsonn, K. P.; Peng, X.; Wilson, T. E.; Loweth, C. J.; Bruchez, M. P.; Schultz, P. G. *Nature* **1996**, *382*, 609-611.

(2) Braun, E.; Eichen, Y.; Sivan, U.; Ben-Yoseph, G. *Nature* **1998**, *391*, 775-778.

(3) Pease, A. C.; Solas, D.; Sullivan, E. J.; Cronin, M. T.; Holmes, C. P.; Fodor, S. P. A. *Proceedings of the National Academy of Sciences of the United States of America* **1994**, *91*, 5022-5026.

(4) Smith, S. B.; Finzi, L.; Bustamantet, C. *Science* **1992**, *258*, 1122-1126.

(5) Storhoff, J. J.; Mirkin, C. A. *Chemical Reviews* **1999**, *99*, 1849-1862.

(6) Mucic, R. C.; Storhoff, J. J.; Mirkin, C. A.; Letsinger, R. L. *Journal of the American Chemical Society* **1998**, *120*, 12674-12675.

(7) Becker, C. F. W.; Wacker, R.; Bouschen, W.; Seidel, R.; Kolaric, B.; Lang, P.; Schroeder, H.; Miller, O.; Niemeyer, C. M.; Spengler, B.; Goody, R. S.; Engelhard, M. *Angewandte Chemie International Edition* **2005**, *44*, 7635 –7639.

(8) Georgiadis, R.; Peterlinz, K. P.; Peterson, A. W. *Journal of the American Chemical Society* **2000**, *122*, 3166-3173.

(9) Kimura-Suda, H.; Petrovykh, D. Y.; Tarlov, M. J.; Whitman, L. J. *Journal of the American Chemical Society* **2003**, *125*, 9014-9015.

(10) Gong, P.; Lee, C.-Y.; Gamble, L. J.; Castner, D. G.; Grainger, D. W. *Analytical Chemistry* **2006**, *78*, 3326-3334.

(11) Casero, E.; Darder, M.; Díaz, D. J.; Pariente, F.; Martín-Gago, J. A.; Abruña, H.; Lorenzo, E. *Langmuir* **2003**, *19*, 6230-6235.

(12) Petrovykh, D. Y.; Kimura-Suda, H.; Tarlov, M. J.; Whitman, L. J. *Langmuir* **2004**, *20*, 429-440.

(13) Dai, S.; Zhang, X.; Du, Z.; Dang, H. *Materials Letters* **2004**, *59*, 423– 429.

(14) Kumar, A.; Pattarkine, M.; Bhadbhade, M.; Mandale, A. B.; Ganesh, K. N.; Datar, S. S.; Dharmadhikari, C. V.; Sastry, M. *Advanced Materials* **2001**, *13*, 341-344.

(15) Wang, J.; Rivas, G.; Jiang, M.; Zhang, X. *Langmuir* **1999**, *15*, 6541-6545.

(16) Zhang, D.; Chen, Y.; Chen, H.-Y.; Xia, X. H. *Analytical and Bioanalytical Chemistry* **2004**, *379*, 1025–1030.

(17) Herne, T. M.; Tarlov, M. J. *Journal of the American Chemical Society* **1997**, *119*, 8916-8920.

(18) Lee, C.-Y.; Canavan, H. E.; Gamble, L. J.; Castner, D. G. *Langmuir* **2005**, *21*, 5134-5141.

(19) Lee, C.-Y.; Gong, P.; Harbers, G. M.; Grainger, D. W.; Castner, D. G.; Gamble, L. J. *Analytical Chemistry* **2006**, *78*, 3316-3325.

(20) May, C. J.; Canavan, H. E.; Castner, D. G. *Analytical Chemistry* **2004**, *76*, 1114-1122.

(21) Mohaddes-Ardabili, L.; Martínez-Miranda, L. J.; Silverman, J.; Christou, A.; Salamanca-Riba, L. G.; Al-Sheikhlya, M.; Bentley, W. E.; Ohuchi, F. *Applied Physics Letters* **2003**, *83*, 192-194.

(22) Sastry, M.; Ramakrishnan, V.; Pattarkine, M.; Ganesh, K. N. *Journal of Physical Chemistry B.* **2001**, *105*, 4409-4414.

(23) Millard, M. M.; Macquet, J. P.; Theophanides, T. *Biochimica et Biophysica Acta, Nucleic Acids and Protein Synthesis* **1975**, *402*, 166-70.

(24) Higashi, N.; Takahashi, M.; Niwa, M. *Langmuir* **1999**, *15*, 111-115.

(25) Saprigin, A. V.; Thomas, C. W.; Dulcey, C. S.; Patterson, C. H.; Spector, M. S. *Surface and Interface Analysis* **2004**, *36*, 24-32.

(26) Petrovykh, D. Y.; Kimura-Suda, H.; Whitman, L. J.; Tarlov, M. J. *Journal of the American Chemical Society* **2003**, *125*, 5219-5226.

(27) Leavitt, A. J.; Wenzler, L. A.; Williams, J. M.; Thomas P. Beebe, J. *Journal of Physical Chemistry* **1994**, *98*, 8742-8746.

(28) Powell, C. J.; Jablonski, A. *NIST Electron Effective-Attenuation-Length Database, Version 1.0 (NIST SRD-82)* **2001**.

(29) Corrie, S. R.; Lawrie, G. A.; Trau, M. *Langmuir* **2006**, *22*, 2731-2737.

(30) Schena, M.; Shalon, D.; Davis, R. W.; Brown, P. O. *Science* **1995**, *270*, 467-470.

(31) Lockhart, D. J.; Dong, H. L.; Byrne, M. C.; Follettie, M. T.; Gallo, M. V.; Chee, M. S.; Mittmann, M.; Wang, C. W.; Kobayashi, M.; Horton, H.; Brown, E. L. *Nature Biotechnology* **1996**, *14*, 1675-1680.

(32) Nonglaton, G.; Benitez, I. O.; Guisle, I.; Pipelier, M.; Léger, J.; Dubreuil, D.; Tellier, C.; Talham, D. R.; Bujoli, B. *Journal of the American Chemical Society* **2004**, *126*, 1497-1502.

(33) Benitez, I. O.; Bujoli, B.; Camus, L. J.; Lee, C. M.; Odobel, F.; Talham, D. R. *Journal of the American Chemical Society* **2002**, *124*, 4363-4370.

(34) Wu, A. P.; Talham, D. R. *Langmuir* **2000**, *16*, 7449-7456.

(35) Byrd, H.; Whipps, S.; Pike, J. K.; Talham, D. R. *Thin Solid Films* **1994**, *244*, 768-771.

(36) Peterson, A. W.; Heaton, R. J.; Georgiadis, R. M. *Nucleic Acids Research* **2001**, *29*, 5163-5168.

(37) Shchepinov, M. S.; Case-Green, S. C.; Southern, E. M. *Nucleic Acids Research* **1997**, *25*, 1155-1161.

(38) Frydman, E.; Cohen, H.; Maoz, R.; Sagiv, J. *Langmuir* **1997**, *13*, 5089-5106.

(39) Weng, L. T.; Vereecke, G.; Genet, M. J.; Bertrand, P.; Stone, W. E. E. *Surface and Interface Analysis* **1993**, *20*, 179-192.

(40) Lee, H.; Kepley, L. J.; Hong, H. G.; Mallouk, T. E. *Journal of the American Chemical Society* **1988**, *110*, 618-620.

(41) Lee, H.; Kepley, L. J.; Hong, H. G.; Akhter, S.; Mallouk, T. E. *Journal of Physical Chemistry* **1988**, *92*, 2597-2601.

(42) Thompson, M. E. *Chemistry of Materials* **1994**, *6*, 1168-1175.

(43) Byrd, H.; Pike, J. K.; Talham, D. R. *Chemistry of Materials* **1993**, *5*, 709-715.

(44) Scofield, J. H. *Journal of Electron Spectroscopy and Related Phenomena* **1976**, *8*, 129-137.

(45) The band-gap energy determined from the average UV absorption maxima of the nucleotides, which is 4.8 eV.

(46) An ideal film density of 0.893 g/cm3 was used.

(47) In the referenced paper by Georgiadis and colleagues, they demonstrated that higher salt concentrations, which they used their experiments, can lead to higher probe surface coverages.

(48) Zammatteo, N.; Jeanmart, L.; Hamels, S.; Courtois, S.; Louette, P.; Hevesi, L.; Remacle, J. *Analytical Biochemistry* **2000**, *280*, 143-150.

(49) Halperin, A.; Buhot, A.; Zhulina, E. B. *Langmuir* **2006**, *22*, 11290-11304.

(50) Hong, B. J.; Oh, S. J.; Youn, T. O.; Kwon, S. H.; Park, J. W. *Langmuir* **2005**, *21*, 4257-4261.

(51) Walker, S. L.; Bhattacharjee, S.; Hoek, E. M. V.; Elimelech, M. *Langmuir* **2002**, *18*, 2193-2198.

(52) Guo, Z.; Guilfoyle, R. A.; Thiel, A. J.; Wang, R.; Smith, L. M. *Nucleic Acids Research* **1994**, *22*, 5456-5465.

(53) Pinnavaia, T. J.; Miles, H. T.; Becker, E. D. *Journal of the American Chemical Society* **1975**, *97*, 7198-7200.

(54) Blackburn, E. H. *Nature* **1991**, *350*, 569-573.

(55) Yauk, C.; Berndt, L.; Williams, A.; Douglas, G. R. *Journal of Biochemical and Biophysical Methods* **2005**, *64*, 69–75.

(56) Han, T.; Melvin, C. D.; Shi, L.; Branham, W. S.; Moland, C. L.; Pine, P. S.; Thompson, K. L.; Fuscoe, J. C. *BMC Bioinformatics* **2006**, *7(Suppl 2)*, S17.

(57) Wolf, L. K.; Gao, Y.; Georgiadis, R. M. *Langmuir* **2004**, *20*, 3357-3361.

(58) Giesbers, M.; J. Mieke Kleijn; Stuart, M. A. C. *Journal of Colloid and Interface Science* **2002**, *248*, 88–95.

(59) Becker, C. F. W.; Wacker, R.; Bouschen, W.; Seidel, R.; Kolaric, B.; Lang, P.; Schroeder, H.; MuIler, O.; Niemeyer, C. M.; Spengler, B.; Goody, R. S.; Engelhard, M. *Angewandte Chemie International Edition* **2005**, *44*, 7635–7639.

(60) Berger, M. F.; Philippakis, A. A.; Qureshi, A. M.; He, F. S.; Estep, P. W.; Bulyk, M. L. *Nature Biotechnology* **2006**, *24*, 1429-1435.

(61) Brockman, J. M.; Frutos, A. G.; Corn, R. M. *Journal of the American Chemical Society* **1999**, *121*, 8044-8051.

(62) Bulyk, M. L. *Current Opinion in Biotechnology* **2006**, *17*, 422–430.

(63) Bulyk, M. L.; Gentalen, E.; Lockhart, D. J.; Church, G. M. *Nature Biotechnology* **1999**, *17*, 573-577.

(64) O'Brien, J. C.; Stickney, J. T.; Porter, M. D. *Journal of the American Chemical Society* **2000**, *122*, 5004-5005.

(65) Shumaker-Parry, J. S.; Zareie, M. H.; Aebersold, R.; Campbell, C. T. *Analytical Chemistry* **2004**, *76*, 918-929.

(66) Smith, E. A.; Erickson, M. G.; Ulijasz, A. T.; Weisblum, B.; Corn, R. M. *Langmuir* **2003**, *19*, 1486-1492.

(67) Sato, N.; Ohta, N. *Nucleic Acids Research* **2001**, *29*, 2244-2250.

(68) Shoeman, R. L.; Hartig, R.; Traub, P. *Biochemistry* **1999**, *38*, 16802-16809.

(69) Tsung, K.; Brissette, R. E.; Inouye, M. *The Journal of Biological Chemistry* **1989**, *264*, 10104 -10109.

(70) Park, S.-M.; Lu, C.-D.; Abdelal, A. T. *Journal of Bacteriology* **1997**, *179*, 5309–5317.

(71) Gong, P.; Harbers, G. M.; Grainger, D. W. *Analytical Chemistry* **2006**, *78*, 2342-2351.

(72) Meinkoth, J.; Wahl, G. *Analytical Biochemistry* **1984**, *138*, 267-284.

(73) Vainrub, A.; Pettitt, B. M. *Biopolymers* **2002**, *68*, 265–270.

(74) Howley, P. M.; Israel, M. A.; Law, M.-F.; Martin, M. A. *The Journal of Biological Chemistry* **1979**, *254*, 4876-4883.

(75) Zhu, H.; Bilgin, M.; Bangham, R.; Hall, D.; Casamayor, A.; Bertone, P.; Lan, N.; Jansen, R.; Bidlingmaier, S.; Houfek, T.; Mitchell, T.; Miller, P.; Dean, R. A.; Mark.Gerstein; Snyder, M. *Science* **2001**, *293*, 2101-2105.

(76) Kambhampti, D. *Protein Microarray Technology* **2004**, Wiley-VCH Verlag, Weinham.

(77) Cha, T.; Guo, A.; Zhu, X.-Y. *Proteomics* **2005**, *5*, 416-419.

(78) Keller, T. A.; Duschl, C.; Kroger, D.; Anne-Francoise; Sevin-Landais; Vogel, H.; Cervigni, S. E.; Dumy, P. *Supramolecular Science* **1995**, *2*, 155-160.

(79) Nieba, L.; Nieba-Axmann, S. E.; Persson, A.; Hamalainen, M.; Edebratt, F.; Hansson, A.; Lidholm, J.; Magnusson, K.; Karlsson, A. F.; Pluckthun, A. *Analystical Biochemistry* **1997**, *252*, 217–228.

(80) Santra, S.; Bagwe, R. P.; Dutta, D.; Stanley, J. T.; Walter, G. A.; Tan, W.; Moudgil, B. M.; Mericle, R. A. *Advanced Materials* **2005**, *17*, 2165-2169.

(81) Brittain, H. G. *Inorganic Chemistry* **1978**, *17*, 2762-2766.

(82) Crosby, G. A.; Whan, R. E.; Freeman, J. J. *Journal of Physical Chemistry* **1962**, *66*, 2493-2499.

(83) Chrysochoos, J.; Evers, A. *Chemistry Physics Letters* **1973**, *20*, 174.

(84) Zhong, G.-L.; Wang, Y.-H.; Wang, C.-K.; Yang, K.-Z. *Luminescence* **2001**, *385*, 234-238.

(85) Zhong, G.; Yang, K. *Langmuir* **1998**, *14*, 5502.

(86) Lenaerts, P.; Storms, A.; Mullens, J.; D'Haen, J.; Go¨rller-Walrand, C.; Binnemans, K.; Driesen, K. *Chemistry of Materials* **2005**, *17*, 5194-5201.

(87) Rodriguez-Mendez, M. L.; Aroca, R.; DeSaja, J. A. *Chemistry of Materials* **1992**, *4*, 1017-1020.

(88) Riegel, E. R.; Zwilgmeyer, F. *Organic Syntheses* **1937**, *17*, 40.

(89) King, H.; Ware, L. L. *Journal of the Chemical Society* **1939**, 873.

(90) Cooper, C. G. F.; MacDonald, J. C.; Soto, E.; McGimpsey, W. G. *Journal of the American Chemical Society* **2004**, *126*, 1032-1033.

(91) Vogel. *Vogel's Textbook of Practical Organic Chemistry* **1978**, Longman, London ; New York.

(92) Borkowski, P. R.; Horn, J. S.; Rapoport, H. *Journal of the American Chemical Society* **1978**, *100*, 276-281.

(93) Roy, B. C.; Santos, M.; Sanku Mallik; Campiglia, A. D. *Journal of Organic Chemistry* **2002**, *68*, 3999-4007.

(94) Somfai, P.; Marchand, P.; Torsell, S.; Lindstro¨m, U. M. *Tetrahedron* **2003**, *59*, 1293–1299.

(95) Lin, W.; Zhang, X.; He, Z.; Jin, Y.; Gong, L.; Mi, A. *Synthetic Communications* **2002**, *32*, 3279–3284.

(96) Cui, Y.; Chen, L.; Qian, G.; Wang, M. *Dyes and Pigments* **2006**, *70*, 232-237.

BIOGRAPHICAL SKETCH

Sarah Lane was born in Pensacola, FL the day after Christmas way back in 1978. She graduated from Escambia High School, home of the fightin' gators, in 1997. Subsequently, she began attending the University of Florida as a psychology major, but her major quickly switched to environmental science. Lacking direction, she dropped out for a semester to wait tables at a diner in Pensacola. After which, she settled on a major in chemistry. In December 2001, she graduated with a BS in chemistry and continued at the University of Florida with graduate studies in surface chemistry. She defended her PhD dissertation in July 2007.